

REFERENCE SECTION,
REVISED STRATIGRAPHY AND FACIES
ANALYSIS OF THE ORDOVICIAN NAMBEET
FORMATION, CANNING BASIN,
WESTERN AUSTRALIA

by
LM Dent, LS Normore and SK Martin



Government of **Western Australia**
Department of **Mines, Industry Regulation**
and **Safety**

REPORT 211

REFERENCE SECTION, REVISED STRATIGRAPHY AND FACIES ANALYSIS OF THE ORDOVICIAN NAMBEET FORMATION, CANNING BASIN, WESTERN AUSTRALIA

by
LM Dent, LS Normore and SK Martin

PERTH 2021



Geological Survey of
Western Australia

MINISTER FOR MINES AND PETROLEUM
Hon Bill Johnston MLA

DIRECTOR GENERAL, DEPARTMENT OF MINES, INDUSTRY REGULATION AND SAFETY
David Smith

EXECUTIVE DIRECTOR, GEOLOGICAL SURVEY AND RESOURCE STRATEGY
Jeff Haworth

REFERENCE

The recommended reference for this publication is:

Dent, LM, Normore, LS and Martin, SK 2021, Reference section, revised stratigraphy and facies analysis of the Ordovician Nambeet Formation, Canning Basin, Western Australia: Geological Survey of Western Australia, Report 211, 69p.

ISBN 978-1-74168-915-0

ISSN 1834-2280



A catalogue record for this
book is available from the
National Library of Australia

Grid references in this publication refer to the Geocentric Datum of Australia 1994 (GDA94). Locations mentioned in the text are referenced using Map Grid Australia (MGA) coordinates, Zones **51** and **52**. All locations are quoted to at least the nearest 100 m.

Disclaimer

This product uses information from various sources. The Department of Mines, Industry Regulation and Safety (DMIRS) and the State cannot guarantee the accuracy, currency or completeness of the information. Neither the department nor the State of Western Australia nor any employee or agent of the department shall be responsible or liable for any loss, damage or injury arising from the use of or reliance on any information, data or advice (including incomplete, out of date, incorrect, inaccurate or misleading information, data or advice) expressed or implied in, or coming from, this publication or incorporated into it by reference, by any person whosoever.

Based on consultation with the Western Desert Lands Aboriginal Corporation (WDLAC) on the cultural significance of the name, Waukarlycarly, it has been agreed to change the name of the well to Barnicarndy 1 and the tectonic subdivision to Barnicarndy Graben. This and all future publications will now refer to the Barnicarndy 1 stratigraphic drillhole (previously Waukarlycarly 1) and the Barnicarndy Graben (previously Waukarlycarly Embayment).

Published 2021 by the Geological Survey of Western Australia

This Report is published in digital format (PDF) and is available online at <www.dmirs.wa.gov.au/GSWApublications>.



© State of Western Australia (Department of Mines, Industry Regulation and Safety) 2021

With the exception of the Western Australian Coat of Arms and other logos, and where otherwise noted, these data are provided under a Creative Commons Attribution 4.0 International Licence. (<http://creativecommons.org/licenses/by/4.0/legalcode>)

Further details of geoscience publications are available from:

Information Centre
Department of Mines, Industry Regulation and Safety
100 Plain Street
EAST PERTH WESTERN AUSTRALIA 6004
Telephone: +61 8 9222 3459 Email: publications@dmirs.wa.gov.au
www.dmirs.wa.gov.au/GSWApublications

Cover image: Image montage featuring characteristics of the Nambeet Formation

Contents

Abstract	1
Introduction	1
Defining the Nambeet Formation	1
Type section	1
Type section review and new reference section	2
Geological setting of the Canning Basin	4
Structure and evolution	4
Lower Ordovician stratigraphy	4
Revised Nambeet Formation stratigraphy	8
Nambeet Formation – Willara Formation boundary	8
New members	8
Fly Flat Member (new name)	12
Lithostratigraphy	12
Diagenesis	17
HyLogger spectral data	17
Biostratigraphy	18
Geochronology	18
Samphire Marsh Member (new name)	18
Lithostratigraphy	18
Diagenesis	27
HyLogger spectral data	29
Biostratigraphy	31
Geochronology	35
Sequence stratigraphic setting	35
Supersequence A0	36
Supersequence A1	36
Depositional model	38
Correlation	40
Interformation correlation	40
Wilson Cliffs Sandstone	40
Prices Creek Group	41
Intraformation member correlation	41
Chemostratigraphy	41
Economic geology	41
Reservoir potential	41
Fly Flat Member	41
Samphire Marsh Member	43
Source and hydrocarbon potential	43
Fly Flat Member	43
Samphire Marsh Member	43
Conclusions	47
References	47

Figures

1. Location map showing subsurface intersections of the Nambeet Formation in the Canning Basin	2
2. Stratigraphic chart showing the age of formations in the Olympic 1 core	5
3. Ordovician stratigraphy in the Canning Basin	6
4. SEEBASE map of the Canning Basin	7
5. Key facies associations interpreted in Olympic 1 core	9
6. Conodont sample depths, species ranges and biozones recorded in Olympic 1	11
7. HyLogger data recorded from the Olympic 1 core	13
8. Major facies and parasequence cyclicity of SFA1	16
9. Diagenetic sequence of siliciclastic facies in Olympic 1	18
10. Thin section and SEM images showing cements and porosity in the Fly Flat Member	19
11. Schematic diagram showing the epeiric sea ramp model	20
12. Major facies and sedimentary features of CFA1	22
13. Major facies and sedimentary features of CFA2	24
14. Core photos of the major facies of CFA3 and CFA4	25
15. Core photos of the major facies of CFA5	26
16. Core photos of the major facies of CFA6 and CFA7	28
17. Paragenetic sequence of diagenetic events in carbonate–mudstone facies of the Nambeet Formation	29
18. Images of cements and porosity in carbonate–mudstone facies of the Nambeet Formation	30
19. Distribution of macrofossil records throughout the Samphire Marsh Member for various groups	32
20. Examples of graptolites from the Samphire Marsh Member	34
21. Sequence stratigraphic framework for the Olympic 1 cored section	37
22. Image showing the first major transgressive boundary in the Olympic 1 cored section	38

23.	Concentration of heavy rare earth elements through the Nambheet Formation.....	39
24.	Chemostratigraphic packages of Olympic 1 correlated to Nicolay 1 and Sally May 2.....	42
25.	Measured core porosity and permeability recorded from Olympic 1	44
26.	Core images showing a 30 cm-long residual hydrocarbon show in Olympic 1	45
27.	Source potential of the Nambheet Formation.....	46

Tables

1.	Type section locations and details of Lower–Middle Ordovician formations in the Canning Basin.....	3
2.	Core recovered from Samphire Marsh 1, Willara Sub-basin	3
3.	Siliciclastic facies associations of the Fly Flat Member in Olympic 1	10
4.	Carbonate facies associations of the Samphire Marsh Member in Olympic 1	10
5.	Geochronology samples and data collected from ash beds in the Olympic 1 cored section.....	11
6.	Facies interpreted in the Fly Flat Member in Olympic 1 well.....	14
7.	Bioturbation index categories	15
8.	Facies interpreted in the Samphire Marsh Member in Olympic 1 well	21
9.	Distinguishing geochemical characteristics of the chemostratigraphic packages identified in Olympic 1	43

Appendices

1.	Revised stratigraphic picks for the top of the Nambheet Formation and equivalent formations	50
2.	Formation definition card — Fly Flat Member	52
3.	Formation definition card — Samphire Marsh Member	55
4.	Micro-brachiopod report by I Percival (Appendix plates 1–3 available with the PDF of this Report as an accompanying digital resource)	58
5.	Hydrocarbon shows recorded in the Nambheet Formation and laterally correlative units.....	62

Plates

1.	Correlation panel through wells on the Broome Platform and Willara Sub-basin
2.	Correlation panel through wells on the Broome Platform, Mowla Terrace and Barbwire Terrace
3.	Correlation panel of wells where the Wilson Cliffs Sandstone has been identified
4.	Seismic lines showing interpreted Nambheet Formation, Willara Formation and Goldwyer Formation packages in three sections across the Canning Basin

Reference section, revised stratigraphy and facies analysis of the Ordovician Nambeet Formation, Canning Basin, Western Australia

by

LM Dent, LS Normore and SK Martin

Abstract

The Olympic 1 petroleum exploration well is proposed as a reference section for the Lower Ordovician Nambeet Formation of the Canning Basin. The well recovered 319.53 m of continuous core that includes the conformable contact between the Nambeet Formation and overlying Willara Formation, and 277.53 m of the Nambeet Formation. At total depth of 1447.53 m, the well and base of the core is predicted to be around 20 m above Precambrian basement, and thus above the base of the Nambeet Formation.

Biostratigraphy and geochronology confirm a Lower Ordovician (Tremadocian–Floian) age for the Nambeet Formation. Eleven bentonite beds were recovered, seven of which yielded $^{206}\text{Pb}/^{238}\text{U}$ zircon dates that ranged from 479.37 ± 0.18 Ma to 470.18 ± 0.13 Ma. Deposition of the overlying Willara Formation commenced in the latest Floian or earliest Dapingian. The bentonite ages were used to constrain four conodont biozones identified within the cored section: *Jumudontus gananda*, *Oepikodus communis*, *Prioniodus oepiki* – *Serratognathus bilobatus* and *Paroistodus proteus*. The four biozones show continuous deposition of the Nambeet and Willara Formations between the Tremadocian and Dapingian (Lower–Middle Ordovician) and provide a basis to correlate the Olympic 1 cored section to outcrop and other subsurface sections.

It is proposed that the Nambeet Formation should be divided into two formal members: the upper Samphire Marsh Member and the underlying Fly Flat Member. The Samphire Marsh Member is dominated by mudstone and carbonate lithologies. Seven facies associations are identified (CFA1–7) and record deposition in a low-angle carbonate/epiiric ramp setting. The Fly Flat Member is sandstone dominated, and three facies associations are identified, SFA1–3, between upper and lower shoreface depositional environments. The Fly Flat Member comprises the lowstand deposits of the initial second-order supersequence in the Canning Basin. The Samphire Marsh Member makes up the remainder of this supersequence, the transgressive to falling stage deposits, and the beginning of the successive Canning Basin supersequence.

The Samphire Marsh Member has good hydrocarbon source potential with total organic compound values of up to 3.28% recorded from the lower mudstone interval. Reservoir potential of both the Fly Flat and Samphire Marsh Members is limited by low porosity and permeability, although a 30 cm-thick interval of core with a residual oil show is present at the top of the Fly Flat Member indicating hydrocarbon migration.

KEYWORDS: biostratigraphy, Canning Basin, Fly Flat Member, geochronology, Nambeet Formation, Ordovician, reference section, Samphire Marsh Member

Introduction

The Olympic 1 well, drilled by Buru Energy Limited in 2015, recovered 319.53 m of continuous core through the Lower–Middle Ordovician Nambeet and Willara Formations in the Canning Basin (Fig. 1). Drilled on the Broome Platform, the Olympic 1 well recovered the most complete cored section currently available through the Nambeet Formation, including the uppermost contact with the overlying Willara Formation. This well significantly increased the amount of cored material available from the Nambeet Formation and provides an opportunity to reconsider and refine information about the formation. Although the well did not reach basement, the seismic interpretation predicts that it is within 20 m below the total depth (TD) of the well (1447.53 m). The excellent

quality of the recovered core allowed an extensive range of sampling to be undertaken through the Olympic 1 Nambeet Formation section. The results from these analyses, detailed in Normore and Dent (2017a) provide better constraints on the identification of the Nambeet Formation and result in its subdivision into two formal members: the upper Samphire Marsh Member and the underlying Fly Flat Member.

Defining the Nambeet Formation

Type section

The Nambeet Formation type section is designated from petroleum exploration well Samphire Marsh 1,

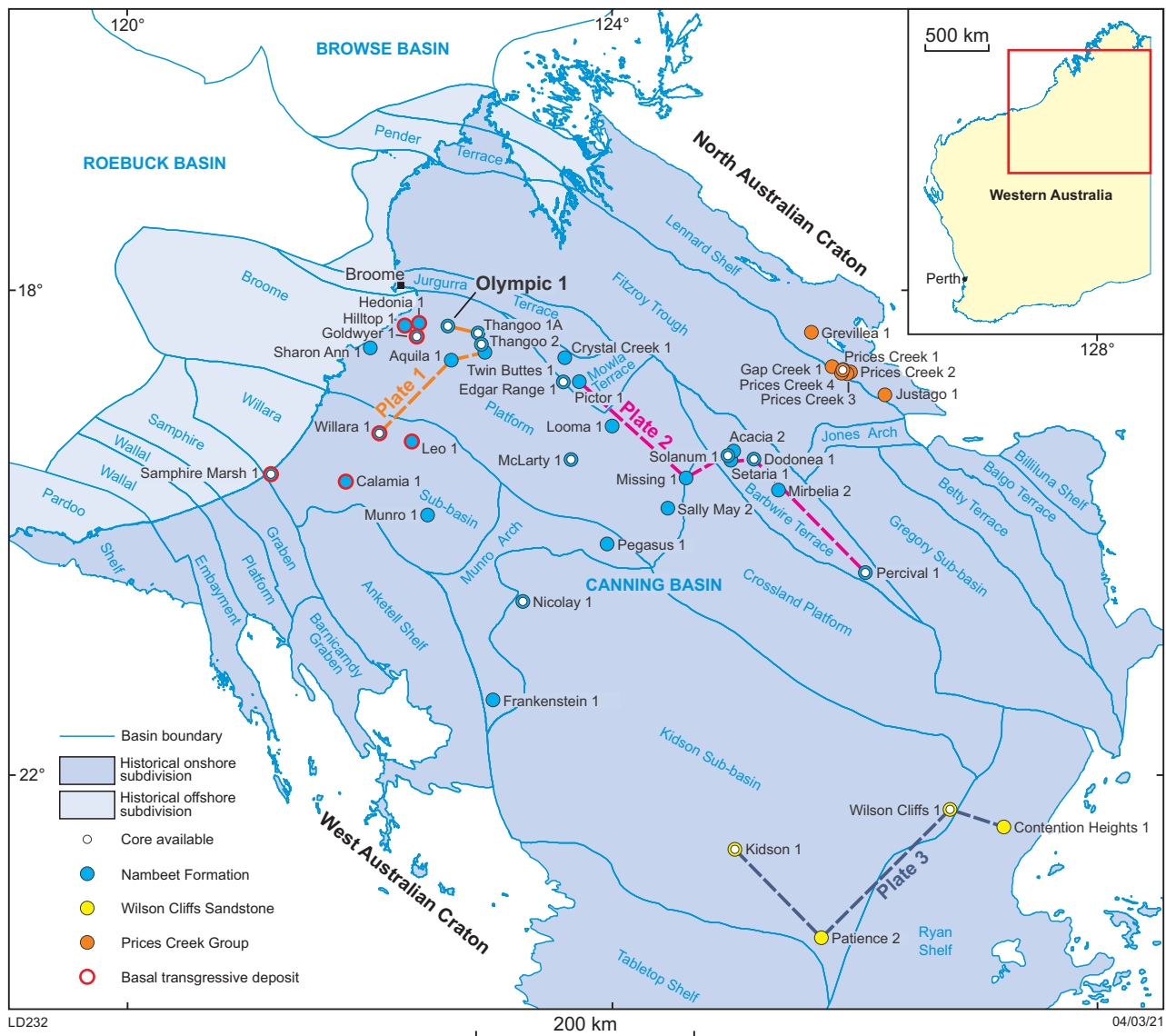


Figure 1. Locations of petroleum wells and stratigraphic holes that intersect the Nambeet Formation or equivalent strata in the Canning Basin, coloured according to formal classification. Wells with cored material available from the Nambeet Formation or equivalent formations are marked. Wells that record a 'basal transgressive unit' are highlighted

drilled in 1958 on the southern edge of the Willara Sub-basin (Fig. 1). The formation was first described in the subsequent well completion report (Johnstone, 1961) with the type section formally defined by Playford et al. (1975) (Table 1). The type section constitutes 775 m of 'Lower Ordovician' strata between 1240 and 2015 m depth. Twelve cores were attempted from this well, with only 12.6 m of core recovered from the Nambeet Formation (Table 2). Basement rocks were intersected directly below the Nambeet Formation at the base of Samphire Marsh 1, which were originally interpreted as Precambrian, but recent studies have determined a Cambrian igneous crystallization age of 505 ± 4 Ma (Haines et al., 2018; Wingate et al., 2018). At the type section, the Nambeet Formation is described as having a basal unit of fine- to coarse-grained quartz sandstone, overlain by a unit of green-grey shale with lesser interbedded limestone. A major unconformity separates the eroded top of the Nambeet Formation from the overlying Grant Group (Playford et al., 1975). Conodont biostratigraphy is available for two intervals: 1246.95 – 1335.20 m from which the *Prioniodus elegans* – *Bergstroemognathus extensus*

biozone is interpreted; 1687.50 – 1786.30 m from which the *Drepanastodus* – *Paltodus* biozone is interpreted (Nicoll, 1993).

Type section review and new reference section

The Nambeet Formation section in Samphire Marsh 1 does not satisfy the ideal components of a type section as defined by the Australian Stratigraphy Commission. The four main issues with the current section are: a) poor exposure, with only about 2% of the formation represented by cored material (Table 2); b) unclear formation boundaries and lack of typical boundary relationships, with both the top and base of the formation bound by major unconformities; c) atypical biostratigraphy when compared to other Nambeet Formation sections; d) lack of a standard suite of wireline logs, in particular the gamma-ray (GR) log. Elsewhere in the Canning Basin, the Nambeet Formation is conformably overlain by the Lower–Middle Ordovician Willara Formation. The base Permian unconformity overlying the Nambeet Formation in the type section is atypical, and Samphire Marsh 1 is the only well where this stratal relationship is observed (Forman and

Table 1. Type section locations and details of Lower–Middle Ordovician formations in the Canning Basin

Group	Formation/Member	Type section	Type section location	Type section specification	Defining work
	Willara Formation	Willara 1	19°10'48"S 122°04'14"E	2610–3142 m	Playford et al. (1975) after proposal by RA McTavish
	Nambeet Formation	Samphire Marsh 1	19°31'13"S 121°10'58.9"E	1240–2015 m	Playford et al. (1975)
	Samphire Marsh Member	Olympic 1	18°17'57.60"S 122°38'23.40"E	1170.00 – 1383.57 m	This Report
	Fly Flat Member	Olympic 1	18°17'57.60"S 122°38'23.40"E	1383.57 – 1447.53 m	This Report
	Wilson Cliffs Sandstone	Wilson Cliffs 1 (exploration well)	22°16'33.9"S 126°46'59.7"E	2847–3503 m	McTavish and Legg (1976)
Prices Creek Group	Gap Creek Formation	Near Gap Creek	18°38'S 125°55'E	192 m of outcrop	Guppy and Opik (1950); amended by Guppy et al. (1958)
Prices Creek Group	Emanuel Formation	Emanuel Creek	18°39'S 125°55'E	594 m of outcrop	Guppy and Opik (1950); amended by Guppy et al. (1958)
Prices Creek Group	Kudata Dolomite	BMR Noonkanbah 3	18°39'37"S 125°54'9.5"E	88 m, cores 1–3	Nicoll et al. (1993)
Prices Creek Group	Kunian Sandstone	BMR Noonkanbah 3	18°39'37"S 125°54'9.5"E	82 m, cores 4–6	Nicoll et al. (1993)

Table 2. Core recovered from Samphire Marsh 1, Willara Sub-basin

Core number	Start depth (m)	End depth (m)	Cored interval (m)	Recovery (%)	Recovery (m)	Stratigraphy
1	749.09	755.18	6.10	50	3.05	Grant Group
2	1039.63	1044.21	4.57	47	2.13	Grant Group
3	1168.60	1173.48	4.88	63	3.05	Grant Group
4	1246.04	1249.09	3.05	80	2.44	Nambeet Formation
5	1352.13	1355.18	3.05	80	2.44	Nambeet Formation
6	1503.96	1506.10	2.13	71	1.52	Nambeet Formation
7	1656.10	1659.15	3.05	0	0.00	Nambeet Formation
8	1686.59	1690.24	3.66	25	0.91	Nambeet Formation
9	1783.23	1786.28	3.05	100	3.05	Nambeet Formation
10	1884.76	1885.37	0.61	100	0.61	Nambeet Formation
11	1947.26	1950.30	3.05	100	3.05	Nambeet Formation
12	2030.18	2031.71	1.52	60	0.91	Basement

Wales, 1981). The Nambheet Formation is also atypically thick at the type section, even before considering the unknown amount lost to erosion.

The Olympic 1 well provides a continuously cored section including 277.53 m of the Nambheet Formation with almost 100% core recovery (Fig. 2). The conformable contact between the upper Nambheet Formation and Willara Formation is also present in the cored section. Precise U–Pb zircon geochronology (DTIMS) dates are available from bentonites throughout the Olympic 1 core and conodont biostratigraphy is well defined providing excellent age and biostratigraphic constraints for the age of the formation (Zhen et al., 2017; Normore et al., 2018). We propose that the Olympic 1 section (–18°17′57.60″S, 122°38′23.40″E), be cited as a new reference section for the Nambheet Formation.

The factors listed above, as well as the extensive additional information available on this cored section (Dent and Normore, 2017; Normore and Dent, 2017a,b; Zhen et al., 2017; Normore et al., 2018) and the full suite of downhole wireline logs, make it a significantly better constrained and typical section of the Nambheet Formation for reference purposes compared to the original Samphire Marsh 1 type section. A full list of samples and analyses conducted can be found in (Normore and Dent, 2017a). In addition, we propose that the Nambheet Formation be subdivided into two formal members, the lower Fly Flat Member and the upper Samphire Marsh Member (Figs 2, 3).

The primary objectives of this report are to:

- specify a new reference section for the Nambheet Formation
- provide a refined definition for the Nambheet Formation, particularly for identification of the upper contact with the Willara Formation
- propose a subdivision of the formation into two formal members
- map these two new members to Nambheet Formation well intersections throughout the Canning Basin
- interpret depositional facies and the sequence stratigraphic setting of the Nambheet Formation.

Geological setting of the Canning Basin

Structure and evolution

The Canning Basin is a large intracratonic basin with both onshore and offshore portions in Australia's northwest (Fig. 1). Initiated by rifting in the early Ordovician, the Canning Basin evolved through a series of major tectonic events between the Ordovician and Cretaceous, details of which can be found in Drummond et al. (1991), Shaw et al. (1994) and Parra-Garcia et al. (2014). The basin is divided into 20 structural elements (Fig. 1; Hocking et al., 1994), the most prominent of which are two northwest-trending depocentres separated and flanked by platforms, shelves and terraces (Fig. 1). The results of recent modelling of the Canning Basin

architecture by Frogtech Geoscience (2017) provides the most recent data on basin depth and structure (Fig. 4).

The Canning Basin is constrained by significantly older cratons and provinces to the north (North Australian Craton), south (West Australian Craton) and southeast (Musgrave Province; Fig. 1). The northwest margin transitions to the offshore Roebuck and Browse Basins. Onshore basin fill constitutes early Ordovician to late Cretaceous sedimentary rocks with a thin Cenozoic cover. Canning Basin stratigraphy was deposited in four first-order events or megasequences defined and discussed in Kennard et al. (1994) and Romine et al. (1994). The Lower Ordovician Nambheet Formation is currently considered to be the oldest formally identified formation in the basin comprising the basal deposit of the first megasequence, although, Haines (2011) suggests there may be an older unit underlying the Nambheet Formation in the Kidson Sub-basin.

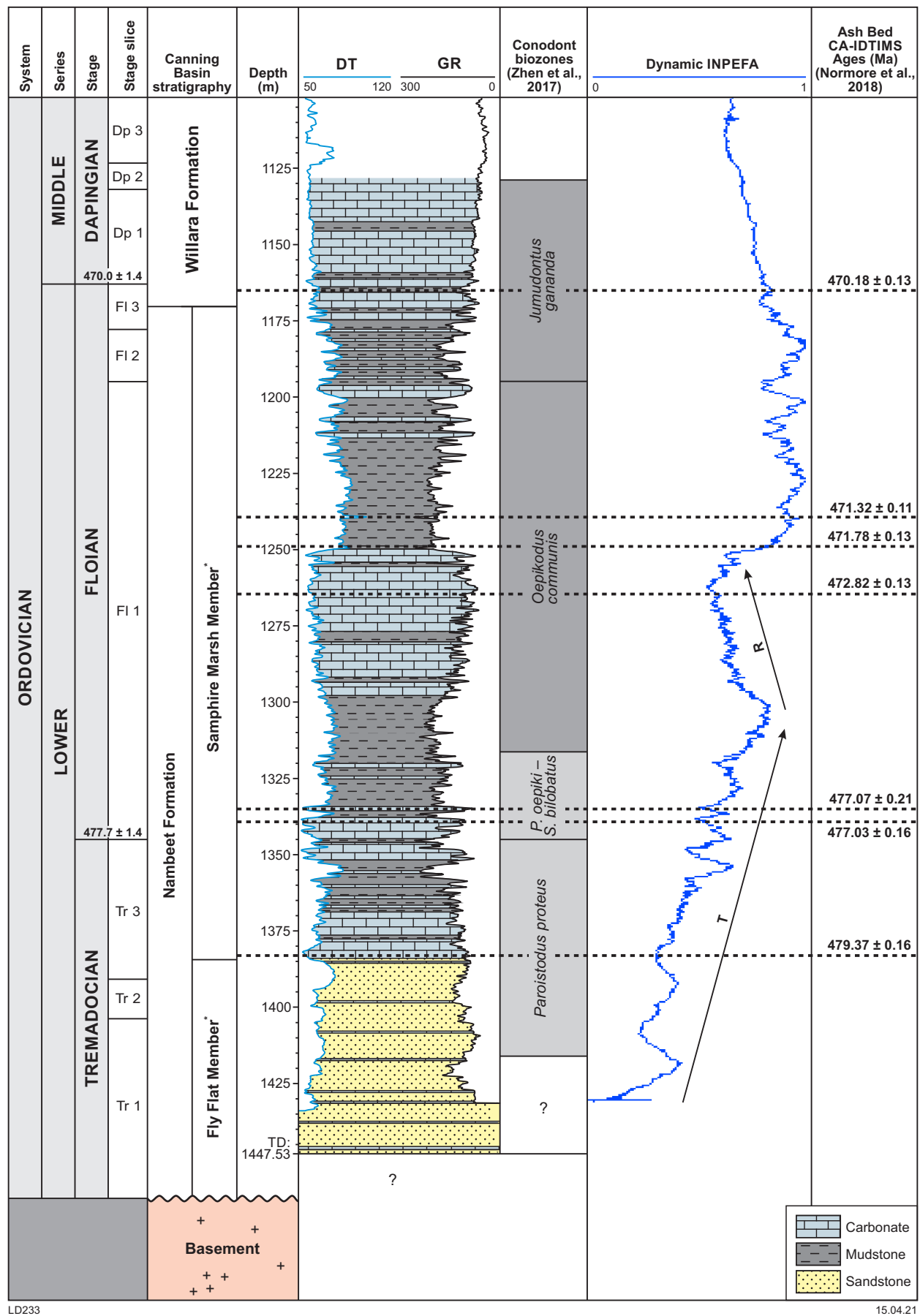
Lower Ordovician stratigraphy

Lower Ordovician strata deposited between the Willara Formation and basement in the Canning Basin has been defined under three lithostratigraphic schemes, largely based on location.

The major points of comparison and basis for correlation of the three schemes are stratigraphic position, lithology and conodont biostratigraphy. The Nambheet Formation is recognized across the northwestern and central basin areas (Fig. 1, blue dots). The equivalent Wilson Cliffs Sandstone is recognized from the subsurface, in the far southeast of the basin, but is recorded in only four wells (Fig. 1, yellow dots). Along the Lennard Shelf, in the northeast Canning Basin, the Nambheet Formation equivalent succession consists of four formations: Gap Creek Formation (lowermost sections only), Emanuel Formation, Kudata Dolomite and Kunian Sandstone, belonging to the Prices Creek Group (Figs 1, 3; Nicoll et al., 1993).

The Nambheet Formation and Wilson Cliffs Sandstone are recorded only in the subsurface, while the Prices Creek Group is observed in both outcrop and subsurface sections. The Carranya Formation, also observed in outcrop, was originally believed to be laterally equivalent to the Wilson Cliffs Sandstone, Nambheet Formation and Kunian Sandstone (Kennard et al., 1994; Haines and Wingate, 2007), but recent work by Normore (2017) has indicated that it is more likely a proximal, lateral equivalent to the middle Ordovician Goldwyer Formation (Fig. 3). Type section information for the Wilson Cliffs Member, Gap Creek Formation, Emanuel Formation, Kudata Dolomite and Kunian Sandstone is provided in Table 1.

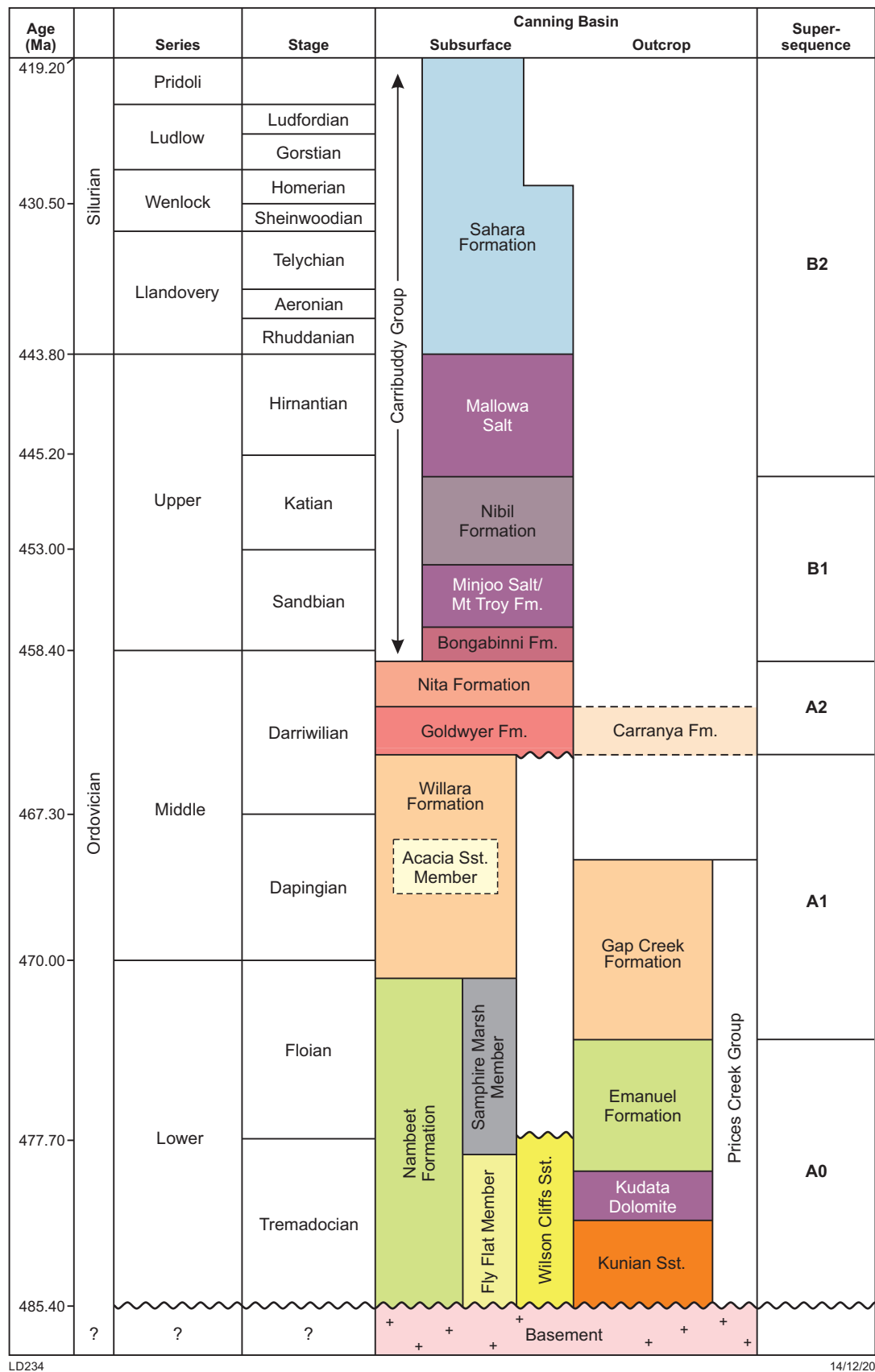
Original correlation of the Lower Ordovician sedimentary rocks was based on their stratigraphic position; underlying the Willara Formation and overlying basement (Fig. 3), and later confirmed with conodont biostratigraphy (Nicoll, 1993). Basin-scale lithological variation is addressed by the definition of equivalent formations, with Wilson Cliffs Sandstone named because of a sandstone-dominated composition. The Nambheet Formation type section records two distinct lithological units, a lower sandstone unit and an overlying carbonate–mudstone unit, although the presence of two units is not consistent across all drilled intervals of the formation.



LD233

15.04.21

Figure 2. Stratigraphic chart showing age of formations in the Olympic 1 core. Figure adapted from Normore et al. (2018) showing conodont biozones interpreted from core samples (Zhen et al., 2017) and CA-IDTIMS U–Pb zircon dates from ash beds (Normore et al., 2018) that constrain the ages of the Nambeet and Willara Formations in this well. Transgressive (T) and regressive (R) D-INPEFA trends are indicated. Unit names marked with an asterisk are proposed new members based on the evidence outlined in this Report



LD234

14/12/20

Figure 3. Ordovician stratigraphy in the Canning Basin modified from Haines (2004) to include proposed new members and updated stratigraphic relationships. Supersequences adapted from Kennard et al. (1994). Age (Ma) according to the 2020 chronostratigraphic chart by Cohen et al. (2020)

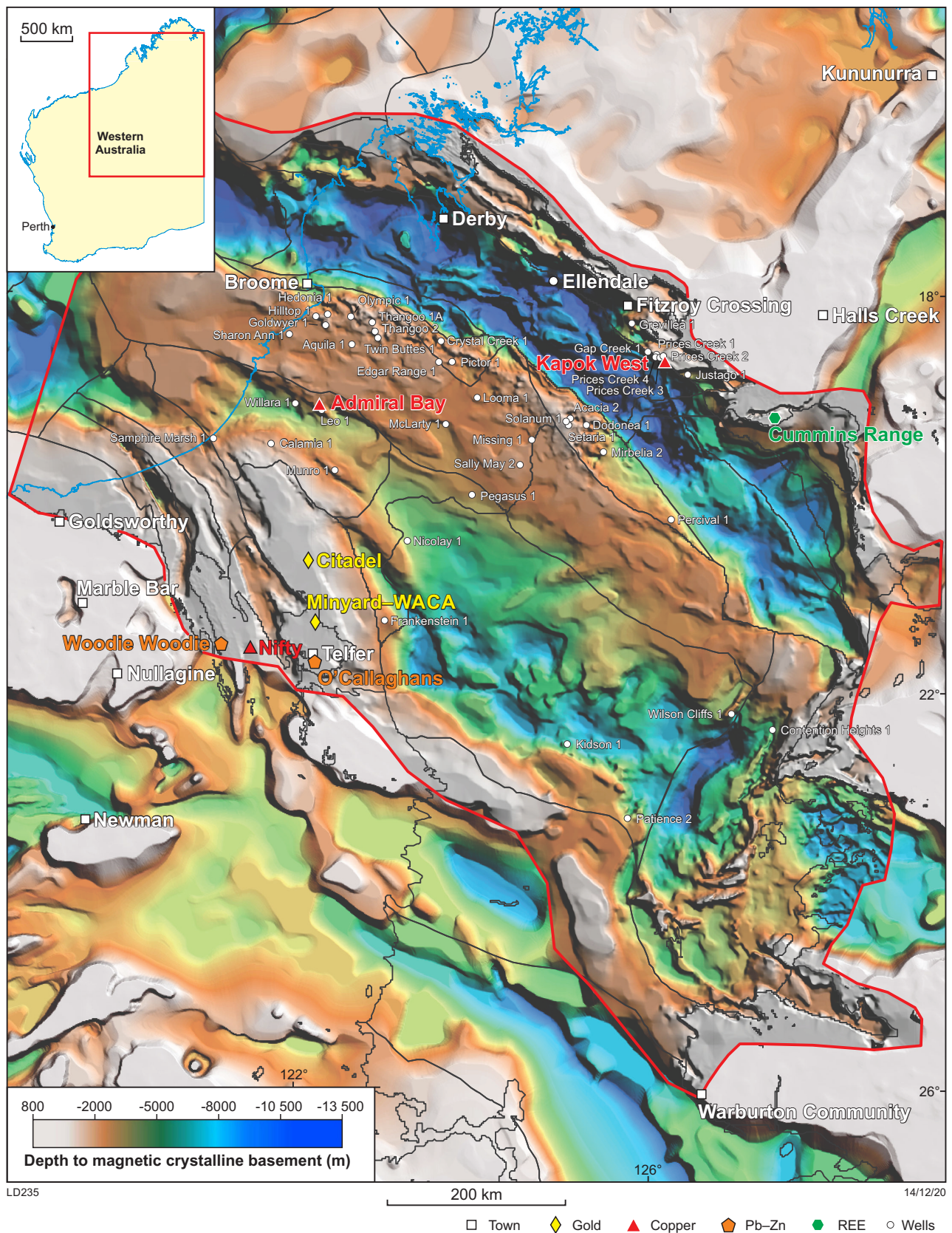


Figure 4. SEEBASE map of the Canning Basin (Frogtech Geoscience, 2017) showing depth to basement and location of petroleum wells and stratigraphic drillholes that intersect the Nambett Formation and equivalent units

Some wells record only a limestone–shale sequence overlying basement (e.g. Edgar Range 1, Jacque et al., 1968a), others record only a sandstone unit between basement and the Willara Formation (e.g. McLarty 1, Jacque et al., 1968b).

Revised Nambeet Formation stratigraphy

Nambeet Formation – Willara Formation boundary

There is no single feature that defines the boundary between the Nambeet and Willara Formations. The Willara Formation is commonly described as carbonate dominated (McTavish and Legg, 1976), and the base of the formation is typically identified by the upward change to limestone dominance in a carbonate–mudstone sequence. This approach is flawed for two reasons. First, the lowest portion of the Willara Formation is not always carbonate. The Acacia Sandstone Member, generally identified in the middle of the Willara Formation in southeastern areas of the Canning Basin, is interpreted to directly overlie the Nambeet Formation in some locations (e.g. Calamia 1, Crystal Creek 1, Hedonia 1; Fig. 1) with apparent conformity.

Second, the relative abundance of carbonate to mudstone throughout the underlying Nambeet Formation is variable and the dominant lithology may switch many times within the formation. Due to this, a distinct lithological change from mudstone to carbonate cannot be relied upon to identify a change of formation. In Olympic 1, limestone becomes the dominant lithology in three places across the Nambeet Formation to Willara Formation sequence (Fig. 2). The first is directly above the Fly Flat Member, the second is between two mudstone-dominated nodular carbonate units, and the third is at the top of the cored section where the interbedded carbonate–mudstone sequence gradually increases in carbonate content moving up-section (Fig. 2). It should also be expected, given the spatial extent of both formations, that the ratio of carbonate to mudstone will vary depending on structural position during deposition (i.e. deposition on platforms or structural highs vs within depocentres).

Sequence stratigraphic position is a more consistent method to identify the boundary between the Nambeet and Willara Formations than lithology. Basin-scale sequence stratigraphy of the Ordovician originally undertaken by Romine et al. (1994) and Kennard et al. (1994) remains the reference work for the Lower Ordovician sequence in the Canning Basin. The second-order sequence or supersequence scheme from these publications is presented in Figure 3. The Willara Formation represents the regressive phase of the second-order A1 supersequence and is overlain by the transgressive phase (Goldwyer Formation) of the following supersequence (A2). Second-order transgressive–regressive patterns can be identified from GR logs using Dynamic Integrated Prediction Error Filter Analysis (D-INPEFA; Fig. 2). D-INPEFA-GR is a derivative parameter calculated from the raw GR data by CycloLog software (Nio et al., 2005, 2006). The D-INPEFA-GR curves illustrate general transgressive–regressive trends within the measured stratal sequence. Transgressive sequences show a positive trend and regressive sequences show a negative trend (Fig. 2).

The regressive phase of the A1 supersequence is identified on the D-INPEFA-GR curve by a turning point preceding a steep negative trend (R), contrary to the underlying transgressive phase (T; Fig. 2). This turning point is present in the majority of wells where the contact between the Nambeet and Willara Formations is observed (Plates 1–4). The D-INPEFA-GR signature varies slightly where the stratal package is thicker than average due to greater accommodation space, for example, Willara 1 and Leo 1 (Plates 1–4). Thicker sections preserve third-order sequences more readily (Romine et al., 1994), and these higher order sequences are reflected in the D-INPEFA-GR curve.

Identification of the negative D-INPEFA-GR trend indicating regression, in combination, with a lithological change from mudstone-dominated lithology in the Nambeet Formation to carbonate-dominated lithofacies, or sandstone in the Willara Formation, is a better way to interpret the position of the formation boundary and reduce misidentification of carbonate-rich packages in the Nambeet Formation. Using this method, original formation picks from well completion reports were revised. The new formation picks are presented in Appendix 1 and will be used in all further figures in this Report.

New members

Two new members are proposed for the Nambeet Formation (Fig. 3), the lower Fly Flat Member (Appendix 2) and the upper Samphire Marsh Member (Appendix 3). These members are defined and described based on the core from Olympic 1 and correlated to intersections of the Nambeet Formation in other wells. Definition of the new members from Olympic 1 mainly rely on four datasets: facies analysis, biostratigraphy, geochronology and HyLogger spectral signature.

Key facies associations are interpreted from the core based on lithology, sedimentary structures and petrographic characteristics (Fig. 5). Three siliciclastic facies associations (SFA) occur within the siliciclastic-dominated Fly Flat Member (Table 3) and seven carbonate facies associations (CFA) make up the carbonate–mudstone-dominated Samphire Marsh Member (Table 4).

Conodont analysis of 18 samples covering the entire cored section from Olympic 1 identified four biozones (Zhen et al., 2017): *Jumudontus gananda*, *Oepikodus communis*, *Prioniodus oepiki* – *Serratognathus bilobatus* and *Paroistodus proteus* (Figs 2, 6). The biozone succession in the Olympic 1 well implies continuous deposition between the Lower–Middle Ordovician (Tremadocian–Dapingian). Sample location, identification and biozonation details are presented in Figure 6 (Zhen et al., 2017). Biozones were age calibrated with CA-IDTIMS ²⁰⁶Pb/²³⁸U zircon dates from bentonite beds also recovered from the Olympic 1 core (Normore et al., 2018). Biozones in Olympic 1 are correlated to conodont biostratigraphy undertaken by Nicoll (1993) in other Canning Basin wells.

Geochronological data for the Olympic 1 section is presented in Figure 2 and Table 5 and a full discussion of results can be found in Normore et al. (2018). Eleven bentonite beds were identified in the core between 1165.44 and 1383.27 m. Four samples were unsuitable for analysis due to absent or

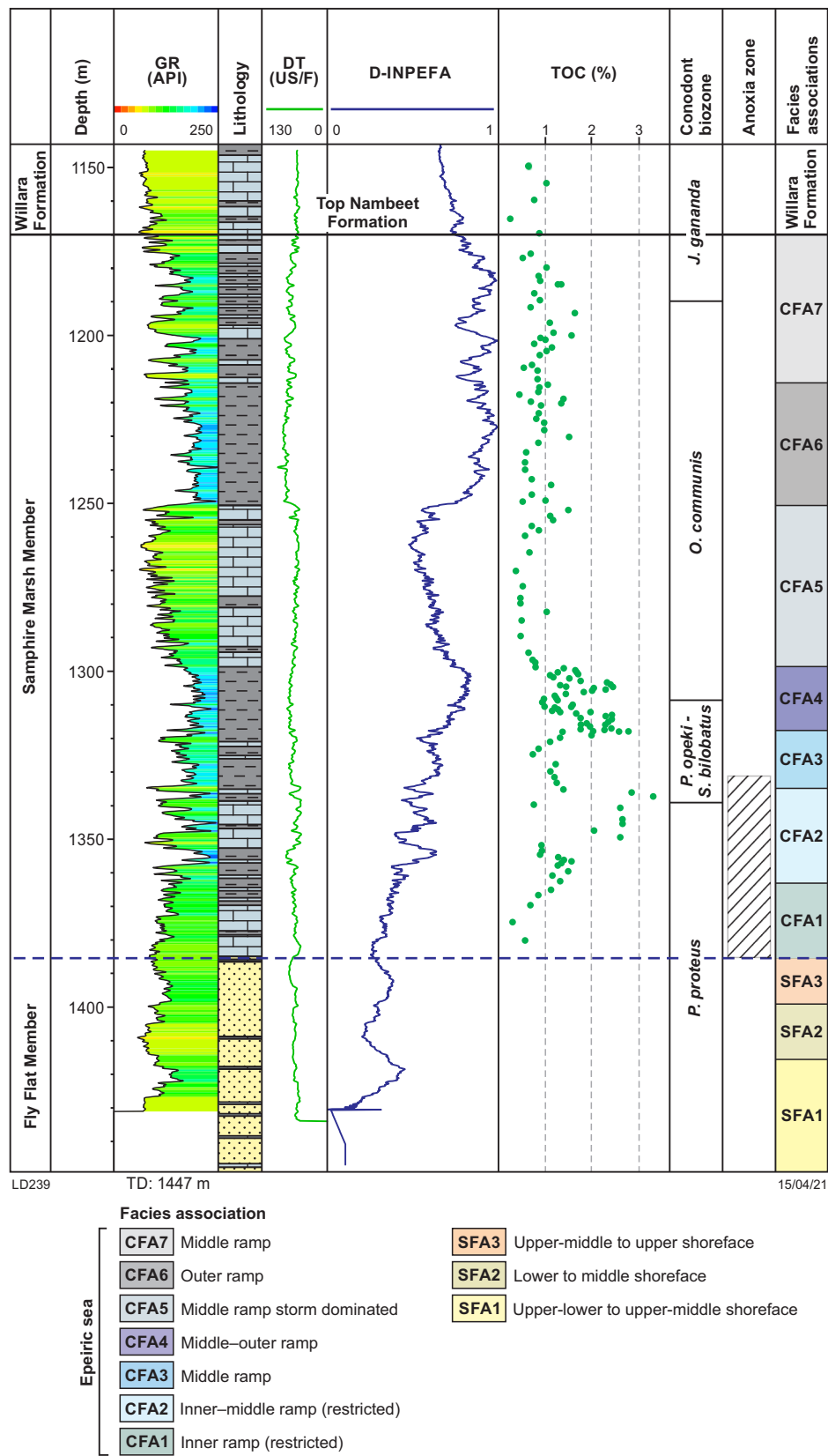


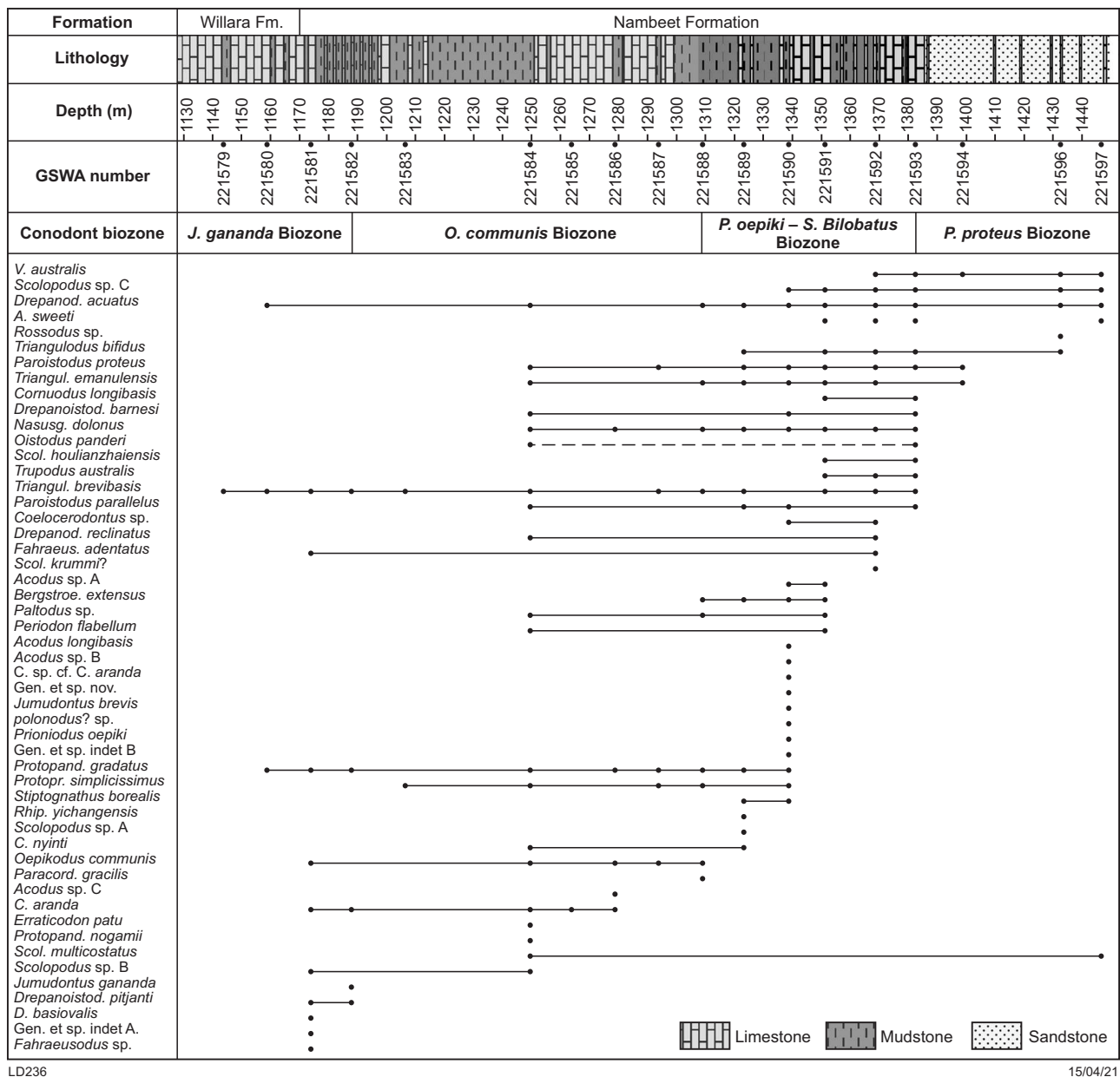
Figure 5. Key facies associations in Olympic 1 core plotted adjacent to well logs, conodont biozones after Zhen et al. (2017), total organic carbon (TOC) data and zones of anoxia interpreted from ICP-MS analysis by Chemostrat Australia (2016)

Table 3. Siliciclastic facies associations (SFA) of the Fly Flat Member in the Nambeet Formation, Olympic 1

Facies association	Depositional setting	Major facies	Minor facies	Depth interval (m)
SF1	Upper-lower to upper-middle shoreface	Calcareous sandstone (<i>Ls</i>), bioturbated sandstone (<i>Hb</i>), sandstone with calcareous grains (<i>Sm</i>)	Sandy carbonate (<i>Cs</i>), planar-laminated sandstone (<i>Sp</i>), cross-stratified sandstone (<i>Sx</i>)	1417.0 – 1447.8
SF2	Lower shoreface	Bioturbated sandstone (<i>Hb</i>), sandstone with calcareous grains (<i>Sm</i>)	Calcareous sandstone (<i>Ls</i>)	1393–1417
SF3	Upper-middle to upper shoreface	Planar-laminated sandstone (<i>Sp</i>), flaser bedded sandstone (<i>Sf</i>)	Cross-stratified sandstone (<i>Sx</i>), bioturbated sandstone (<i>Hb</i>)	1383.57 – 1393.95

Table 4. Carbonate facies associations (CFA) of the Samphire Marsh Member in the Nambeet Formation, Olympic 1

Facies association	Depositional setting	Major facies	Depth interval (m)
CFA 1	Restricted proximal inner epeiric ramp	Bioclastic wackestone–packstone (<i>Lc</i>), nodular mudstone (<i>Ln</i>)	1362.0 – 1383.57
CFA2	Restricted inner epeiric ramp	Bioclastic packstone–grainstone (<i>Hn</i>), nodular mudstone (<i>Ln</i>)	1334–1362
CFA 3	Epeiric middle ramp	Nodular mudstone (<i>Ln</i>)	1319–1334
CFA 4	Epeiric middle to outer ramp	Laminated mudstone with nodules (<i>Mc</i>)	1296–1319
CFA 5	Epeiric middle ramp storm dominated	Interbedded mudstone and wackestone–packstone (<i>La</i>), bioclastic packstone–wackestone (<i>Lc</i>), nodular mudstone (<i>Ln</i>) and laminated fossiliferous mudstone (<i>MI</i>)	1250–1296
CFA 6	Epeiric outer ramp	Laminated mudstone (<i>Mo</i>) and laminated fossiliferous mudstone (<i>MI</i>)	1213–1250
CFA 7	Epeiric middle ramp	Heterolithic mudstone–limestone (<i>Hp</i>) and laminated fossiliferous mudstone (<i>MI</i>)	1180–1213



LD236

15/04/21

Figure 6. Conodont sample depths, species ranges and biozones recorded from the core in Olympic 1 (after Zhen et al., 2017)

Table 5. Geochronology samples and data collected from the Olympic 1 cored section in the Samphire Marsh Member and Willara Formation and analysed by CA-IDTIMS. Dates published in Normore et al. (2018)

Depth (m)	GSWA sample number	Calculated age (Ma)	Mean square weighted deviation
1165.44	221598	470.18 ± 0.13	1.9
1239.27	221599	471.32 ± 0.11	1.0
1249.31	221600	471.78 ± 0.13	1.7
1264.61	221474	472.82 ± 0.13	0.6
1279.96	221475	Unproductive sample (non-uniform zircons)	-
1317.05	221476	Unproductive sample (non-uniform zircons)	-
1335.03	221477	477.07 ± 0.21	3.8
1339.56	221478	477.03 ± 0.16	1.4
1369.38	221479	Unproductive sample (non-uniform zircons)	-
1376.44	221496	Unproductive sample (no zircons)	-
1383.27	221480	479.37 ± 0.16	0.6

poor-quality zircons. Seven samples were analysed by CA-IDTIMS at Boise State University, Idaho. The $^{206}\text{Pb}/^{238}\text{U}$ dates obtained from the seven productive samples ranged from 479.37 ± 0.18 Ma to 470.18 ± 0.13 Ma with ages decreasing up-section.

The entire Olympic 1 core was scanned using the Geological Survey of Western Australia (GSWA) HyLogger-3 and results interpreted with The Spectral Geologist software. The HyLogger, housed at the Perth Core Library, is a spectral scanner that uses visible and infrared spectroscopy for mineral detection. Thermal infrared (TIR) and short-wave infrared (SWIR) electromagnetic spectra were measured (Fig. 7). Thermal infrared data provides details on the main mineral components (including quartz, calcite, muscovite, albite and microcline) and their variation throughout the spectrum. Short-wave infrared data of carbonate minerals highlights the variability of carbonate composition throughout the section (Fig. 7).

Fly Flat Member (new name)

Lithostratigraphy

The Fly Flat Member (Appendix 2) is named for the neighbouring Fly Flat and is equivalent to the previously informal 'lower sandstone unit' of the Nambheet Formation, including the basal transgressive deposits (Kennard et al., 1994). This unit will herein be referred to as the Fly Flat Member. The member is defined as the siliciclastic section between 1383.57 and 1447.53 m depth (63.96 m thick) in the Olympic 1 well. The well did not intersect the base of the Fly Flat Member, and therefore did not penetrate the complete unit but TD is interpreted to be around 20 m above the top of the basement based on seismic interpretation.

Typically, the Fly Flat Member of the Nambheet Formation is described as very fine- to fine-grained sandstone, tight (low porosity and permeability) and hard, with both siliceous and carbonate cements present. Siltstone and shale are sometimes interbedded, and glauconite is commonly recorded, as are traces of pyrite. In six wells, this typified fine-grained sandstone unit is further divided into an upper fine-grained section and an underlying basal sandstone–conglomerate unit of variable character. This basal sandstone–conglomerate is recorded predominantly in the northwest of the Canning Basin (Fig. 1) overlying basement in six wells (Hedonia 1, Hilltop 1, Goldwyer 1, Leo 1, Calamia 1 and Samphire Marsh 1), where descriptions include: conglomerate, medium- to coarse-grained poorly consolidated sandstone and granitic 'basement wash'. These basal deposits are attributed to the transgressive coarse-clastic deposits described by Kennard et al. (1994) that accompanied initial basin subsidence and are inferred to be equivalent to the Kunian Sandstone in the north of the basin (Nicoll et al., 1993). In other wells, this basal unit is absent, and the fine-grained lower sandstone unit directly overlies basement (e.g. Thangoo 1A, Thangoo 2, Pictor 1). The variable occurrence of the basal sandstone–conglomerate unit may be accounted for by original basin conditions which are described by Kennard et al. (1994) as deposition in half-grabens over an irregular land surface.

The basal sandstone–conglomerate unit was not identified in Olympic 1. In Olympic 1, the Fly Flat Member comprises

well-sorted, very fine-grained subarkose sandstones and minor siltstone. Sandstone composition is dominated by quartz and feldspar, with calcareous allochems comprising between 5–50% of grains. Calcareous allochems are predominantly fossil fragments and the incertae sedis cyanobacteria, *Nuia*. Minor to common detrital clay matrix is observed and may be locally enriched in organic material. Glauconite is present in trace amounts. Bioturbation is common ranging from minor to locally extensive, and bored hardgrounds with glauconite veneers are observed in the lower parts of the member. The Fly Flat Member is interpreted as being deposited in an open shallow-marine environment. Three facies associations are identified (Fig. 5; Table 3) and record deposition in upper to lower shoreface settings. Eight key facies are presented in Table 6. Bioturbation is described according to the categories of Taylor and Goldring (1993; Table 7).

SFA1 — upper-lower to upper-middle shoreface (depth 1417.0 – 1447.8 m)

Description

The basal association (SFA1) is dominated by very fine-grained, well-sorted subarkose sandstones with variable amounts of fossil fragments and *Nuia* grains. These are deposited in a series of cycles that progress from weakly bioturbated (BI 2–3) structureless sandstones (*Sm*) at the base of each cycle, to highly bioturbated (BI 5–6) silty sandstones (*Hb*), capped by well-cemented calcareous sandstone with grainstone clasts (*Ls*) at the top of the cycle (Fig. 8a–c; Appendix 4). Cycles vary in thickness from 10 cm to 3.85 m but most are <1 m thick. Cycles commonly contain only two of the three possible facies. Sharp planar or bored hardground surfaces commonly form at cycle tops (Fig. 8a). Lesser, thin, planar-laminated (*Sp*) and cross-stratified (*Sx*) sandstones are also interbedded.

Interpretation

The observed cyclicity in SFA1 indicates frequent changes from high- to low-energy conditions, including episodes of slow sedimentation and non-deposition. They progress upwards with depth from lower to upper-middle shoreface settings and are interpreted as high-frequency transgressive–regressive cycles or parasequences. *Nuia* are generally interpreted as cyanobacterial in origin (Flügel, 2010; Vachard and Téllez-Grión, 1986), associated with shallow environments, either intertidal to supratidal (Flügel, 2010) or shallow high-energy shoals (Donovan, 1992). In this facies association, *Nuia* grains are interpreted to be allochthonous based on micritic rims which indicate reworking (Fig. 8d).

The lack of structure and character of bioturbation at the base of each cycle suggests shifting sandy substrates or storm deposition and therefore high-energy deposition associated with transgression. This is overlain by low-energy, slow deposition of silt-rich, highly bioturbated sandstones (Buatois et al., 2002). These more finely grained, bioturbated intervals represent the most distal deposits in each cycle. Abundant grainstone clasts (Fig. 8e) and *Nuia* are found at the top of each cycle implying a return to shallower high-energy conditions more proximal to intertidal or shallow-marine shoal areas. The *Hb*–*Ls* facies contact is gradational indicating transitional rather than abrupt shallowing. Development of hardgrounds is known to occur

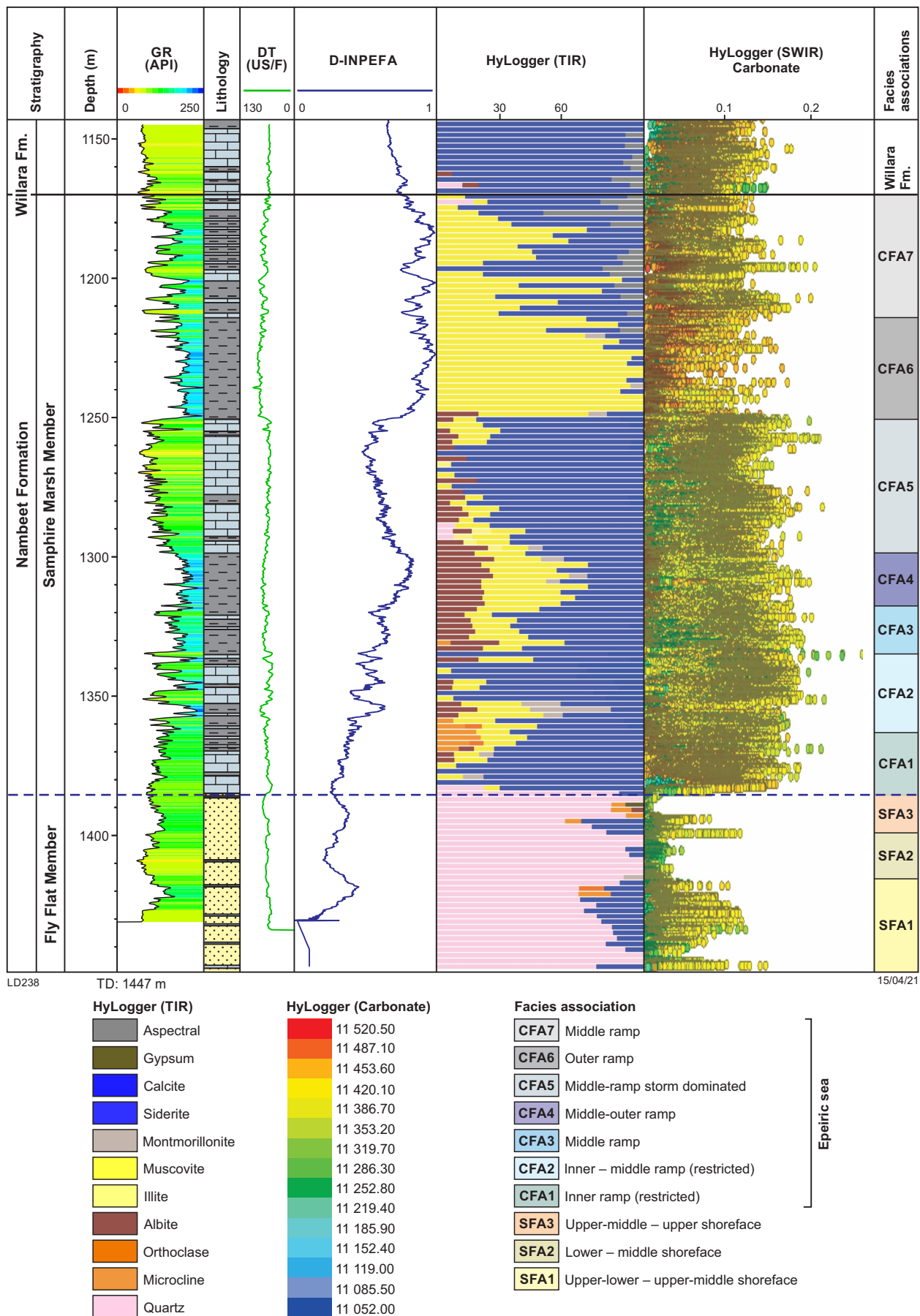


Figure 7. HyLogger data recorded from the Olympic 1 core. Thermal infrared (TIR) and short-wave infrared (SWIR) spectral data of carbonate species are displayed. Carbonates recording a higher wavelength (e.g. 11 520 and represented by warm colours) are interpreted to contain more Fe while those with a lower wavelength (e.g. 11 052 and represented by blue colours) are interpreted to contain higher levels of Mg

Table 6. Facies interpreted in the Fly Flat Member of the Nambeet Formation in the Olympic 1 well. Fossils noted are observed in thin section only

Code	Facies	Lithology	Bedding	Sedimentary structure	Fossils	Bioturbation	Depositional setting	Thin sections (m)
<i>Ls</i>	Calcareous sandstone	Very fine sandstone (subarkose) with carbonate allochems, calcitic shell fragments and <i>Nuia</i> . Minor mudstone. Well sorted	Moderate to thick (6–60 cm). Bed contacts are planar to wavy. Upper contacts are typically abrupt and locally have a thin deep green veneer; lower contacts are sharp to gradational	<i>Nuia</i> grainstone clasts, blue-grey (up to 4 cm wide) are common to abundant. Thin mudstone drapes are weakly deformed around these clasts, becoming stylonodular in places. Locally some grains have dark green ?glauconitic rims. Hardgrounds form commonly at bed tops	Abundant whole and fragmented fossils, well rounded, including echinoderms (crinoids), possible fragments of brachiopods and bivalves	BI 1–2, small, horizontal, cylindrical traces. U-shaped burrows descending from sharp bed contacts. ~0.1 – 0.2 m deep and wide	Moderate- to high-energy events followed by episodes of slow deposition or non-deposition. Normal to restricted open marine conditions	1417.06 1425.18 1427.92
<i>Hb</i>	Bioturbated sandstone	Very fine sandstone (subarkose) and carbonate allochems, <i>Nuia</i> and possible fossil fragments. Minor siltstone. Allochems constitute ~10–30% of grains	Moderate to thick (0.2 – 2.35 m). Bed contacts are planar to irregular. Upper contacts are typically gradational, lower contacts are abrupt to gradational	Faint lamination locally highlighted by alignment of allochem rich layers. Primary fabric is obliterated by intense bioturbation. Siltstone layers are deformed with bioturbation; however, siltstone is commonly more abundant at bed bases. <i>Nuia</i> fragments are highly micritized	Minor fossil fragments and <i>Nuia</i>	BI 5–6, trace fossil assemblage is dominated by horizontal traces but vertical traces are also present, individual forms are difficult to distinguish due to density	Moderate to low-energy, open shallow-marine conditions	1397.08 1040.11 1420.11 1427.11 1430.53 1433.16
<i>Sm</i>	Sandstone with calcareous grains	Very fine sandstone (subarkose) with carbonate allochems, <i>Nuia</i> and fossil fragments	Moderate to thick (0.2 – 2.0 m). Bed contacts are planar. Upper contacts are gradational but sharp locally, lower contacts are sharp	Generally massive in appearance, with some irregular silty, carbonaceous laminae, almost stylonitic in places. Small carbonate clasts are also present – common in places	Minor fossil fragments and <i>Nuia</i>	BI 2–3, low-diversity assemblage dominated by a single type of vertical, cylindrical, silt-lined, sand-filled traces ~1 cm high and 1–2 mm wide. Possible horizontal silt-lined sand-filled cylindrical traces ~1 x 1 cm	Moderate- to high-energy shallow-marine conditions with shifting sandy substrates	1406.92 1427.11
<i>Sc</i>	Convolute sandstone	Very fine sandstone (subarkose) with carbonate allochems, <i>Nuia</i> and fossil fragments	Thin to moderate (7–50 cm). Bed contacts are planar and both upper and lower contacts are sharp	Probable low-angle cross-laminated; original structure altered to chaotic as if slumped. Rare mudstone laminations are present, almost stylonodular in places. Top of beds appear ripple cross-laminated in places	Rare recrystallized clasts present locally, possible fossils	BI 0–1. Escape traces observed locally but rare (<i>Rosselia</i>)	Moderate to high energy with high sediment load and 3D bedform migration in variable but moderate to shallow water depths	1434.73
<i>Sp</i>	Planar-laminated sandstone	Very fine sandstone (subarkose), some siltstone with minor carbonate allochems <i>Nuia</i> and fossil fragments	Thin to thick (1 cm – ~1.5 m). Gradational upper and lower contacts	Thin planar laminations with occasional planar and wavy siltstone laminae	Minor fossil fragments and <i>Nuia</i>	BI 1–2, horizontal, cylindrical traces, unlined and sand filled, approximately 2 x 2 mm in diameter. Associated with siltstone layers, <i>Planolites</i> ?	Shallow water upper flow regime conditions	1393.40 1393.54

Table 6. Facies interpreted in the Fly Flat Member of the Nambeet Formation in the Olympic 1 well. Fossils noted are observed in thin section only

Code	Facies	Lithology	Bedding	Sedimentary structure	Fossils	Bioturbation	Depositional setting	Thin sections (m)
Sf	Flaser-bedded sandstone	Very fine sandstone (subarkose), some siltstone and minor carbonate allochems, <i>Nuia</i> and fossil fragments	Thin to thick (5 cm – >3 m). Gradational upper and lower contacts	Flaser-bedded sandstone and siltstone. Siltstone flays become weakly stylolitic in places. Indistinct mottling with paler sandstone, possibly bioturbation		BI 1–2, horizontal, cylindrical traces, unlined and sand filled, approximately 2 x 2 mm in diameter. Associated with siltstone layers, <i>Planolites</i> ?	Shallow-marine, lower flow regime shallow water settings indicated by flaser bedding style	
Sx	Cross-stratified sandstone	Very fine sandstone (subarkose), some siltstone and minor carbonate allochems, <i>Nuia</i> and fossil fragments	Thin (~5 cm). Gradational upper and lower contacts	Low-angle planar cross-stratification and trough cross-stratification. Commonly only one or two sets thick	Minor fossil fragments and <i>Nuia</i>	BI 0	Shallow-marine water, lower flow regime settings	1386.08 1393.72
Cs	Sandy carbonate	Fine carbonate sandstone	Thick (up to 1.2 m). Sharp and gradational lower contacts and sharp upper contact	Planar and low-angle cross-laminated beds grading into flaser bedding in places. Sandstone also appears massive in places. Lamination is locally defined by carbonaceous material with microcrenulated character	Macrofossils are absent	BI 0	Alternation between upper and lower flow regime conditions	

Table 7. Bioturbation index (BI) categories (Taylor and Goldring 1993). Percent bioturbated values are to be used as a guide

Grade	Percent bioturbated	Classification
0	0	No bioturbation
1	1–4	Sparse bioturbation, bedding distinct, few discrete traces and/or escape structures
2	5–30	Low bioturbation, bedding distinct, low trace density, escape structures often common
3	31–60	Moderate bioturbation, bedding boundaries sharp, traces discrete, overlap rare
4	61–90	High bioturbation, bedding boundaries indistinct, high trace density with overlap common
5	91–99	Intense bioturbation, bedding completely disturbed (just visible), limited reworking, later burrows discrete
6	100	Complete bioturbation, sediment reworking due to repeated overprint

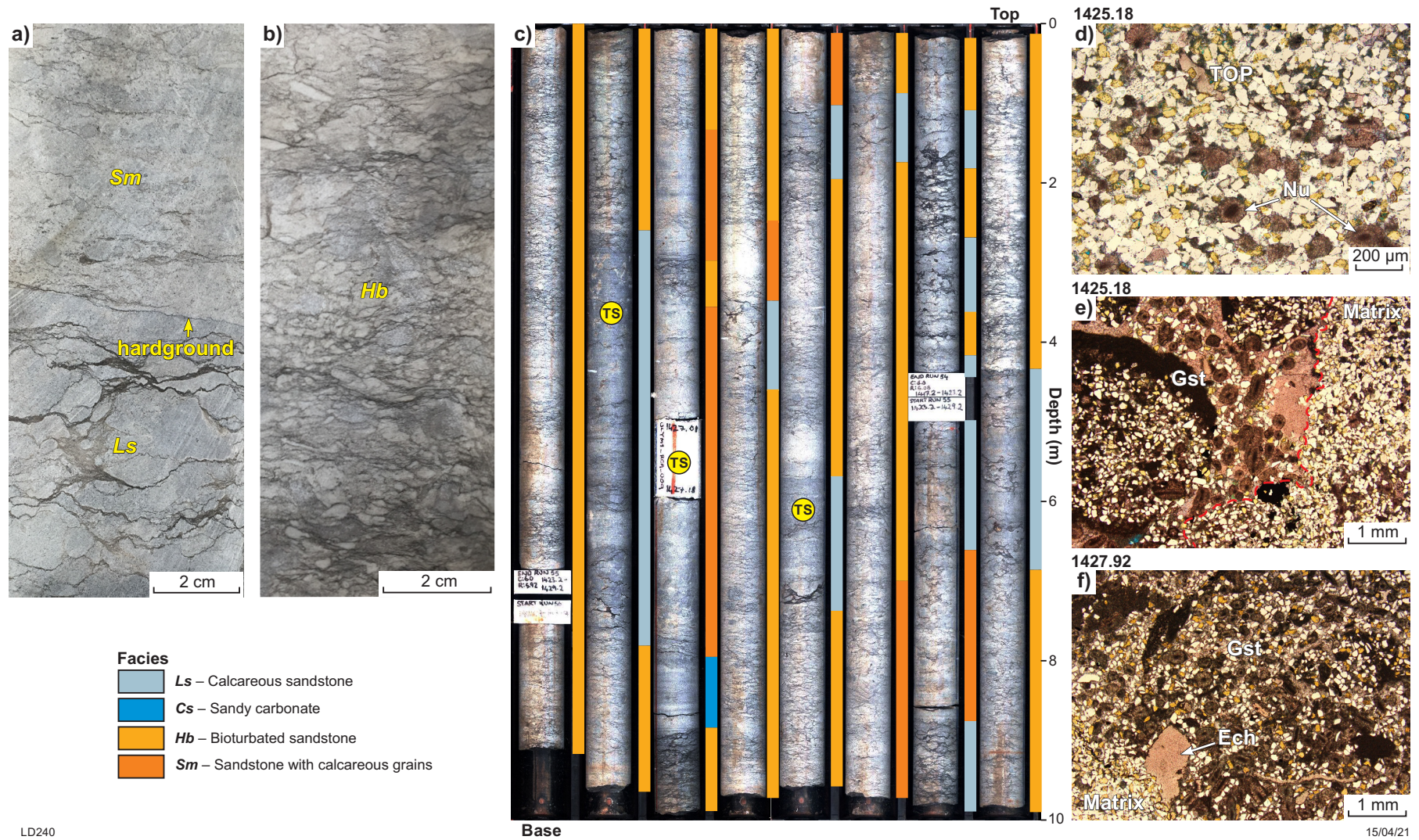


Figure 8. Major facies and parasequence cyclicity of SFA1: a) core photo of Ls facies with planar hardground overlain by Sm facies at ~1446.15 m; b) Hb facies at ~1416.59 m; c) approximately 8 m of cored section showing cyclicity of major facies and position of thin sections (TS) in d, e and f; d) thin section through Ls facies at 1425.18 m showing *Nuia* (Nu) grains with micritic rims; e) thin section through Ls facies at 1425.18 m showing *Nuia* grainstone clast (Gst), outlined in pink, in sandstone matrix; f) Ls facies at 1427.92 m showing *Nuia* grainstone clast (Gst) with possible echinoderm fragment (Ech)

in very shallow wave-agitated conditions and is common at maximum regressive surfaces (Christ et al., 2015). The hardgrounds observed in this sequence are interpreted to represent the final phases of regression.

SFA2 — lower shoreface (depth 1395–1410 m)

Description

This facies association is dominated by thickly bedded, highly bioturbated silty sandstones (*Hb*) with some weakly bioturbated structureless sandstones (*Sm*). Highly bioturbated beds are an amalgamation of thinner, normally graded cycles within which bioturbation increases towards the cycle tops. Thin calcareous sandstone beds with grainstone clasts (*Ls*) are rare. Sandstones in this facies association are carbonate poor and carbonate allochems comprise less than 5% of framework grains. Fossil fragments, including echinoderms and possible brachiopods and bivalves, dominate this allochem assemblage. *Nuia* are sometimes present in trace quantities.

Interpretation

The dominance of lower energy facies, increased abundance of siltstone, reduction of carbonate facies and *Nuia* allochems, and the absence of hardgrounds suggests that SFA2 was deposited under deeper conditions and more distal to carbonate-producing shallow areas than SFA1. Based on this, and the highly bioturbated, silt-rich sandstone facies, lower shoreface settings are interpreted (e.g. Gowland, 1996; Buatois et al., 1999; Olsen et al., 2017). Small-scale depositional cycles are recorded by the gradational packages within bioturbated facies indicating prevailing lower shoreface conditions with slow sedimentation.

SFA3 — upper-middle to upper shoreface (depth 1383.57 – 1393.95 m)

Description

This facies association is dominated by interbedded planar-laminated sandstone (*Sp*) and wavy-to-flaser bedded (*Sf*) very fine-grained sandstone facies and minor cross-stratified sandstone. Bioturbated silty sandstone (*Hb*) is also present in minor amounts, localized to the base of the association where such beds are thinly interbedded with planar and cross bedded (*Sx*) facies. Sandstone in this facies association is dominantly composed of quartz and K-feldspar with minor carbonate allochems, the assemblage of which are mainly fossil fragments with a very minor *Nuia* component. Bioturbation within the planar and wavy-to-flaser facies is limited to small, monospecific assemblages of *Planolites* found in siltstone flays and laminae.

Interpretation

This association is transitional on SFA2 and demonstrates an upward shallowing of the marine system. The interpreted facies frequently switch between upper and lower flow regimes. Overall, the lower portions of siltstone, variable energy and transition to impoverished, opportunistic, trace fossil assemblages suggest upper shoreface conditions (Gowland, 1996; Howell et al., 2008).

Diagenesis

The diagenetic sequence is presented in Figure 9. The order of events is deduced from the crosscutting relationships of cements observed in thin section, under cathodoluminescence and from scanning electron microscope (SEM) analysis. The earliest phase of diagenesis occurred during deposition with the micritization of carbonate allochems (Fig. 10a), followed by an early phase of calcite cementation. Authigenic clays developed early, (Fig. 10b) followed by quartz and feldspar overgrowth cements (Fig. 10c). These events were followed by a phase of dissolution, most notably of K-feldspar grains that are frequently partially dissolved (Fig. 10b,d). A second phase of calcite/Fe-calcite formation occurred after dissolution, partially infilling the secondary porosity generated from feldspar dissolution (Fig. 10d). Dissolution of carbonate allochems occurred late (Fig. 10e) followed by emplacement of bitumen.

X-ray diffraction (XRD) analysis of whole-rock mineralogy measures the variation in sandstone composition with a range of quartz volume from 50.9 to 79.7% and a range of K-feldspar volume from 6.4 to 23.8%. The maximum amount of quartz corresponds to a sample with extremely well-developed quartz overgrowths. Calcite makes up between 10.2 and 31.4% of the whole-rock mineralogy in sandstones, although its presence is strongly controlled by the quantity of allochems in any given sample.

There are two main dissolution events in these sandstones. Dissolution of K-feldspar is common and observed throughout the Fly Flat Member, and sparry calcite cement occasionally forms in the dissolved centre of these grains (Fig. 10b,d). Dissolution of carbonate allochems (Fig. 10e) occurs later and interestingly, is a feature isolated to SFA3 facies occurring between 1386 m and 1404.11 m. Below SFA3, allochems within the sandstones remain intact.

Cathodoluminescence suggests that calcite and Fe-calcite cements in the siliciclastic section formed very early in their deposition. These cements have a bright luminescence similar to that shown by the calcitic matrix and allochems present (Fig. 10f,g). This indicates that they may have formed at the same time as the calcitic matrix and when allochems stabilized, potentially syndeposition or during very early burial. This is consistent with the development of the hardground features observed in the core.

The range in measured core porosity in the Fly Flat Member in Olympic 1 varies from 2.0 to 15.9%, with an average of 9.2%, and is strongly facies controlled with the highest values recorded in SFA3. Quartz overgrowths play the largest role in reducing intergranular porosity (Fig. 10c). Porosity reduction by K-feldspar overgrowths is also significant locally, and porosity reduction by carbonate cement is minor. Microporosity is commonly observed associated with authigenic clays and micrite (Fig. 10h). Significant secondary porosity is generated by the dissolution of K-feldspars (Fig. 10b,d) and by the dissolution of carbonate allochems (Fig. 10e) at the top of the sandstone sequence in SFA3.

HyLogger spectral data

Thermal infrared electromagnetic spectral data distinguishes the Fly Flat Member from the overlying Samphire Marsh Member primarily by the dominance of quartz (Fig. 7).

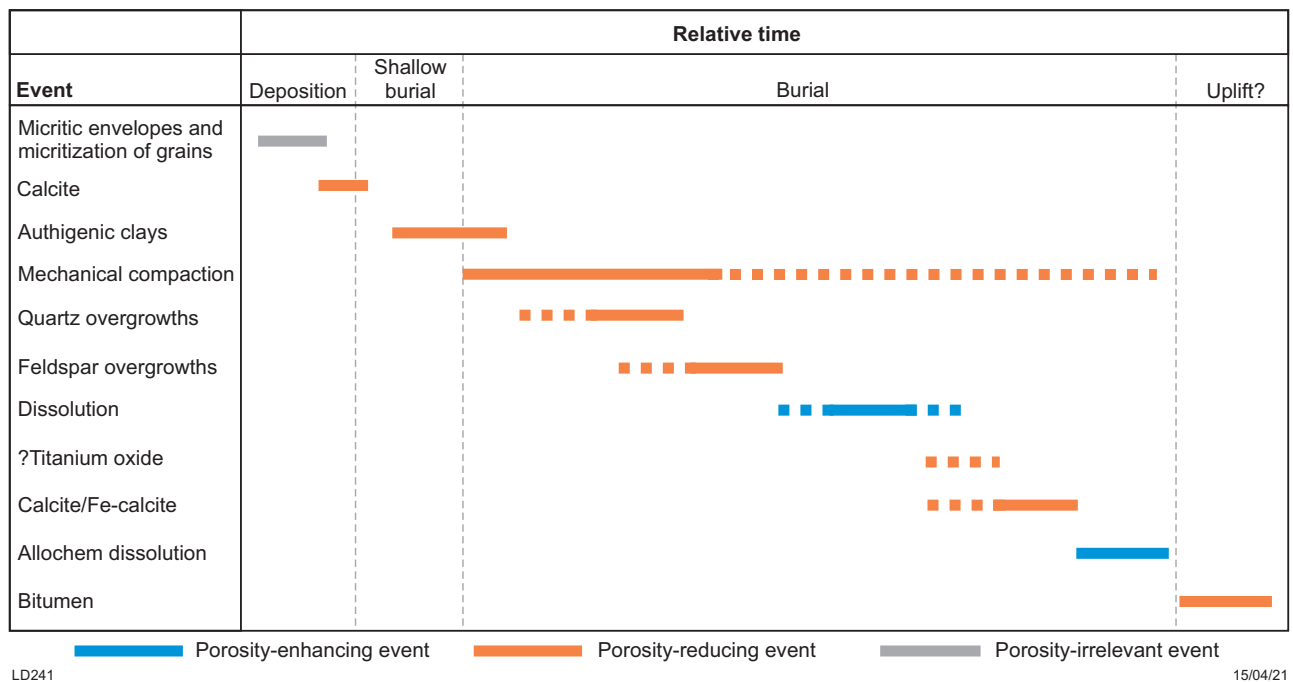


Figure 9. Diagenetic sequence of siliciclastic facies in Olympic 1

A minor carbonate component is also recorded, consistent with the presence of carbonate allochems, *Nuia* and fossil fragments, and minor carbonate cement. Short-wave infrared spectra of carbonate show a distinct decrease in carbonate content between 1385 and 1394 m. This corresponds to SFA3, which contains few carbonate grains and little carbonate cement. The interval between 1418 and 1439 m shows up to 25% carbonate within the sandstone package. This interval is generally equivalent to SFA1, where abundant primary carbonate grains and common calcite cement are observed. The carbonate spectra, particularly in the lower part of the sandstone, indicate that two carbonate species are present. This is consistent with the occurrence of primary carbonate, allochems and secondary diagenetic carbonate in the form of calcite cements.

Biostratigraphy

The conodont biozones *Drepanastodus* – *Paltodus* and *P. elegans* – *Berg. extensus* used by Nicoll (1993) are no longer recognized, and the current scheme is presented in Figure 2. Later work has identified that the *P. elegans* – *Berg. extensus* biozone correlates to the current *P. proteus* and *P. oepiki* – *S. bilobatus* biozones (Zhen and Nicoll, 2009; Zhen et al., 2017).

Paraistodus proteus is the only biozone recorded in the Fly Flat Member in Olympic 1 and spans the contact between the Fly Flat Member and the overlying Samphire Marsh Member (Fig. 2). Where sampled in other wells, the *P. elegans* – *Berg. extensus* biozone is recorded in the Fly Flat Member (e.g. Frankenstein 1, Pegasus 1, Percival 1, Pictor 1, Thangoo 1A) (Nicoll, 1993). In the Goldwyer 1 well, the *P. elegans* – *Berg. extensus* biozone is recorded in the basal conglomerate unit (1387.75 – 1420.36 m), which rests on basement.

In all but one well, *P. elegans* – *Berg. extensus* is the only biozone recorded within the Fly Flat Member, and in three wells (Frankenstein 1, Pictor 1 and Thangoo 1A) this biozone occurs across the Fly Flat Member – Samphire Marsh Member boundary. The single exception occurs in the Samphire Marsh 1 well, where two conodont biozones are recorded, the *Drepanastodus*–*Paltodus* biozone across the Fly Flat Member and base of the Samphire Marsh Member, and the *P. elegans* – *Berg. extensus* biozone in the Samphire Marsh Member only. In this well, the *P. elegans* – *Berg. extensus* biozone is the youngest recorded in the Nambeet Formation although, it is overlain by an unconformity.

Geochronology

No bentonite beds were recorded from the Fly Flat Member in the Olympic 1 well.

Samphire Marsh Member (new name)

Lithostratigraphy

The Samphire Marsh Member (Appendix 3) is named for the Samphire Marsh 1 well where the original type section of the Nambeet Formation is designated. This new member is nominated for the carbonate–mudstone unit between 1170.00 and 1383.57 m in the Olympic 1 well that overlies the lower sandstone, now Fly Flat Member.

In Olympic 1, the Samphire Marsh Member consists of interbedded and nodular carbonate–mudstone sequences. Such sequences are commonly referred to as limestone–marl alternations or limestone–marl rhythmites (Munnecke

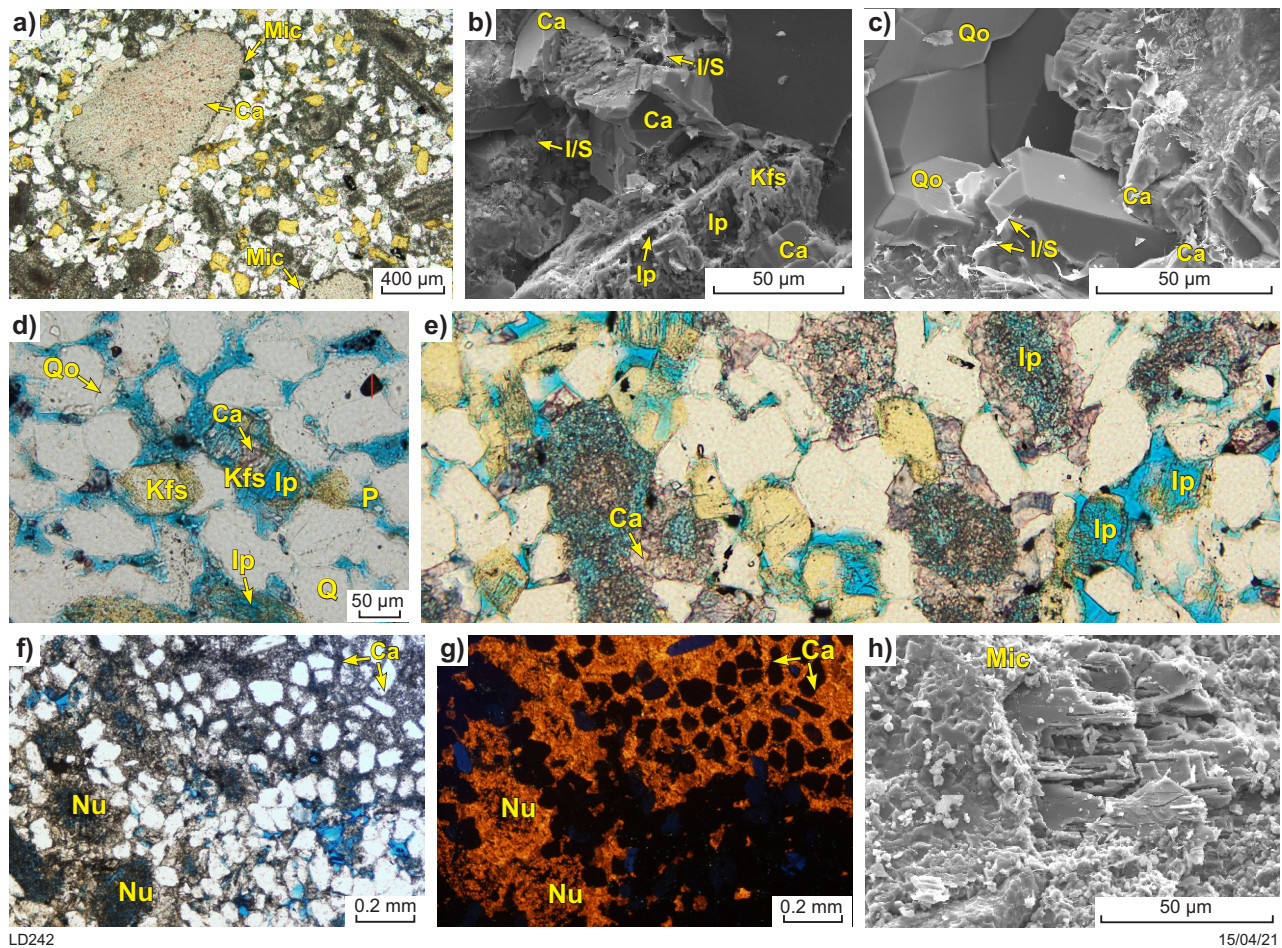


Figure 10. Thin section photomicrographs and SEM images showing cements and porosity in the Fly Flat Member in Olympic 1. All photomicrographs were taken in plane-polarized light (ppl) except g), and the epoxy is stained blue to indicate voids. Labelled features include K-feldspar (Kfs), quartz overgrowths (Qo), calcite cement (Ca), micrite (Mic), illite/smectite (I/S), *Nuia* (Nu), intragranular porosity (Ip) and intergranular porosity (P): a) photomicrograph of sandstone at 1427.90 m showing micritic rims formed around carbonate allochems; b) SEM image of sandstone at 1406.92 m showing partial dissolution of K-feldspar producing intragranular porosity; c) SEM image of sandstone at 1443.16 m with well-developed quartz overgrowths; d) photomicrograph of sandstone at 1406.92 m showing partial dissolution of K-feldspar and occlusion of secondary porosity with calcite cement; e) photomicrograph of sandstone at 1393.54 m showing dissolution of carbonate allochems, possibly *Nuia*, creating secondary porosity; f) photomicrograph of sandstone at 1393.54 m showing *Nuia* grains and calcite-cemented matrix; g) thin section from f) under luminescence showing similar relatively bright fluorescence of both *Nuia* and calcite-cemented matrix; h) SEM image of sandstone at 1427.92 m showing extensive micritic cement

and Samtleben, 1996; Munnecke and Westphal, 2005; Elrick and Hinnov, 2007; Westphal et al., 2008; Amberg et al., 2016). Limestone bed textures range from grainstone to lime mudstone and nodule textures vary from wackestone to lime mudstone. Transitions between interbedded and nodular sections and coarser to finer carbonate fabrics are gradational throughout the sequence. Mudstones in both interbedded and nodular sections are calcareous.

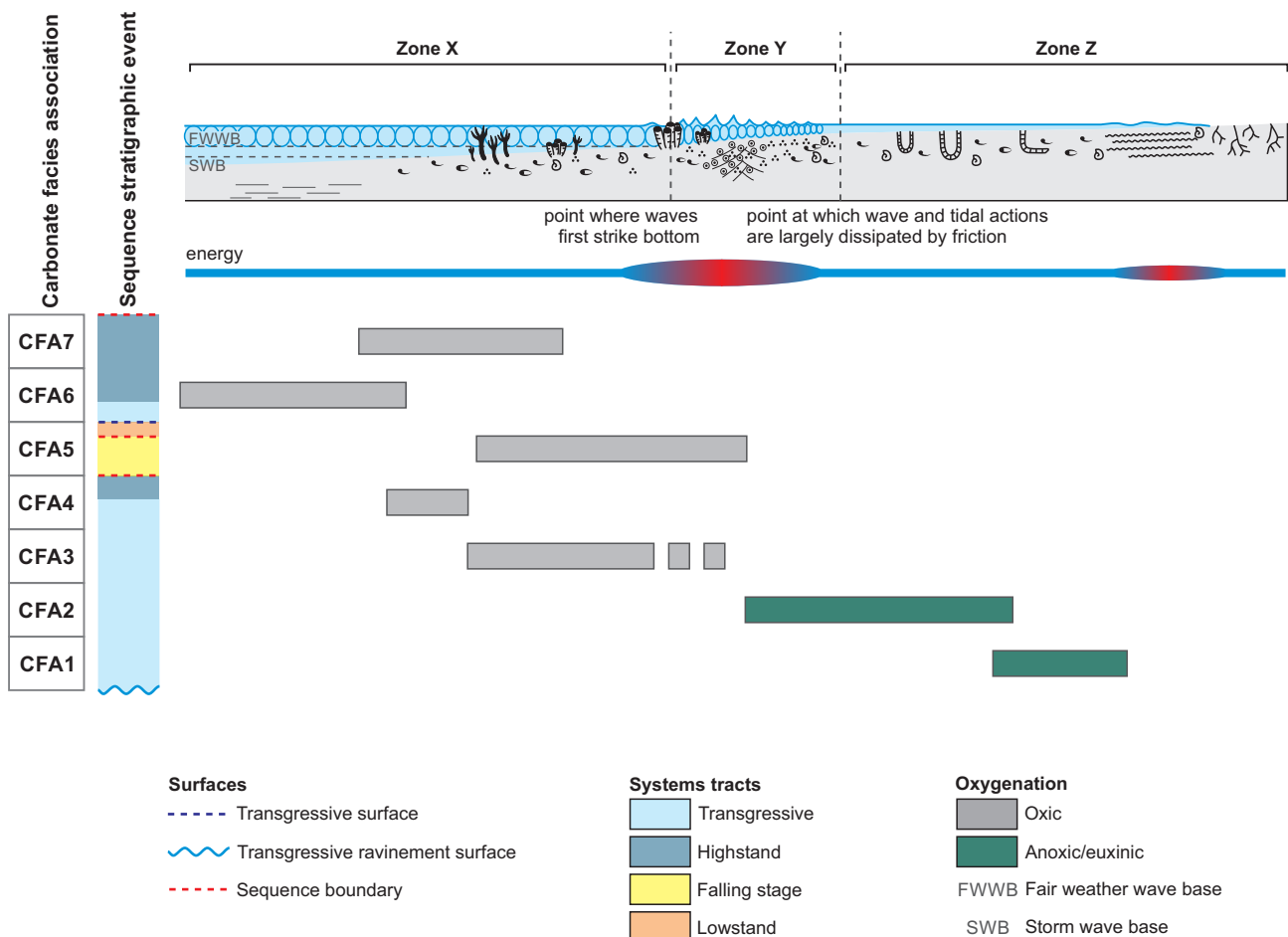
The carbonate–mudstone sequence (Sapphire Marsh Member) in Olympic 1 can be described as being deposited on an epeiric platform or very low-angle epeiric ramp environment developed as the result of a major transgression in the late Tremadocian. It is likely that this transgression resulted in large-scale shoreline back-stepping and the abrupt shutoff of siliciclastic input. The transition from open-marine settings that deposited the underlying siliciclastic system to a widespread epeiric sea is interpreted at a prominent erosive surface where there is an abrupt switch from siliciclastic to low-energy shallow carbonate deposits. Within the carbonate–mudstone succession, a progression from proximal to distal environments along the platform/ramp are represented by the seven facies associations described below (Figs 5, 11; Table 4). Facies associations and depositional setting are interpreted based on limestone fabrics, bioclasts, key features including glauconite and hardgrounds, total organic carbon (TOC) values, and interpreted oxidation conditions based on inductively coupled plasma mass spectroscopy (ICP-MS) of both carbonates

and mudstones. Eight key facies are identified (Table 8). Carbonates are classified according to the Dunham (1962) scheme. Bioturbation is described according to the categories of Taylor and Goldring (1993; Table 7).

CFA1 — Restricted proximal inner ramp (depth 1362.00 – 1383.57 m)

Description

Carbonate Facies Association 1 is dominated by bioclastic packstone–wackestones with minor grainstone (*Lc*). These grade into sequences of nodular mudstones (*Ln*). Carbonate nodules are abundant, small, dense, single phase and most commonly have irregular edges (Fig. 12a). Low-level bioturbation is observed (BI 1–2; Fig. 12a) and some nodules are bioturbated, with traces preserved by recrystallization of a later carbonate cement (Fig. 12b). Packstone and wackestone facies (*Lc*) contain high proportions of micritic cement, and abundant bioclasts, and glauconite is common throughout (Fig. 12c). Echinoderm fragments, including crinoid ossicles, and *Nuia* are observed in lower sections (Fig. 12d). Other fossil fragments include probable molluscs and trilobite sclerites. Hardgrounds are present throughout these facies (*Lc*, *Ln*), but are most common in the lower 4 m (1381–1385 m) where they form in stacked succession. Here the hardgrounds are sometimes bored with glauconitic veneers (Fig. 12c,d).



LD237

15/04/21

Figure 11. Schematic diagram showing the epeiric sea carbonate ramp model (adapted from Schlaich and Aigner, 2017, showing zones X, Y and Z after Irwin, 1965) displaying idealized positions of CFA identified in Olympic 1

Table 8. Facies interpreted in the Sapphire Marsh Member of the Nambeet Formation in the Olympic 1 well

Code	Facies	Lithology	Facies thickness and sedimentary structure	Grain type and composition	Bioturbation	Depositional setting	Thin section (m)
<i>Hn</i>	Bioclastic packstone–grainstone	Packstone–grainstone and mudstone	Medium to thick (20 cm – 2.5 m). Abrupt to gradational contacts. Thin to thick mudstone drapes, stylolitic in parts	Dominantly bioclastic with abundant nautiloids, common to moderate molluscs. Some peloids	Low, BI 1–2 Horizontal, cylindrical, unlined burrows with carbonate fill in mudstone laminations	Moderate-energy settings; above storm wave base; episodes of non-deposition	1339.27 1343.07
<i>Lc</i>	Bioclastic packstone–wackestone	Packstone–wackestone, with minor grainstone and mudstone	Thin to thick (10 cm – 2.8 m). Gradational contacts. Thick mudstone laminae, wavy to stylolitic. Hardgrounds	Dominantly bioclastic with common molluscs, <i>Nuia</i> , crinoids and other echinoderms. Abundant glauconite. Minor peloids	Low, BI 1–2 Horizontal, cylindrical, unlined burrows with carbonate fill in mudstone laminations	Well-oxygenated, restricted marine	1294.86 1365.07 1375.02 1383.24
<i>La</i>	Interbedded mudstone and wackestone–packstone	Wackestone–packstone, grainstone and mudstone	Medium to thick (~20 cm to ~3 m) from log. Abrupt to gradational contacts. Bored hardgrounds. Hardground intraclasts	Bioclastic with common nautiloids, echinoderms, trilobites and unidentified bioclasts. Some ?peloids. Bioclasts are fragmented. Poorly sorted to chaotic		Above storm wave base; intervals of non-deposition between high-energy events; oxygenated	1251.78
<i>Ln</i>	Nodular mudstone (nodular limestone–marl rhythmities)	Mudstone, carbonate nodules	Medium to thick. Gradational contacts. Laminated mudstone. Common carbonate nodules. Thin shell debris lags	Nodules are micrite dominated to bioclastic (wackestone–grainstone) containing recrystallized ?brachiopods and ?nautiloids. Minor glauconite	Common, BI 2–3	Low-energy, possibly restricted conditions	1337.80 1355.29 1369.90 1375.02
<i>Hp</i>	Heterolithic mudstone–limestone	Mudstone, lime mudstone	Thick (1–7 m thick). Planar thin to moderately (1–10 cm) interbedded mudstone and lime mudstone. Minor carbonate nodules in mudstone. Minor fossil fragments	Lime mudstone contains occasional allochems, molluscs and other unidentified bioclasts, possible ?peloids	Low, BI 1–2. Horizontal, cylindrical, unlined traces with carbonate fill in mudstone laminations. ?Chondrites, ?Planolites. Minor bioturbation with crystalline carbonate fill in nodules	Low energy	1188.40
<i>Mc</i>	Laminated mudstone with nodules	Mudstone, packstone–micrite	Thick (17 m) gradational contacts. Laminated mudstone. Large, disseminated carbonate nodules. Minor pyrite	Nodules are dominantly micritic, occasionally having packstone fabric	Low BI 1–2	Very low energy; slow rate of deposition; anoxic	1311.17
<i>MI</i>	Laminated fossiliferous mudstone	Mudstone, packstone–micrite	Medium to thick (~0.3 – 15 m). Gradational contacts. Laminated mudstone. Sparse carbonate nodules	Mudstone is silty in parts and bioclasts are common, including; nautiloids, trilobites and possible ?brachiopods and ?echinoderms. Nodules are bioclastic packstone to micritic in composition	Common BI 2–3. Occurs in carbonate nodules. Horizontal, cylindrical, unlined traces ~0.1 cm diameter. ?Chondrites	Low-energy settings; influence from bottom and distal currents	1192.39 1200.63 1213.12
<i>Mo</i>	Laminated mudstone	Mudstone	Thin to thick (10 cm – 24 m). Gradational contacts. Laminated mudstone. Rare carbonate nodules. Pyrite. Some fossil fragments	Mudstone is silty and calcareous. Fossil fragments include molluscs and echinoderms	Mudstone: possible very small (less than 1 mm), horizontal traces in mudstone. ?Phycosiphon. Carbonate nodules: abundant, BI 3, horizontal and subvertical unlined, carbonate-filled traces. Low-diversity assemblage. Predominantly chondrites	Very low energy; below storm wave base	1235.70 1235.86 1244.35

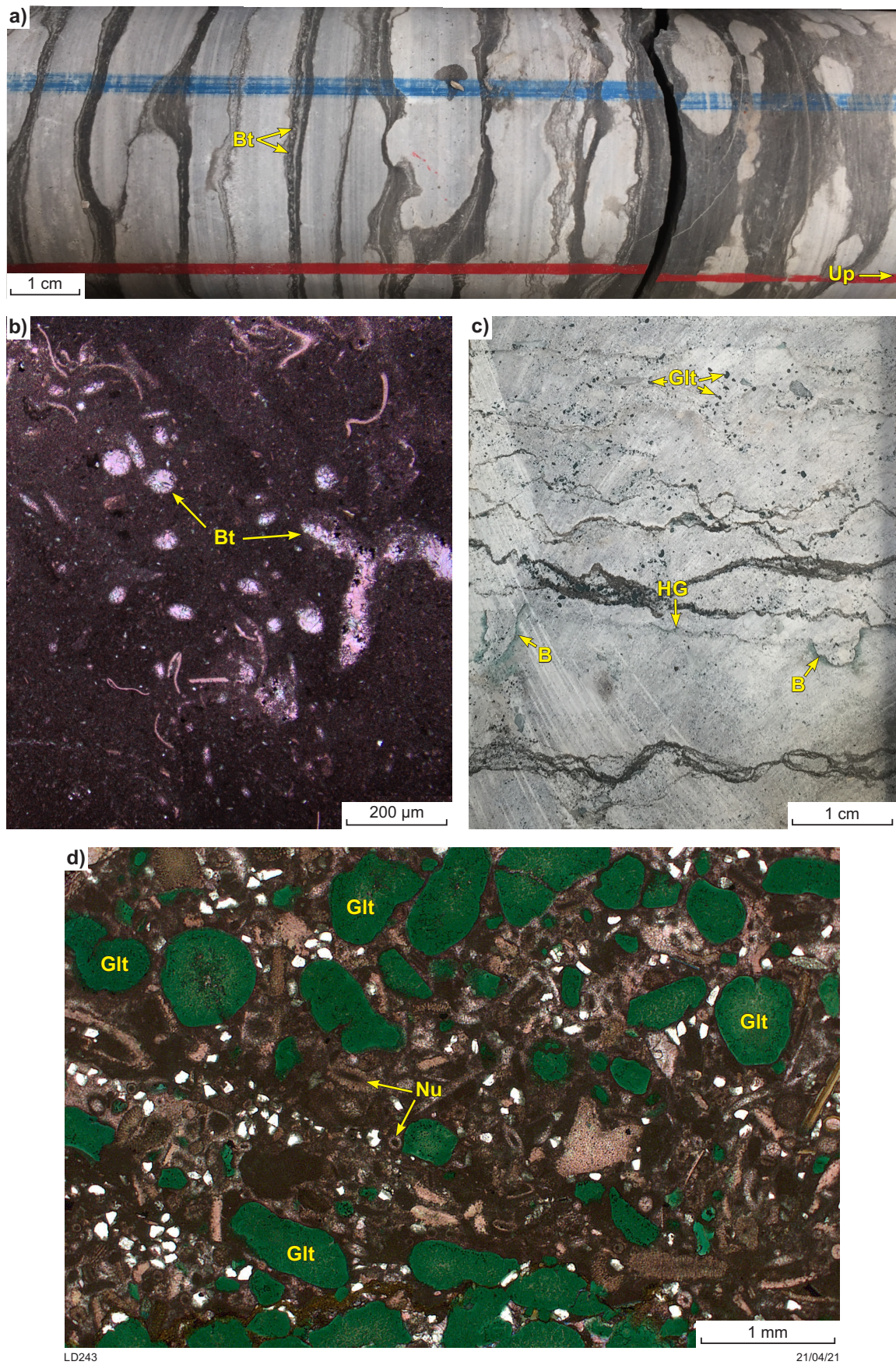


Figure 12. Major facies and sedimentary features of CFA1: a) core photo showing bioclastic packstone-wackestone (Lc) at about 1377.70 m depth with dense irregularly edged nodules in laminated mudstone. Mudstone intervals show evidence of low-level bioturbation (Bt); b) stained thin section viewed in ppl through micritic nodule at 1365.07 m showing recrystallized calcite within bioturbation; c) core photo of a hardground (HG) in wackestone at approximately 1383.45 m. The hardground has a glauconitic veneer and shows boring traces (B), glauconite grains (Glt) are common in the surrounding rock; d) thin section at 1383.24 m viewed in ppl through hardground with glauconitic veneer showing abundance of glauconite and the presence of *Nuia*

The level of organic material is low at the base of the Samphire Marsh Member in Olympic 1, with a TOC content of 0.31 – 0.68%, but increases up-section as mudstone becomes more dominant (Fig. 5). ICP-MS data indicates high levels of enrichment factor of molybdenum (EFMo) and anoxic/euxinic conditions are interpreted across this sequence (Chemostrat Australia, 2016). HyLogger data indicates the absence of quartz as supported by petrographic analysis, except for minor quantities at the base of the Samphire Marsh Member in this facies association. Potassium-rich feldspar species are present towards the top of this facies association (Fig. 7).

Interpretation

The abundance of micritic and nodular carbonate features in this facies association is indicative of persistent low-energy marine conditions. The abundance of hardgrounds with bored surfaces (Fig. 12c) record multiple episodes of non-deposition or erosion (Christ et al., 2015). The presence of glauconitic hardground veneers and dispersed glauconite grains (Fig. 12c,d), along with the anoxic conditions indicated by the low EFMo calculated from ICP-MS data, suggests restricted or marginal marine conditions. Micrite is a common deposit in protected inner-ramp areas and shelf hardgrounds are commonly associated with glauconite and borings (Flügel, 2004). Based on this combination of features, deposition within the inner areas of an epeiric ramp or platform is interpreted (Fig. 11). Further, the micritic rims around the *Nuia* grains suggests reworking of these grains and the likely proximity of this depositional setting to intertidal or supratidal environments or high-energy shoals with which *Nuia* formation is generally associated (Donovan, 1992; Flügel, 2010; Vachard et al., 2017). An increase of the relative mudstone to carbonate ratio of this sequence indicates a deepening-upwards trend transitioning into the overlying CFA2.

CFA2 — restricted inner ramp (depth 1334–1362 m)

Description

This facies association is dominated by thin to thick beds of bioclastic packstone–grainstone (*Hn*) and interbedded nodular mudstone (*Ln*; Fig. 13a). The mudstone is clay dominated, laminated and very dark grey to black in colour with minor silty laminations observed in parts. Low-level bioturbation (BI 1–2) is present throughout *Ln*, commonly as small horizontal traces (?*Planolites* and ?*Chondrites*). Fossil fragments are present but uncommon and are usually parallel or subparallel to laminations. Carbonate nodules are small and dense with both smooth and irregular edges. Nodules are micritic and zoned, with dense crystalline centres and coarse, dispersed crystalline rims (Fig. 13b). They contain recrystallized fossil material and show evidence of bioturbation (Fig. 13c). Single phase forms dominate but multiple phases are observed (Fig. 13d).

Packstone to grainstone beds are extensively recrystallized and comprise two main grain types: unidentifiable extensively micritized grains and recrystallized fossil fragments including common nautiloids (Fig. 13a), and probable mollusc fragments. The conodont zone *P. oepiki* – *S. bilobatus* is interpreted for samples recovered in this facies association (Zhen et al., 2017). Mudstones are organic rich containing up to 3.28% TOC (Fig. 5). High values of Cu and EFMo are present indicating anoxic/euxinic conditions.

Interpretation

Alternating very low-energy and moderate- to high-energy conditions are interpreted based on the interbedded packstone–grainstone and nodular laminated mudstone deposits. Deposition in the restricted inner-ramp areas is indicated based on the continued anoxic conditions and high levels of organic material. The formation of zoned nodules and multiphase nodule associations (Fig. 13d) suggests very low-energy, stable conditions with slow sedimentation during deposition of this facies association. The increased proportion of mudstone to carbonate implies a deeper water setting than CFA1 (Fig. 11). Grainstone to packstone facies (*Hn*) represent episodes of higher energy, possibly short transitions to the deeper but higher energy ramp 'Zone Y' (Fig. 11; Irwin, 1965) or storm deposits.

The mixed grain composition and abundance of pelagic grains and nautiloids in grainstones suggests that a high proportion of grains were imported from shallower settings. Storm deposition is a more likely method of deposition particularly as storms are one of the major processes depositing coarser carbonates on epeiric ramps (Flügel, 2004).

CFA3 — Epeiric middle ramp (depth 1319–1334 m)

Description

This sequence consists of nodular mudstone (*Ln*; Fig. 14a) within the *P. oepiki* – *S. bilobatus* biozone. Mudstones are dark brown to black and laminated with abundant to common fossil fragments; mainly ?trilobites which are preserved parallel to laminae. Low-level bioturbation (BI 1–2) is present. Nodules are very fine crystalline, likely micritic, with smooth edges. Both dense and disseminated forms are present and two phases of nodule formation are observed. Lags of fossil material are common in nodule centres as is bioturbation of nodules. The level of bioturbation is low to moderate, but trace fossil diversity is low. Rare thick grainstone nodules/beds are observed. Organic content is moderate to low, TOC 0.74 – 1.99% (Fig. 5).

Interpretation

Prevailing low-energy settings dominated by pelagic deposition are interpreted based on the dominance of nodular facies, nodular character and development of multiple nodule phases. Grainstone beds and common grain lags in nodules indicate a depth above storm wave base, with the sediment surface occasionally affected by storm activity. This facies association does not contain the geochemical indicators of anoxic/euxinic environments recorded in CFA1 and CFA2. The depositional environment is interpreted to be deeper in a middle-ramp setting outside the zone of restricted circulation as evidenced by the increase in mudstone content and decrease in higher energy packstone–grainstone facies compared to CFA2 (Fig. 11).

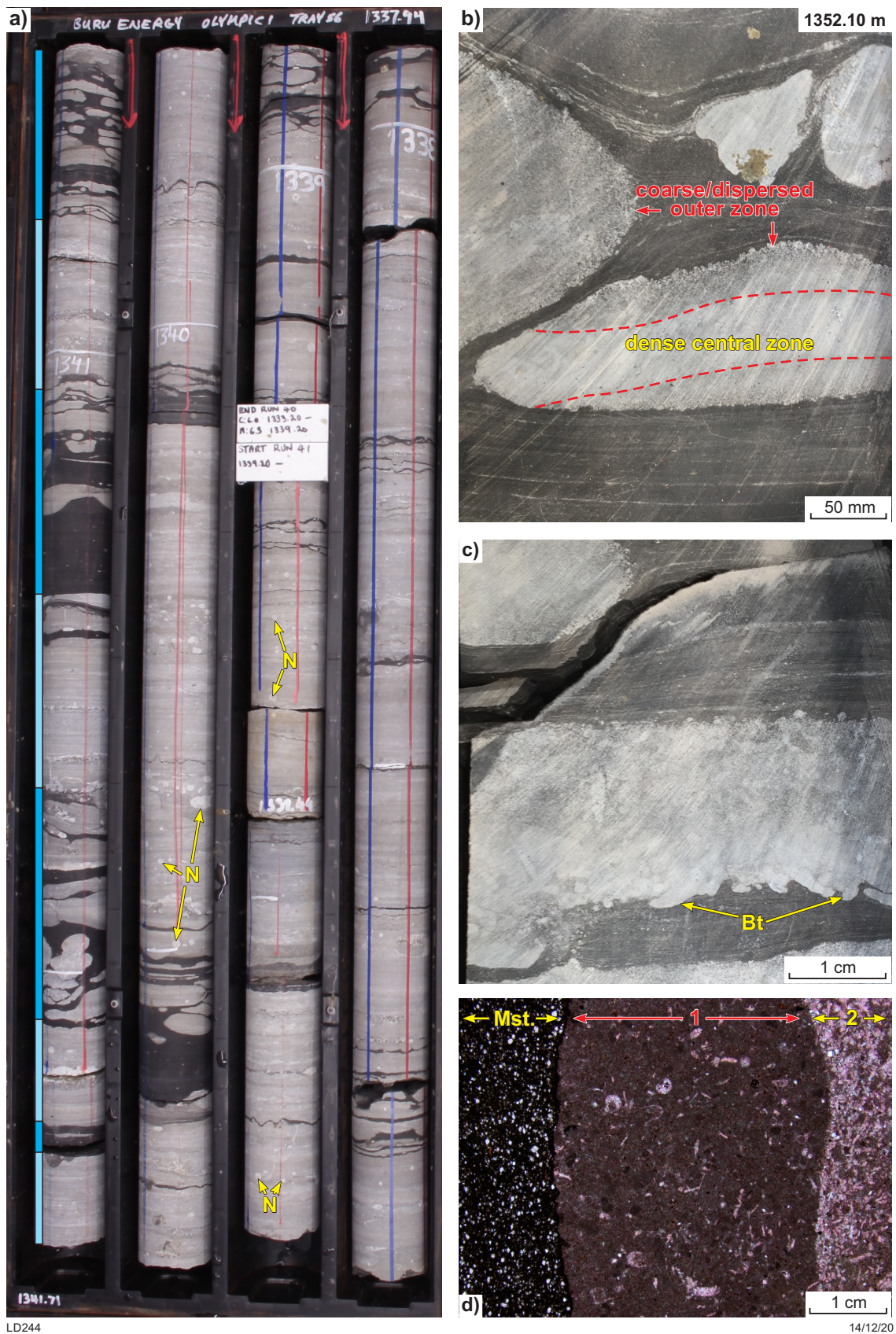


Figure 13. Major facies and sedimentary features of CFA2: a) core photo of interbedded bioclastic packstone-grainstone (*Hn*) in pale blue and nodular mudstone (*Ln*) in bright blue, showing abundant recrystallized nautiloids (*N*) in packstone-grainstone beds; b) core photo of zoned carbonate nodules with dense micritic centre zones and coarser, diffuse outer zones at about 1352.10 m; c) core photo of bioturbation throughout carbonate nodule, particularly evident at the base where burrows extend into underlying mudstone; nodule at ~1351.76 m; d) stained thin section viewed in cross-polarized light through mudstone (*Mst.*) and a multiphase nodule at 1337.80 m, the two phases indicated by numbered zones 1 and 2 and show difference in crystal formation



Figure 14. Core photos demonstrating the major facies of CFA3 and CFA4: a) nodular mudstones (*Ln*) dominate CFA3 at about 1333–1334 m depth; nodules are dense single-phase forms with smooth margins; b) laminated mudstone with nodules (*Mc*) of CFA4 at 1313.50 m depth; nodules are zoned with dense centres and diffuse margins, direction of zoning indicated by red arrows

CFA4 – Epeiric middle–outer ramp (depth 1296–1319 m)

Description

The CFA4 sequence is dominantly mudstone. The main facies is planar-laminated mudstone with nodules (*Mc*), with subordinate laminated fossiliferous mudstone (*MI*). Mudstones are dark brown to black and laminated, and low-level bioturbation (BI 1–2) is present. Nodules are very finely crystalline, likely micritic, with smooth edges. Disseminated nodule forms dominate and show distinct zonation from dense centres to disseminated edges (Fig. 14b). These nodules are typically large, 4.5 cm in diameter and larger, with smaller dense nodules rarely observed. Lags of fossil material and bioturbation are present in nodules but are a minor component. Up-section, the sequence shows a transition to larger more disseminated nodules within the *Mc* facies. The base of the sequence is within the *P. oepiki* – *S. bilobatus* conodont biozone, whereas the top lies inside the *O. communis* conodont biozone (Fig. 5). Organic content is moderate to high, with a maximum of 2.78% at 1318.29 m (Fig. 5).

Interpretation

Low-energy conditions below storm wave base are interpreted based on lithology and relative sparsity of fossil fragments compared to CFA1–3. The broad disseminated

character of nodules and high organic content of this association suggest very slow deposition and long residence times on a stable, undisturbed seafloor. A deeper marine setting than CFA3 is interpreted and CFA4 is likely deposited in a middle–outer ramp setting, supported by the transition of shallow conodont faunas of the *P. oepiki* – *S. bilobatus* biozone to deeper conodont faunas of the *O. communis* biozone (Zhen et al., 2017) within this association.

CFA5 – Epeiric middle ramp storm dominated (depth 1250–1296 m)

Description

This sequence is characterized by interbedded mudstone and wackestone–packstone facies (*La*), bioclastic packstone–wackestone and occasional grainstone beds (*Lc*) interbedded with nodular mudstone (*Ln*) and laminated fossiliferous mudstone (*MI*) facies (Fig. 15a). The nodules in *Ln* contain a high proportion of fragmented bioclasts similar to the wackestone–packstone beds. They are typically small and dense with wavy or irregular edges. *Lc* and *La* limestone beds are chaotic with irregular bed boundaries and fossil fragments within are abundant and disordered. Bioturbation is high. Fossil fragments are generally not micritized although some highly micritized, unidentifiable grains are present. Nautiloids are abundant

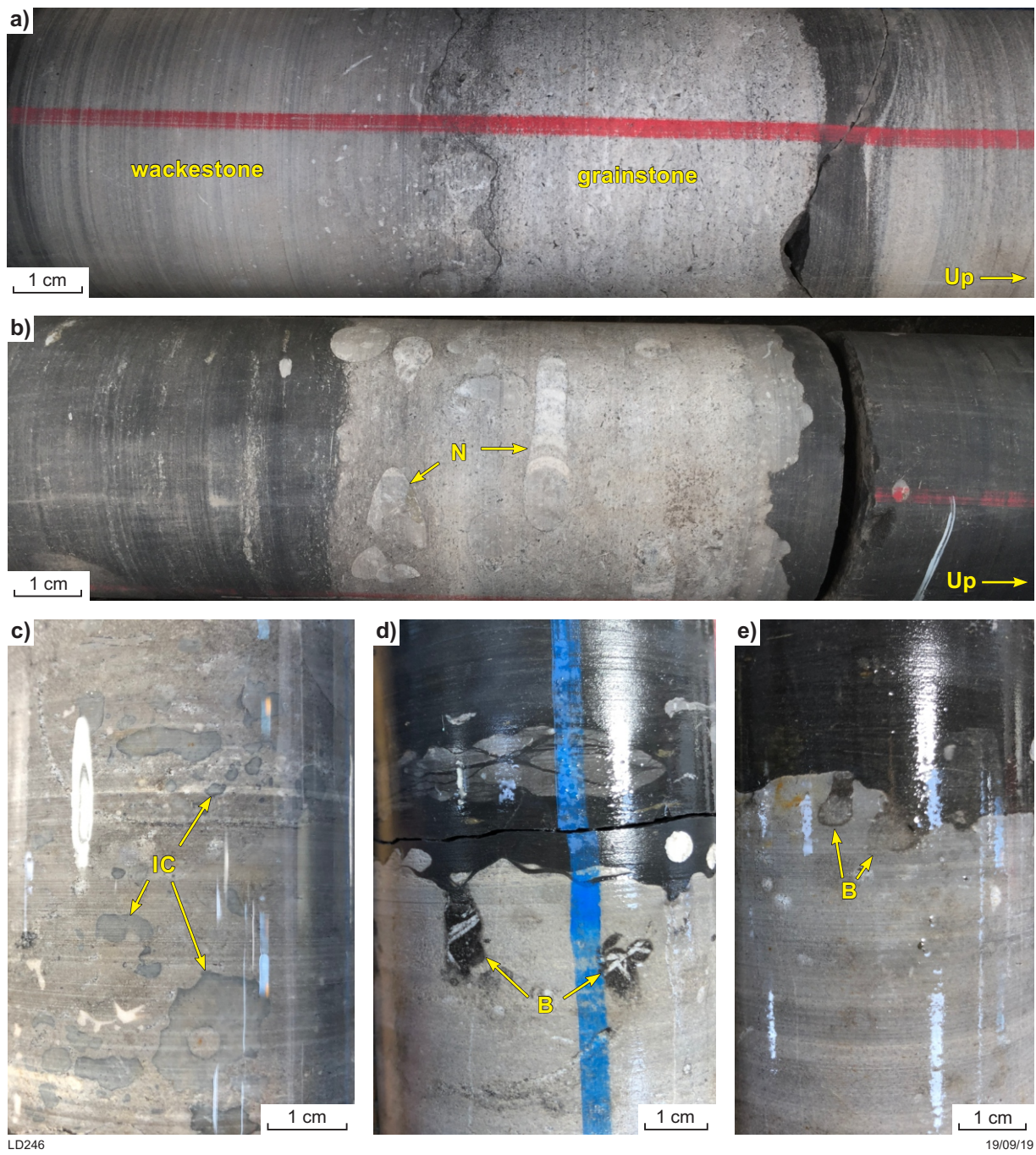


Figure 15. Core photos of CFA5: a) Facies *La*, grainstone bed abruptly overlying wackestone bed at about 1252.50 m; b) facies *La*, wackestone-packstone bed containing abundant recrystallized nautiloid shells (N) at about 1252.50 m; c) hardground intraclasts (IC) with green-grey rims in chaotic wackestone-packstone bed at about 1281.55 m; d) and e) bored surfaces of wackestone-packstone beds, bored trace (B) filled with mudstone and fossil fragments at d) 1257.59 m and e) 1256.98 m

in the uppermost wackestone–packstone beds (Fig. 15b) and the *O. communis* biozone is recorded throughout the sequence.

Hard ground intraclasts are common in facies *Lc* and coated or rimmed with deep green or dark grey veneers possibly glauconite or manganese (Fig. 15c). Hardgrounds are common at higher stratigraphic intervals within the CFA5, and style varies from cemented eroded surfaces between two carbonate beds, to veneered or bored (Fig. 15a,d,e). Bioturbation is notably higher (BI 2–3) than in underlying CFA4. This facies association has low organic content with a TOC range of 0.38 – 1.49% and an average of 0.72%. Geochemical data suggests deposition in an oxygenated environment, and TIR spectral data records an influx of quartz at the base of the sequence (Fig. 7).

Interpretation

Packstone–grainstone deposits are interpreted as storm deposits due to their chaotic character, the abundance of pelagic fossils, nautiloids and the presence of hardground intraclasts within beds. Nodular mudstone interbeds and the formation of bored hardground surfaces between carbonate beds suggests intervals of low energy, non-deposition and lithification of the sea floor between storm events. The occurrence of the *O. communis* conodont biozone is consistent with the interpretation of deeper conditions (Zhen et al., 2017), likely between storm and fair weather wave base. The dramatic increase in bioturbation in this setting is consistent with the indications of an oxic depositional environment as recorded by the geochemical data, which is potentially due to a change to conditions with good circulation and an oxygenated water column.

CFA6 – Epeiric outer ramp (depth 1213–1250 m)

Description

This sequence is defined by a thick section of laminated mudstone (*Mo*) with rare, small carbonate nodules (Fig. 16a) and minor laminated fossiliferous mudstone (*MI*). The mudstone in both facies is dark grey to brown with abundant graptolites, including phyllograptid and dichograptid forms (see Biostratigraphy), and trilobite fragments well preserved and aligned with laminae. Some recrystallized nautiloid shells are present but in much smaller quantities than in the underlying carbonate beds of CFA5. Carbonate nodules are small, micritic and single phase with smooth margins and micritic crystals forming the nodules range from densely packed to disseminated through the mudstone. Low-level, indistinct bioturbation is present throughout the section and organic content is generally low, with a TOC range of 0.46 – 1.50%, and an average of 0.90%. Geochemical data indicates that the system remains oxygenated and the *O. communis* biozone is recorded throughout (Fig. 5). TIR data show that mica dominates the mudstone mineral assemblage, and the feldspar that was present in lower stratigraphic sections is absent (Fig. 7). Short-wave infrared hyperspectral data records an increased wavelength of carbonate species measured, which is attributed to Fe enrichment of the carbonate species present. The signature appears abruptly at the base of the package and is retained throughout.

Interpretation

Low-energy, unrestricted marine settings likely below storm wave base and dominated by pelagic deposition are indicated based on lithology, conodont fauna and the excellent preservation of whole pelagic specimens in mudstone. The sparse and diminished nodules suggest very limited carbonate input into the system. Depositional environments are deeper than the preceding CFA5 sequence, with the base of the sequence recording a dramatic change from carbonate-dominated to mudstone-dominated facies indicating the presence of a major flooding surface. This is also coincident with a sharp increase in values on the GR log (Fig. 5). The sequence shows a shallowing up trend with an increasing carbonate–mudstone ratios towards the top. This is consistent with a change in conodonts, from faunas of the deeper *O. communis* biozone, to shallower faunas of the *J. gananda* biozone (Zhen et al., 2017) in the overlying facies association CFA7. The source of the Fe-enriched carbonate is not obvious from XRD data or thin section analysis.

CFA7 – Epeiric middle ramp (depth 1170–1213 m)

Description

This association is dominated by two facies, laminated fossiliferous mudstone (*MI*) and heterolithic mudstone – lime mudstone (*Hp*; Fig. 16b). Laminated mudstone beds are dark grey as seen in previous associations and contain small, dense, carbonate nodules with irregular margins. Bioclasts are common with variable orientation, and shell lags are observed. Heterolithic mudstone – lime mudstone facies are planar bedded with distinct bed boundaries between lithologies. Beds are 1–10 cm thick, and lime mudstone beds are gradational with dense centres grading out to disseminated margins. Minor fossil fragments and bioturbation are present in both facies. Geochemical data indicates that the system remains oxygenated. This association cannot be separated from the underlying CF6 from HyLogger data.

Interpretation

This association is gradational with the underlying CFA6 interval. Interbedded mudstone and lime mudstone lithologies indicate low-energy conditions. When compared to CFA6, shallower and slightly higher energy settings are suggested based on the increased abundance of shell fragments and carbonate in the system. The distinctive planar bedding of the heterolithic facies may be a function of more regular and extensive carbonate beds forming at the time of deposition, possibly due to increased distribution by bottom currents.

Diagenesis

Carbonate facies in Olympic 1 range from lime mudstone to grainstone fabrics. Calcite, Fe-calcite, dolomite and Fe-dolomite are the major cement compositions found in these facies. Lesser quantities of pyrite, authigenic clays, authigenic quartz, baryte and bitumen are also present. A proposed diagenetic sequence is presented in Figure 17. The order of events is interpreted from the crosscutting relationships observed in thin section, under cathodoluminescence and from SEM analysis. The earliest phase of diagenesis occurred during deposition



Figure 16. Core photos demonstrating the major facies of CFA6 and CFA7: a) laminated mudstones (*Mo*) with rare small carbonate nodules that dominate CFA6 between 1238.51 and 1242.41 m; b) heterolithic mudstone-limestone (*Hp*) facies that dominate CFA7 between 1196.12 and 1199.93 m

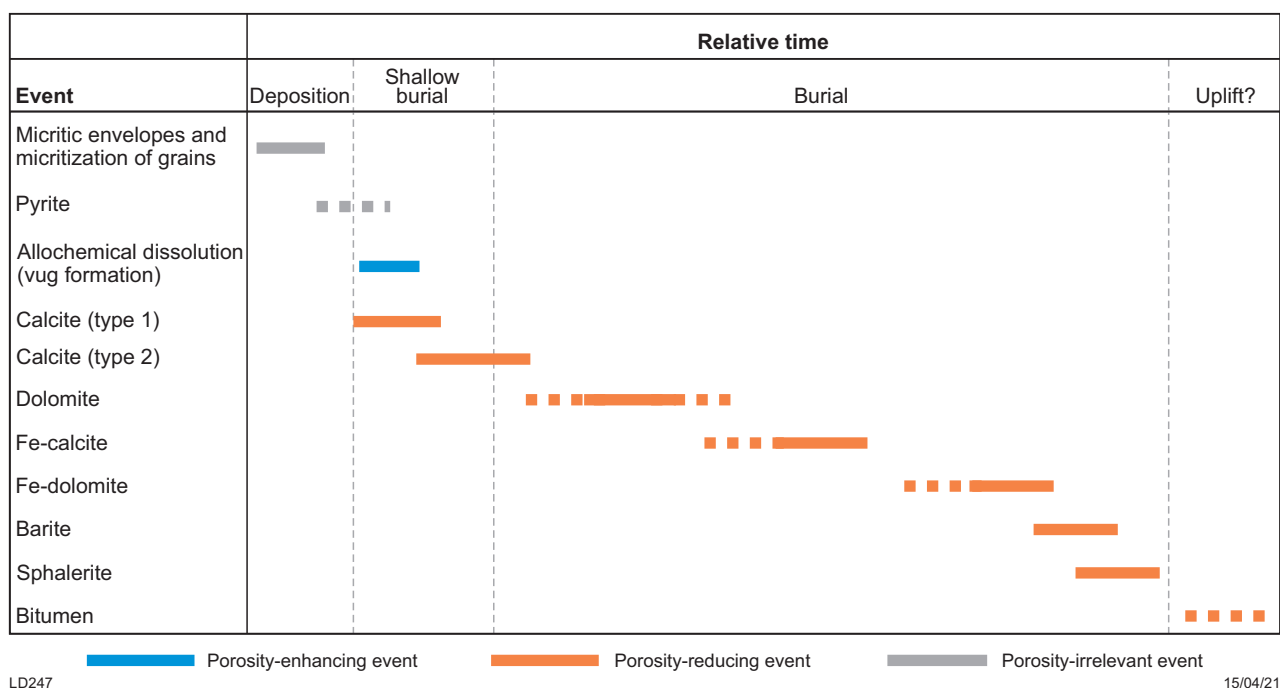


Figure 17. Paragenetic sequence of diagenetic events in carbonate-mudstone facies of the Nambett Formation in Olympic 1

with the micritization of carbonate allochems, followed by formation of authigenic pyrite (Fig. 18a), and an early phase of calcite cementation. Dissolution of carbonate allochems and development of vugs also occurred early (Fig. 18b). Next calcite and dolomite cements were generated (Fig. 18c,d). This was followed by formation of fractures, then development of a Fe-calcite and finally Fe-dolomite cements (Fig. 18d,e). Barite and sphalerite formed later along with stylolites, and bitumen was emplaced last (Fig. 18e).

X-Ray diffraction analysis of whole-rock mineralogy measures the volumetric ranges of calcite (9.9 – 85.9%), dolomite (0 – 12.2%), quartz (4.1 – 29.8%) and total clay (3.8 – 43.8%) from limestone and mudstone facies throughout the section. Elevated quartz values generally correspond to mudstone lithofacies, although the highest reading is derived from a wackestone sample in the lower part of the section. X-Ray diffraction readings do not differentiate between standard and Fe-rich forms of calcite and dolomite. Two of the four highest dolomite readings are attributed to extensive formation of Fe-dolomite (1200.63 and 1235.70 m), and the other two are attributed to the dominance of non-ferroan forms (1235.70 and 1213.12 m).

Iron-dolomite is more common in mudstone beds and layers replacing the detrital clay matrix. Rhombic Fe-dolomite forms in isolation or around existing dolomite crystals, and occurs within laminated mudstone beds, in mudstone surrounding nodular carbonate, and in mudstone laminae between limestone beds (Fig. 18c,d). Rhombs are more prolific next to carbonate clasts and crystals appear to be better developed in mudstone laminae than mudstone beds (Fig. 18d). In tight limestones where mudstone is absent, Fe-dolomite is observed forming in vuggy and mouldic pore spaces that formed after dissolution of carbonate allochems (Fig. 18f).

Cathodoluminescence suggests that two phases of calcite cementation occurred, a possible very early marine cement followed by a second phase during shallow burial. This second phase is interpreted to have occurred at the same time as recrystallization and stabilization of the calcitic matrix. Dolomite is also interpreted to have formed relatively early replacing matrix clays and carbonate grains. Iron-calcite, which fills fractures and vugs, formed later and Fe-dolomite much later still during deep burial.

Measured core porosity from 25 samples of limestone and mudstone facies in the Sapphire Marsh Member ranges from 0.2 to 8.0%. There is no correlation between porosity and permeability in the member, and neither porosity nor permeability show a depth-related trend. In all limestone and mudstone samples, microporosity is the principal pore type occurring between detrital clay flakes and micritic crystals (Fig. 18g). A weak positive correlation is present between increased total clay content and porosity of samples. Increased porosity values show a good positive correlation ($r^2 = 0.797$) to elevated levels of chlorite. No correlation of porosity to other components is evident, neither is there a correlation between permeability and specific components. Porosity may be locally enhanced by the presence of rare vugs and fractures. Minor levels of porosity are associated with organic material in some samples (Fig. 18h).

HyLogger spectral data

The Sapphire Marsh Member contains two distinct mudstone-dominated sequences, both of which grade upwards into carbonate-dominated units. The lower mudstone sequence constitutes CFA2–4, while the upper is represented by CFA6. The TIR data differentiate these two mudstone-dominated sequences by the presence of feldspars in the lower interval (~1300–1335 m), and a mica-dominated mineralogical assemblage in the upper mudstone

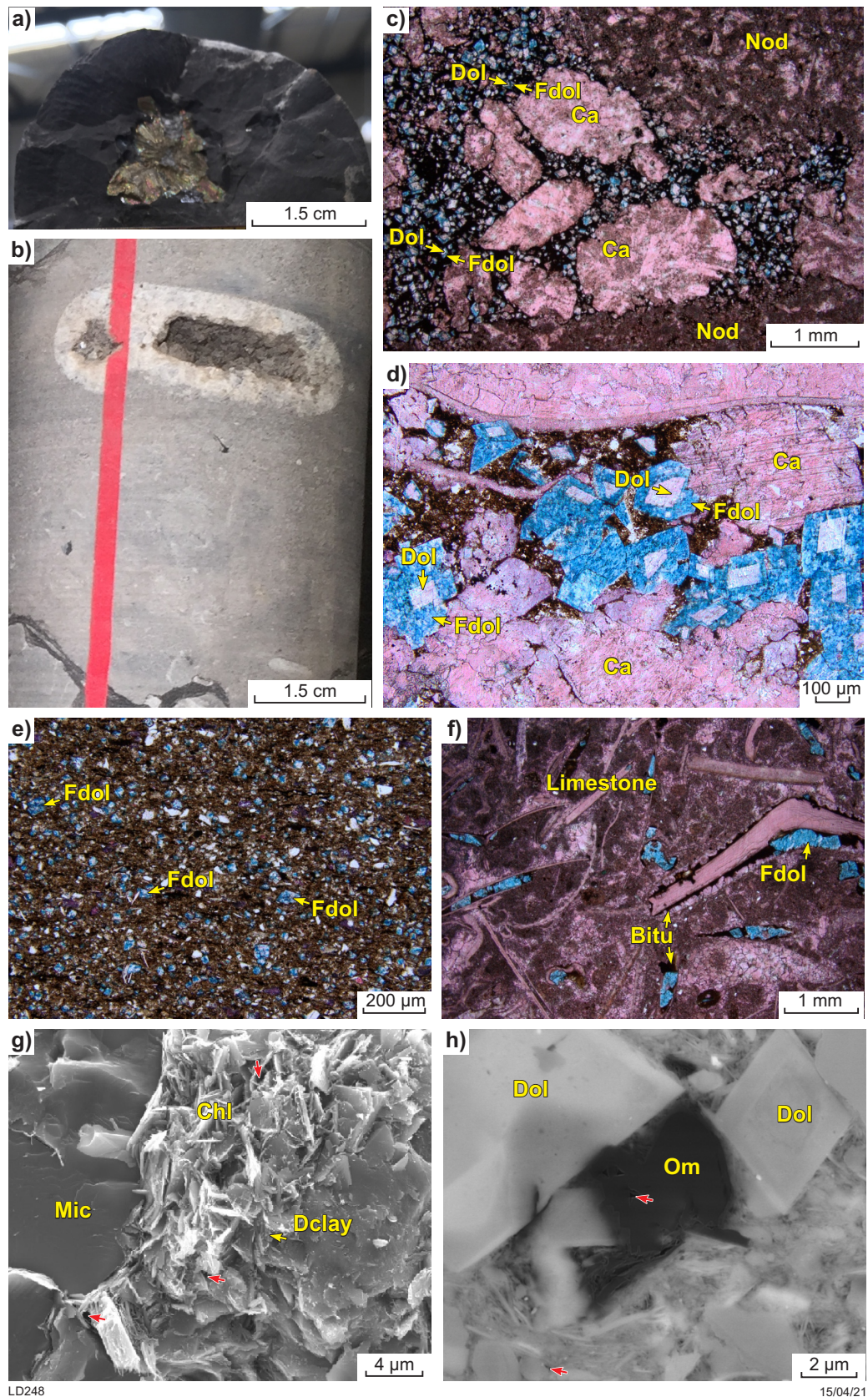


Figure 18. Cements and porosity in carbonate-mudstone facies of the Nambet Formation in Olympic 1: a) authigenic pyrite in mudstone at 1331 m; b) dissolution of nautiloid shell and recrystallization with calcite cement at 1178.83 m; c) stained thin section photomicrograph of nodular carbonate-mudstone at 1337.80 m showing calcite cement forming between nodules along with dolomite (Dol) and later Fe-dolomite (F-Dol); d) stained thin section photomicrograph of mudstone seam in limestone at 1396.90 m showing Fe-dolomite forming around dolomite cores; e) thin section photomicrograph of mudstone at 1311.17 m showing Fe-dolomite rhombs replacing detrital clay matrix; f) stained thin section photomicrograph of limestone at 1251.78 m showing Fe-dolomite formation in mouldic pore spaces; g) SEM image at 1251.78 m showing microporosity associated with detrital clays (red arrows); h) argon-ion milled SEM image at 1200.63 m showing microporosity associated with organic material (Om) and surrounding detrital clay (Dclay, red arrows). Abbreviations: Bitu, bitumen; Chl, chlorite; Nod, limestone nodules

package. The feldspar-rich signature of the lower mudstone is consistent throughout the transition to carbonate-dominated facies. The transition of the upper mudstone interval shows an up-sequence decline in mica to an almost 100% carbonate composition (Fig. 7), which marks the top boundary of the Samphire Marsh Member and base of the overlying Willara Formation.

The difference between the two mudstone-dominated packages is also highlighted by the SWIR carbonate data which shows a sharp change from non-ferroan to Fe-rich carbonate species in the second mudstone package starting at 1250 m (Fig. 7). The cause of this Fe enrichment is not clear. One possibility is an increase in the level of Fe-rich cements such as Fe-calcite and Fe-dolomite; however, an increase in these cements is not obvious from thin section. The SWIR carbonate spectra also show a notable change in carbonate composition from Fe rich to Mg rich at the approximate position of the boundary between the Nambett and Willara Formations. With further study this difference may be valuable as an additional tool to help identify the Nambett – Willara Formation boundary.

Biostratigraphy

Conodonts

Conodont sampling and analysis of the entire cored section from Olympic 1 identified four biozones (Zhen et al., 2017); *J. gananda*, *O. communis*, *P. oepiki* – *S. bilobatus* and *P. proteus* (Figs 2, 6). Their succession in the Olympic 1 well records continuous deposition between the Lower–Middle Ordovician (Tremadocian–Dapingian). Sample location, identification, and biozonation details are presented in (Fig. 6) from Zhen et al. (2017). Biozones were age calibrated with CA-IDTIMS $^{206}\text{Pb}/^{238}\text{U}$ dates recovered from bentonite beds within the Olympic 1 core (Normore et al., 2018). The biozones in Olympic 1 are cross correlated to conodont biostratigraphy undertaken by Nicoll (1993) in other Canning Basin wells.

In Olympic 1, the Samphire Marsh Member begins in the *P. proteus* biozone and extends through the *P. oepiki* – *S. bilobatus*, *O. communis* biozones. The upper contact with the Willara Formation occurs in the *J. gananda* biozone just above the *O. communis* – *J. gananda* biozone boundary (Fig. 2). The *P. adami* – *S. bilobatus* biozone was defined by Zhen and Nicoll (2009) and later updated to the *P. oepiki* – *S. bilobatus* biozone based on material in the Olympic 1 well (Zhen et al., 2017). Therefore, to date, it is not identified in any Canning Basin well except Olympic 1. In other wells, the top of the Nambett Formation generally occurs in the *O. communis* or *J. gananda* biozones (Nicoll, 1993). The onset of Willara Formation deposition is tied to a second-order regressive event, so it should be expected that this contact will be diachronous, younging towards the west. The position of the formation top in the *J. gananda* biozone in Olympic 1 is consistent with this expected diachroneity.

In Olympic 1, the *O. communis* biozone begins in CFA4, in the lower of the two mudstone-dominated packages identified in this well (Fig. 5). A similar lithological sequence, a carbonate-dominated section between two mudstone-dominated packages, is commonly observed in wells on the Broome Platform; however, the existing conodont samples are not extensive enough to verify this onset position of this biozone.

Palynology

Palynological analysis of the Canning Basin's Ordovician strata was first undertaken by Combaz and Peniguel (1972) and was later regrouped and presented in McTavish and Legg (1976) although, these zones have not been widely used.

Palynological analysis was carried out across the Olympic 1 cored interval between 1130.54 and 1442.45 m. Twenty-two samples were collected and analysed but the palynomorphs recovered were strongly degraded barring any taxonomic identification; however, general identification of botryoidal algal colonies and indeterminate acanthomorphic acritarchs was achieved between 1189.22 and 1432.69 m and interpreted to indicate a Middle Ordovician age. This interpretation was general only, details can be found in Playford and Wicander (2016). Thermal alteration index of the recovered palynomorphs was 3+ to 4– based on the Pearson (1984) standard, indicating thermal maturity in the dry gas – over mature zone. This interpretation, however, is not supported by other maturity data which interpret lower levels of maturity (see Dent and Normore, 2017).

Two additional palynological samples were collected from cuttings between 760 and 860 m. These samples indicate the presence of the *Microbaculispora tentula* palynozone, and the lack of spinose acritarchs is consistent with non-marine deposition (Hannaford, 2016). The presence of the *M. tentula* palynozone indicates a Permocarboiferous age (Partridge, 2006; Hannaford, 2016) and is consistent with the Grant Group at the sampled depth interval. This supports the interpreted base-Grant unconformity overlying the Willara Formation at about 898 m depth in the Olympic 1 well (Dent and Normore, 2017).

Macrofossils

Macrofossils are preserved throughout the Samphire Marsh Member but appear to be completely absent from the underlying Fly Flat Member (~1384 m to TD). A wide range of groups are recorded in the assemblage, with the most prominent being trilobites, graptolites, brachiopods, bivalves and nautiloids sensu lato (defined here as including early cephalopod groups now generally considered separate suborders and those of uncertain placement, but excluding Coleoidea and Ammonoidea). Notable minor taxa including gastropods, macheridians, bryozoans and scolecodonts. Of particular importance are the trilobites and graptolites, both of which are useful for biostratigraphy during the Ordovician, and could be used to support and supplement microfossil biostratigraphy and radiometric geochronology. Scolecodonts have also been used for biostratigraphy in the past, but do not seem to be particularly plentiful in the succession. These and other groups would provide insights into environmental changes during deposition of the Nambett Formation with further work. At present, no taxonomic work has been completed on the fossils in this well and environmental interpretations are highly preliminary, although a number of general trends have been observed.

The macrofossil abundance within the Samphire Marsh Member as recorded in Olympic 1 can be separated into two distinct sections, with the lower part of the member (CFA1–5) having variable and constantly changing abundances, and the upper part (CFA5–7) characterized by slightly higher and more even changes in fossil abundance (Fig. 19a).

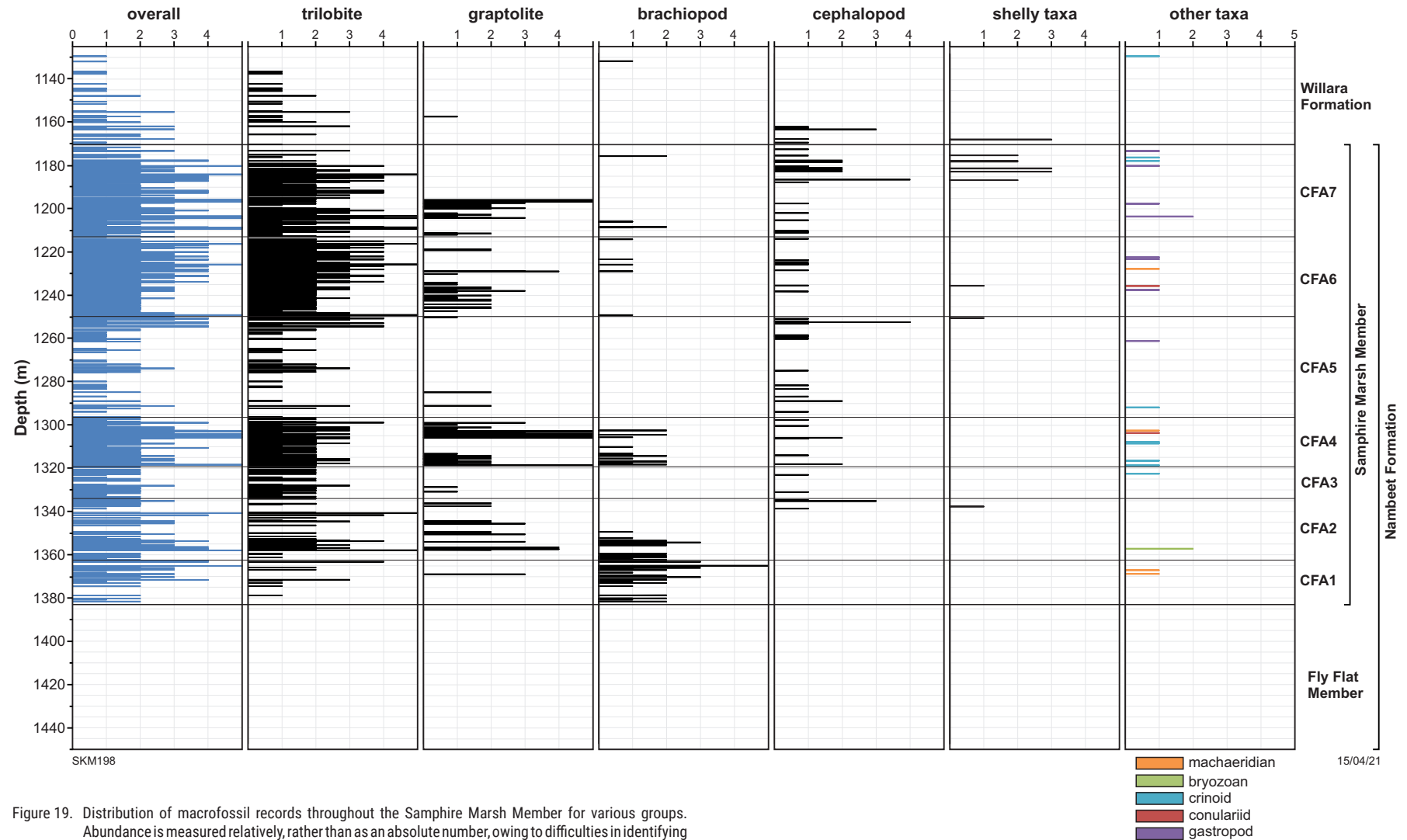


Figure 19. Distribution of macrofossil records throughout the Samphire Marsh Member for various groups. Abundance is measured relatively, rather than as an absolute number, owing to difficulties in identifying the numbers of individuals in overlapping or disarticulated taxa. Abundance scale: 1 = single element or specimen; 2 = few, 0–25% of the core surface covered with macrofossils; 3 = rare, 25–50% of the core surface; 4 = common, 50–75% of the core surface; 5 = abundant, 75–100% of the core surface. Note that abundances measured in this way are dependent on the size of individual taxa; fewer large taxa, such as the asaphid trilobites and cephalopods, are required to cover a core surface compared to smaller taxa, such as brachiopods or graptolites

More specifically, CFA1 is characterized by low but gently increasing abundance, CFA2 and CFA3 by short peaks of abundance surrounded by generally low fossil abundance, CFA4 has consistently moderate to high abundance, and much of CFA5 has low to very low abundance. At about 1255 m (middle of CFA5), the overall fossil abundance increases steadily to a series of peaks from 1225 to 1180 m (CFA6 and CFA7), after which the overall fossil abundance decreases slowly and evenly to the top of the member. Note that the abundance estimates here are qualitative due to the preliminary nature of the study; no species richness or other formal diversity measures have been calculated for this assemblage to date.

Of the individual groups seen in the Samphire Marsh Member (Fig. 19b–g), trilobites are the most commonly recorded macrofossils, and their abundances mostly mirror that of the macrofossil assemblage as a whole; trilobites are also more notably abundant in CFA7 and CFA2 when compared to other groups. Trilobites of Superfamily Asaphoidea are the most commonly noted group and are recorded across the entire Samphire Marsh Member. These trilobites are often easy to identify, even from small fragments, and as a result there is a likely collector's bias towards reporting taxa of this group, to the detriment of identifying other groups, particularly smaller or less distinctive taxa. However, it is obvious from a cursory examination of the core that a wide range of trilobite forms, shapes and sizes are preserved within the Nambeet Formation, indicating a wide diversity of species, both within the asaphoids and more broadly. There is a general sense of faunal change down the core within all trilobite taxa; however, extracting any useful environmental and biostratigraphic information from this assemblage will require careful and detailed taxonomic work that could not be completed within the timeframe of the present project. Many forms appear similar to species already described elsewhere in the Lower Ordovician of the Canning Basin (e.g. Legg, 1976; Laurie and Shergold, 1996a,b). Most of the trilobite fossils within the core are disarticulated and fragmentary; of the 634 core surfaces within the Samphire Marsh Member preserving trilobite material, only 39 (6%) show evidence of sclerite articulation, most of which are associations of thoracic segments. This suggests that beds mostly preserve accumulations of moulted material, or material disarticulated and accumulated after death, rather than in situ or life-position assemblages.

Graptolites are less abundant than trilobites in the Samphire Marsh Member, but where recorded they are rarely preserved singly, commonly filling core surfaces with individuals of the same species. It has also been observed that graptolites are rarely preserved on the same surfaces as trilobites, suggesting either a taphonomic or environmental separation between the two groups. Graptolites are most abundant within CFA4, with a brief but strong abundance peak in CF7 at about 1195–1200 m. Graptolites are preserved predominantly as carbonized films, or occasionally as replacements by an unknown dun-coloured mineral (?jarosite). Phyllograptid and dichograptid forms are the most commonly preserved in the assemblage (Fig. 20) and including forms likely assignable to *Didymograptus* (*Expansograptus*), *Tetragraptus* and *Pseudophyllograptus* – all broadly reminiscent of Floian taxa elsewhere in Australia (e.g. Rickards and Chapman, 1991; Vandenburg and Cooper, 1992). Of particular interest is the presence and distribution of rare multiramous graptolites including specimens

reminiscent of both *Loganograptus* and *Clonograptus*. Previous workers (Cooper et al., 1991, 1998, 1999) have suggested that particular graptolite taxa are indicators of deeper water, with Egenhoff and Maletz (2007) designating multiramous dichograptids in particular as mesopelagic species and using their distribution to identify maximum flooding surfaces within a sequence of deep-water shelf successions in Sweden. This might suggest that the presence of these taxa within the Samphire Marsh Member (in CFA6 at 1240.98 and 1242.41 m, CFA2 at 1345.20 and 1356.44 m, and in CFA1 at 1368.93 m) indicates deepening or maximum flooding events, an interpretation supported by the mostly complete preservation of these delicate, complex fossils, suggesting deposition in low-energy environments or minimal transport prior to burial. However, a number of these occurrences (in CFA1 and CFA2) are in sections interpreted as restricted inner-ramp settings, which would not be expected to preserve mesopelagic species. Complete taxonomic description will be required before any detailed environmental analysis can be attempted.

Brachiopods are relatively rare in the Nambeet Formation and are primarily recorded in three zones at 1206–1229 m (CFA6 and CFA7), 1302–1318 m (CFA4) and 1349–1381 m (CFA1 and CFA2), but are most intensely recorded in the deepest of those sections. In fact, brachiopods become the most commonly logged fossil below 1350 m, a section in which no molluscs are recorded. Inarticulate (likely linguloid) brachiopods are relatively common throughout the formation, but are the dominant group recorded from 1313 m downward to the base of the fossiliferous section at 1384 m. The range of forms and sizes present suggests multiple inarticulate taxa are preserved within the assemblage, and the relatively good preservation of many specimens makes this group suitable for later in-depth taxonomic work. Other groups are visible although less completely preserved in most cases, and include likely rhynchonellids, strophomenids and orthides.

Orthoconic and planispiral nautiloids (s.l.) are relatively common throughout the Nambeet Formation, although there are distinct concentrations towards the top of the Samphire Marsh Member at 1175–1188 m (CFA7) and at 1250–1260 m (CFA5). As with other molluscs, no cephalopods are seen deeper than 1340 m. Cephalopods are generally recorded singularly in limestone-dominated beds, where they tend to be preserved in three dimensions and filled with recrystallized calcite; for these records, the intersection of the fossil with the core surface is generally at an oblique angle and the calcitic fill is often irregular in form, meaning the septal features are difficult to discern without additional preparation, such as sectioning perpendicular to the shell walls. Where cephalopods are noted on mudstone surfaces, they are preserved as impressions and no internal features can be discerned. Most of the records are orthoconic in form (~85%), although few of these specimens can be identified to even the subclass level at present. Most of the planispiral records are assumed to be nautiloids (s.s.), although again, their preservation is generally insufficient to allow detailed identification. Other molluscs are relatively rare. There are no obvious records of bivalves on core surfaces, although some are tentatively identified in cross-section in shell-lag layers, and there are only five partial, poorly preserved gastropods recorded throughout the Nambeet Formation, although it is also possible that unrecognized gastropods form part of shell lags.

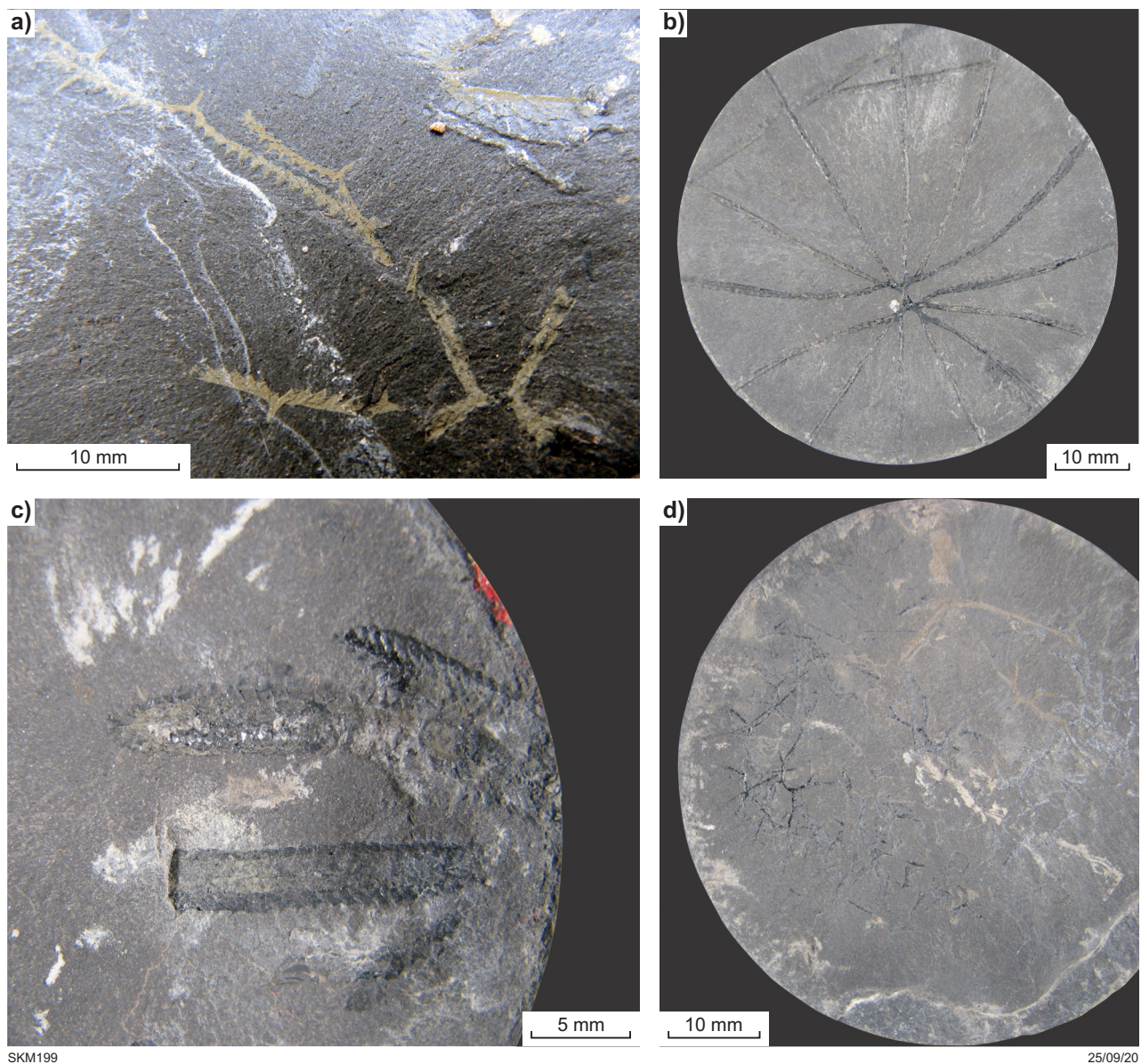


Figure 20. Examples of graptolites from the Samphire Marsh Member: a) a collection of graptolites including specimens likely assignable to the genera *Didymograptus* and *Tetragraptus*, 1197.24 m, CFA7; b) large stellate dichograptid, possibly *Loganograptus*, 1242.41 m, CFA6; c) graptolite group, all likely assignable to *Pseudophyllograptus*, 1244.10 m, CFA6; d) numerous fragmented stellate dichograptids, likely *Clonograptus*, 1356.44 m, CFA2. Note the variation in preservation, with b–d) preserved as carbonized compressions, and a) replaced with a dun-coloured material, possibly jarosite

As mentioned previously, an interpretation of paleoenvironmental change through the member as indicated by the macrofossils requires detailed taxonomic work and could not be achieved during the present project, although it is clear that ample material is available for a study of this type. Overall, the assemblage is strongly dominated by epibenthic taxa, with pelagic (mostly epiplanktic) graptolites and nautiloids *sensu lato* (mostly nekctic) being the main exceptions. Some trilobites are also assumed to be nekto-benthic in nature, although no obvious examples were identified; similarly, there are no obviously infaunal taxa, although semi-infaunal and infaunal inarticulate brachiopods are known from the Lower Ordovician elsewhere in the world and can probably be assumed here (Baliński and Sun, 2013). When considering feeding ecologies, the assemblage includes a wide range of suspension-feeding taxa, including graptolites, brachiopods,

bryozoans and crinoids. Like modern cephalopods, fossil nautiloids *sensu lato* are interpreted to be active predators. Different groups of gastropods and trilobites have various feeding habits, but include likely detritivores, predators and sediment ingesters. All groups are considered euhaline. The dominance of benthic taxa throughout the member suggests mostly shallow (i.e. shelfal, rather than deep basinal water depths) conditions, as pelagic taxa tend to dominate in deep-water assemblages. This agrees well with the interpreted epeiric nature of the Canning Basin during the Ordovician. Despite the preliminary nature of the interpretation, two distinct faunal changes are noted within the Samphire Marsh Member, which will be discussed further here. The first can be observed at around 1340 m (upper CFA2). The section below this depth has no recorded molluscs or crinoids, brachiopods are very common – becoming more common than trilobites – and the only bryozoan fragments appear.

The reason for the different assemblage seen at the base of the Samphire Marsh Member is unclear, but it is unlikely to be entirely attributable to shallow-water conditions, as graptolites, including a small number of supposedly mesopelagic taxa, are present in this lower section. However, some of the mesopelagic graptolites seen in this section are partly jumbled and incomplete compared to records higher up, which might suggest they were transported prior to burial and therefore allochthonous. Alternative interpretations for the unusual assemblage in this section include a strong taphonomic influence, with diagenetic conditions preferentially removing the aragonitic molluscs; or an environment with suboptimal or unstable water oxygenation, water salinity or nutrient levels, with the taxa preserved more tolerant of unstable conditions (or allochthonous). Environmental instability is presently the favoured interpretation, as widespread anoxic conditions are interpreted for CFA1 and CFA2 (see facies association description above), and would certainly have had a strong effect on benthic taxa. An unusual macrofossil assemblage is also recorded in CFA5, with this Facies Assemblage recording much lower rates of macrofossil abundance than the remainder of the Samphire Marsh Member; of the groups recorded in this section only the nautiloids (s.l.) continue with apparently unchanged regularity, with brachiopod, trilobite and graptolite records all strongly reduced or completely absent. This is more likely a taphonomic influence, possibly reflecting the storm-dominated environment interpreted for this Facies Association, with the high levels of oxygenation and periods of high energy likely reducing the preservation potential of smaller, more delicate or more chitinous taxa in preference of larger, more robust, and calcitic taxa (or a combination of these influences). On this basis, the more consistent assemblages seen in the other Facies Associations can probably be interpreted as iterations of more 'normal' death assemblages; that is, those accumulated slowly under average and mostly stable marine-ramp conditions.

Taphonomy

Most fossils were observed in siltstone or shale lithologies, with fewer fossils recorded in limestone sections. This preference is at least partly due to the more regular bedding and higher fissibility of the fine-grained clastic rocks compared to limestones. In Olympic 1, the shale lithologies regularly break apart along bedding surfaces into individual slivers of core a centimetre or so in thickness, although the degree of bedding and fissibility does vary extensively across the cored section. In contrast, limestone beds rarely fracture naturally in any particular orientation, and some calcareous sections are competent for the entire length of the core tray (~1 m). As a result, the surface area of limestone exposed over the entire length of the Olympic core is far less than that of the shales, decreasing the chances for fossils to be exposed and identified. This difference in cementation probably results in a collection bias against fossils preserved in limestone. Due to the fewer core section exposures, most of the limestone-hosted fossils were observed in cross-section in the sides of the core, oriented roughly parallel to bedding. This introduces additional collection and identification biases due to the difficulties inherent in adequately identifying fossils in this orientation; for example, it is difficult to differentiate brachiopod and bivalve shells in cross-section.

Diagenetic processes may also contribute to the fewer fossils observed within limestones. Most of the limestones within the borehole are stylolitic or stylo-nodular in texture, with stylolites developed roughly parallel to bedding. Stylolitic textures are considered indicative of pressure solution during diagenesis, and have been linked to recrystallization, bed-thickness and porosity reduction, and cementation processes (e.g. Tada and Siever, 1989). Although closely associated spatially, the shales and siltstones appear mostly unaffected by dissolution textures, with the effects perhaps ameliorated in part by the low porosity and relatively compressible nature of these clastic sediments, thereby insulating the fossils within. However, the shale-hosted fossils are distinctly flattened (compressions, carbonaceous films, and flattened impressions) compared to fossils in the limestone lithologies, which are commonly rounded and regularly infilled with crystalline (calcitic) cements.

In addition to the relative numbers of fossils, a distinction between the lithology and types of fossils preserved was also observed, with molluscs and brachiopods seen more regularly in limestone, and trilobites, graptolites and chitinous taxa observed almost exclusively within clastic lithologies. Although this superficially suggests a strong association between taxa and lithology, this fossil distribution is just as likely to reflect sampling and post-depositional taphonomic and diagenetic influences. Further work will be needed to tease out all the influences on fossil preservation and preserved fauna in this well.

Micro-brachiopods

Micro-brachiopods were recovered from both carbonate- and mudstone-dominated facies but could not be used to determine age (Appendix 4).

Geochronology

Ten bentonite beds were analysed by CA-IDTIMS at Boise State University, to determine zircon crystallization dates. Six of the 10 samples produced zircons that were able to be dated. One additional bed from the lowermost Willara Formation was analysed and produced a date.

The bentonite bed at 1383.27 m depth at the base of the Samphire Marsh Member was dated at 479.37 ± 0.16 Ma (Fig. 2) or late Tremadocian. A bentonite bed sampled at 1165.44 m from the lowermost Willara Formation returned a date of 470.18 ± 0.13 Ma, which is latest Floian or earliest Dapingian (Fig. 2; Normore et al., 2018).

These dates indicate that deposition of the Nambett Formation began in at least the Tremadocian and continued until the latest Floian or earliest Dapingian and deposition of the Samphire Marsh Member occurred over about a 9–10 Ma period between the Tremadocian and Dapingian. A bentonite bed at the base of CFA6 and the second major mudstone sequence at 1249.31 m, yielded a date of 471.78 ± 0.13 Ma and thus provides a date for the estimated onset of supersequence A1.

Sequence stratigraphic setting

The sequence stratigraphic scheme for the Olympic 1 cored section is based on: a) core lithology, sedimentary

and biostratigraphic features; b) wireline logs and the derivative D-INPEFA logs. The original sequence stratigraphic framework for the Canning Basin was developed by Romine et al. (1994) and Kennard et al. (1994) and remains the reference work for the Ordovician stratigraphy in the basin. These publications describe three sequence levels: first-order cyclicity (megasequences), second-order cyclicity (supersequences) and third-order cyclicity (sequences). This terminology is used throughout this Report. Both Kennard et al. (1994) and Romine et al. (1994) define megasequences, supersequences and sequences as transgressive–regressive (T–R) cycles. In this report supersequences are described in more detail following the terminology of van Wagoner et al. (1990) and Hunt and Tucker (1995).

The Nambet and Willara Formations form the early transgressive phase of the Ordovician–Silurian megasequence defined by Kennard et al. (1994). Supersequences A0 and A1 are identified in the Olympic 1 cored section (Fig. 21) and are clearly defined by the D-INPEFA log trace.

Supersequence A0

The basal siliciclastic sections of the core (SFA1–3) are shallow marine, representing the lowstand phase of supersequence A0. This interval presents as a retrogradational stacking pattern on the GR log and forms the base of a D-INPEFA transgressive trend (Fig. 21). Stacked hardgrounds observed in the lower sections indicate very slow, possibly interrupted sedimentation classic of lowstand deposition where generation of accommodation space is slow. The loss of hardgrounds up-section may be interpreted as a reflection of increasing rates of base-level rise. This siliciclastic sequence overlies basement in other wells and deposition was likely driven by rift-related transgressive sedimentation during initial basin subsidence and subsequent marine incursion.

A major transgressive surface is encountered at 1384.15 m and marks the end of the lowstand systems tract (transgressive ravinement surface on Fig. 19). This surface is preserved as an abrupt erosive contact in the core where a thin grainstone lag overlies the sandstone of the basal siliciclastic sequence (Fly Flat Member; Fig. 22). This is preceded by a brief return to sandstone facies before rapidly transitioning to carbonate facies and the beginning of a >200 m-thick carbonate–mudstone sequence (base of the Sapphire Marsh Member). This boundary also shows a significant concentration of rare earth elements including both light and heavy, and other elements (Fig. 23). Given the erosive nature of this boundary and its position overlying upper shoreface facies, it is interpreted as a transgressive ravinement surface (Nummendal et al., 1987; Catuneanu et al., 2009).

The base of the overlying transgressive sequence consists of sediments deposited in restricted shallow-marine conditions. The initial deposition rate was slow as indicated by stacked and bored hardgrounds. Such slow sedimentation features have been recorded above wave ravinement surfaces in other studies (e.g. Roberts and Boyd, 2011). Transgression is interpreted from the deepening-upwards succession from CFA1 to CFA4. A series of distinct flooding surfaces occur throughout and a significant increase in water depth

is interpreted at about 1351.20 m. This is coincident with a peak in macrofossil abundance at around 1355 m and likely attributed to an increased rate of base eustatic sea level rise. Here the sequence changes up-section from bioclastic packstone–grainstones (*Hn*) interbedded with nodular mudstone (*Ln*) to nodular mudstone dominated by pelagic fossils increasing in abundance up-section. The presence of multiramous graptolites at three depth locations within this transgressive sequence between 1345.20 and 1368.93 m may represent higher order flooding events (compare with Egenhoff and Maletz, 2007).

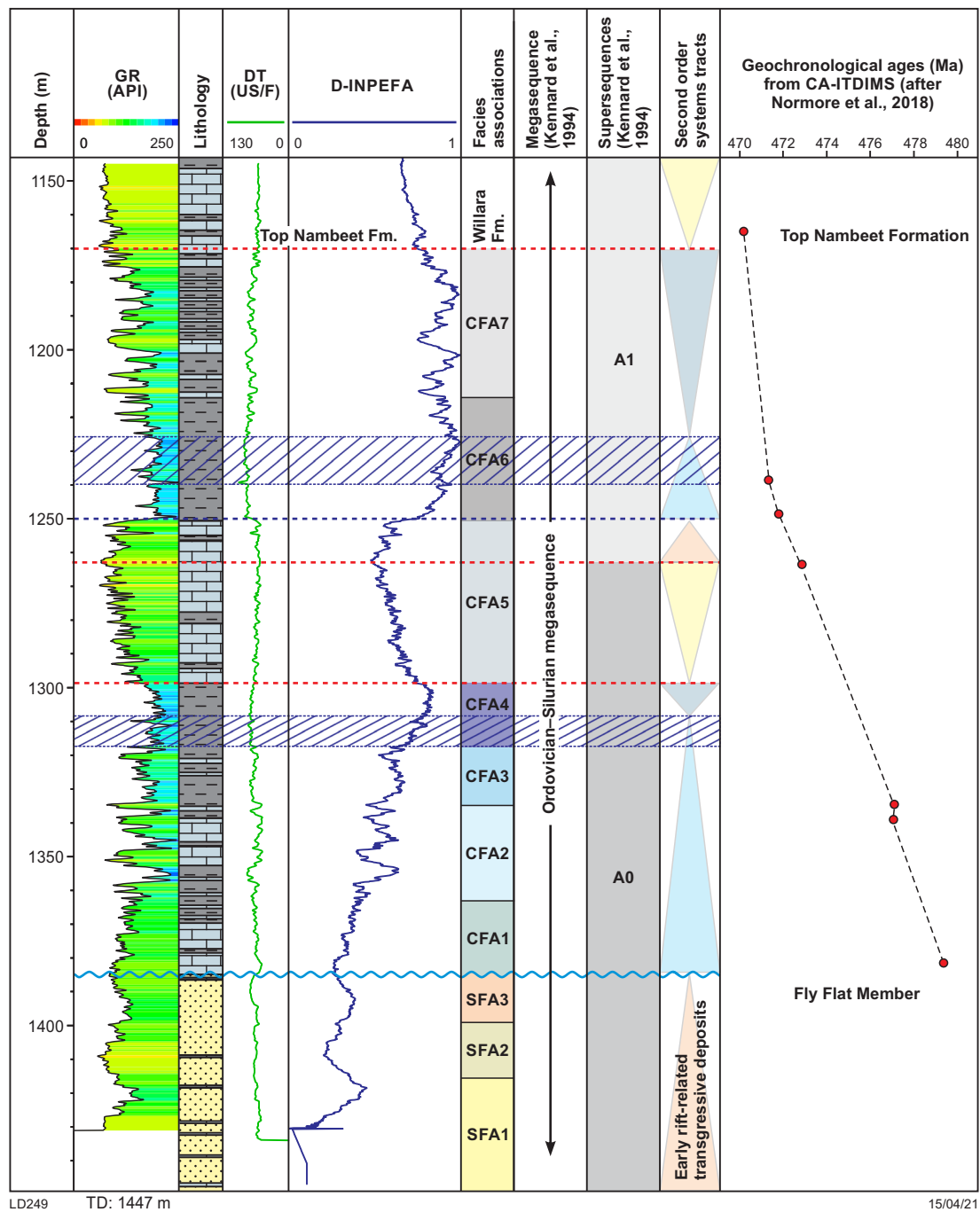
Maximum transgression or the maximum flooding zone (MFZ) is placed between 1319.50 and 1309.50 m. Here the maximum mudstone to carbonate ratio is reached, reflected on the GR log, and the deepest depositional environment of the sequence is interpreted as outer epeiric ramp (CFA4; Fig. 19). The style and character of the carbonate nodules suggests a long residence and slow growth time and a condensed zone is probable given the position in the sequence (Catuneanu et al., 2009). At this point the D-INPEFA trace also reaches a turning point after which it begins a negative trend (towards zero) indicating the beginning of regressive conditions (Fig. 21).

The highstand systems tract is interpreted as a thin interval in the Olympic 1 well. With increasing water depth, carbonate production is not optimal and therefore the distinct aggradational – stacked progradational trends common in siliciclastic systems are not observed. The sequence boundary between highstand and falling stage systems tracts is placed at ~1298 m where the first distinct shallowing of the system occurs. This is identified by the first chaotic carbonate beds or storm beds. These beds contain frequent hardground intraclast lags, which may suggest the development of up-dip hardgrounds during highstand conditions. At ~1285 m, a zone of elemental concentration is recorded in the ICP-MS data as shown by increased values of Th, Pb, Sn, Nb, Ga, Ni, Co, V, Be and Sc, which may suggest up-dip erosive processes commonly associated with sequence boundaries. The upper sequence boundary is picked at 1263 m where there is a turning point in the D-INPEFA log, and a 1.5 m-thick breccia is present.

Supersequence A1

Deposits of the supersequence A1 lowstand are carbonate dominated. These are distinguished from the underlying supersequence A0 sediments deposited during the falling sea-level stage by the presence of distinct well-developed hardgrounds with borings. The appearance of boring trace fossils indicates not only lithification and slow sedimentation but may also indicate episodes of non-deposition (Christ et al., 2015) interpreted as the slow change of base level associated with lowstand conditions. Lowstand deposition in supersequence A1 occurred in deeper water settings than in lowstand deposition in supersequence A0 due to the progression of the concurrent first-order (megasequence) Ordovician–Silurian transgression.

The A1 transgressive surface is placed at 1250 m depth. This major flooding surface is identified by the rapid change in lithology from carbonate-dominated to mudstone, an abrupt deepening of depositional setting from middle ramp (CFA5) to outer ramp (CFA6), and a distinct increase in GR log values (Fig. 21). The MFZ within supersequence A1 is placed within



Facies association	
CFA7	Middle ramp
CFA6	Outer ramp
CFA5	Middle-ramp storm dominated
CFA4	Middle-outer ramp
CFA3	Middle ramp
CFA2	Inner-middle ramp (restricted)
CFA1	Inner ramp (restricted)
SFA3	Upper-middle – upper shoreface
SFA2	Lower – middle shoreface
SFA1	Upper-lower – upper-middle shoreface

Surfaces	
---	Transgressive surface
~~~~~	Transgressive ravinement surface
▨	Maximum flooding zone
---	Sequence boundary

System tracts	
Light blue	Transgressive
Dark blue	Highstand
Yellow	Falling stage
Orange	Lowstand

Figure 21. Sequence stratigraphic framework for the Olympic 1 cored section. Geochronological ages plotted against depth to illustrate general deposition rate



the depth range of about 1225–1240 m coinciding with the second peak in macrofaunal abundance, a close proximity (within 3 m) to multiramous dichograptids occurrences, and the highest GR values corresponding to the interval of zero carbonate content recorded by the TIR spectral data (Fig. 7). A second major concentration of elements is recorded in the ICP-MS data at this point in the sequence, including increased concentrations of light rare earth elements Sm, Nd, Pr, Ce, La, Gd, Eu, redox sensitive elements Co, Cr and V and others including Cs, Sn, Nb, Rb, Gd, Ni, Be and Sc, and may be the result of a condensed zone.

The beginning of the A1 highstand systems tract is interpreted to start at approximately 1225 m where carbonate lithologies reappear and gradually increase upwards. After this point in the sequence CA-IDTIMS dates suggest a rapid increase in sedimentation rate. If bentonite dates are plotted against sediment thickness to produce a rudimentary estimate of sediment accumulation rates, a threefold increase in depositional rate is observed in the approximately 74 m above 1239.27 m when compared to the 144 m below (Fig. 21). This estimate does not consider the effect of condensed sections or the small hiatuses indicated by hardgrounds. Differential compaction of mudstone and carbonate lithologies are also not considered in this estimate.

The falling stage systems tract is tentatively placed at about 1170 m. No distinct features were observed in the cored section here, but the D-INPEFA signature begins a major regressive trend around this depth and the TIR spectral data shows a small influx of quartz into the system followed by almost total domination of carbonate lithologies (Fig. 7). The beginning of the falling stage is also coincident with the beginning of the Willara Formation.

## Depositional model

The Fly Flat Member in Olympic 1 was deposited in open-marine, upper-lower shoreface settings and is evidence of a marine incursion into the newly rifted Canning Basin. The consistent fine-grained character of the member, dominance of lower energy deposits and development of shallow-marine hardgrounds suggests a protected setting with low wave energy (Clifton, 2006) or microtidal conditions. Such conditions could be attributed to an epeiric sea-type environment (e.g. Choi and Simo, 1998), consistent with a shallow transgressive sea filling a rifted basin. The immaturity of the deposits is reflected in the high K-feldspar content of the sandstones, which can be up to 23.8 weight percent (wt%) of the rock determined by XRD analysis.

With so little cored section available through the Nambeet sandstone section, interpretation of depositional setting in a broader context is limited. At the time of Nambeet Formation deposition the Broome Platform was dipping gently to the north (Romine et al., 1994). Borehole data from Looma 1, located to the south east of Olympic 1 on the Broome Platform (Fig. 1), indicates north–south-trending paleocurrents on low-angle bedding. The sandstone section in this well is interpreted as a shallow-marine shelf–shoreline system that trends east–west, consistent with the shallow-marine shoreface model for Olympic 1 presented in this Report. Stream mouth bars and tidal channels are also interpreted (Phipps et al., 1998). This model is further

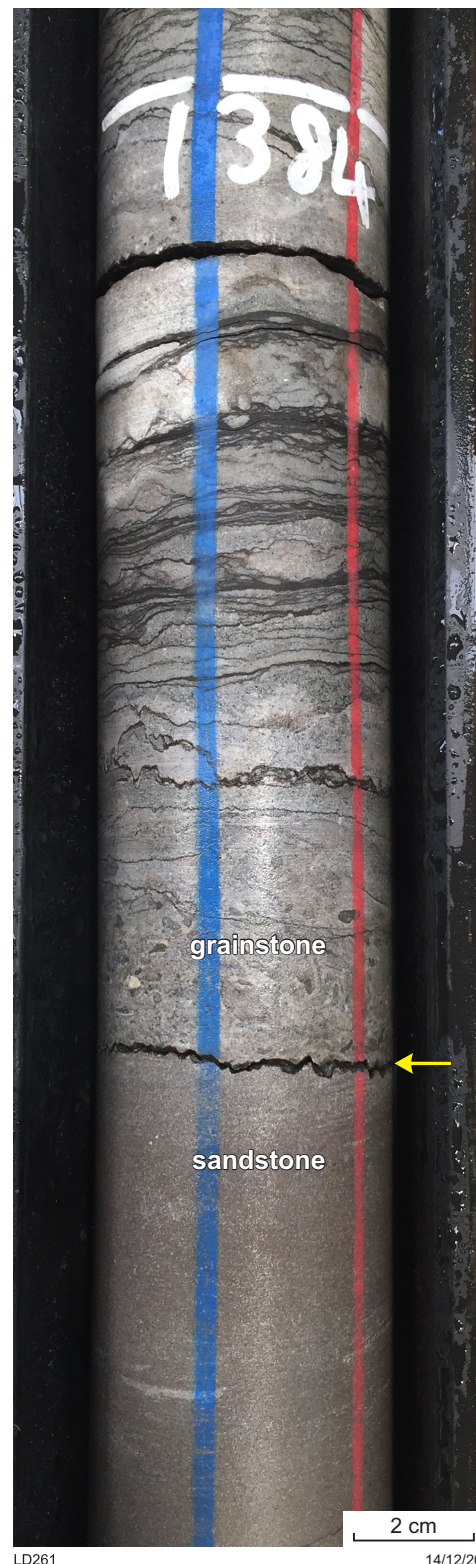


Figure 22. Core photograph showing the first major transgressive boundary (yellow arrow) in the Olympic 1 cored section, where an abrupt erosive contact occurs between sandstone and overlying grainstone at 1384.15 m



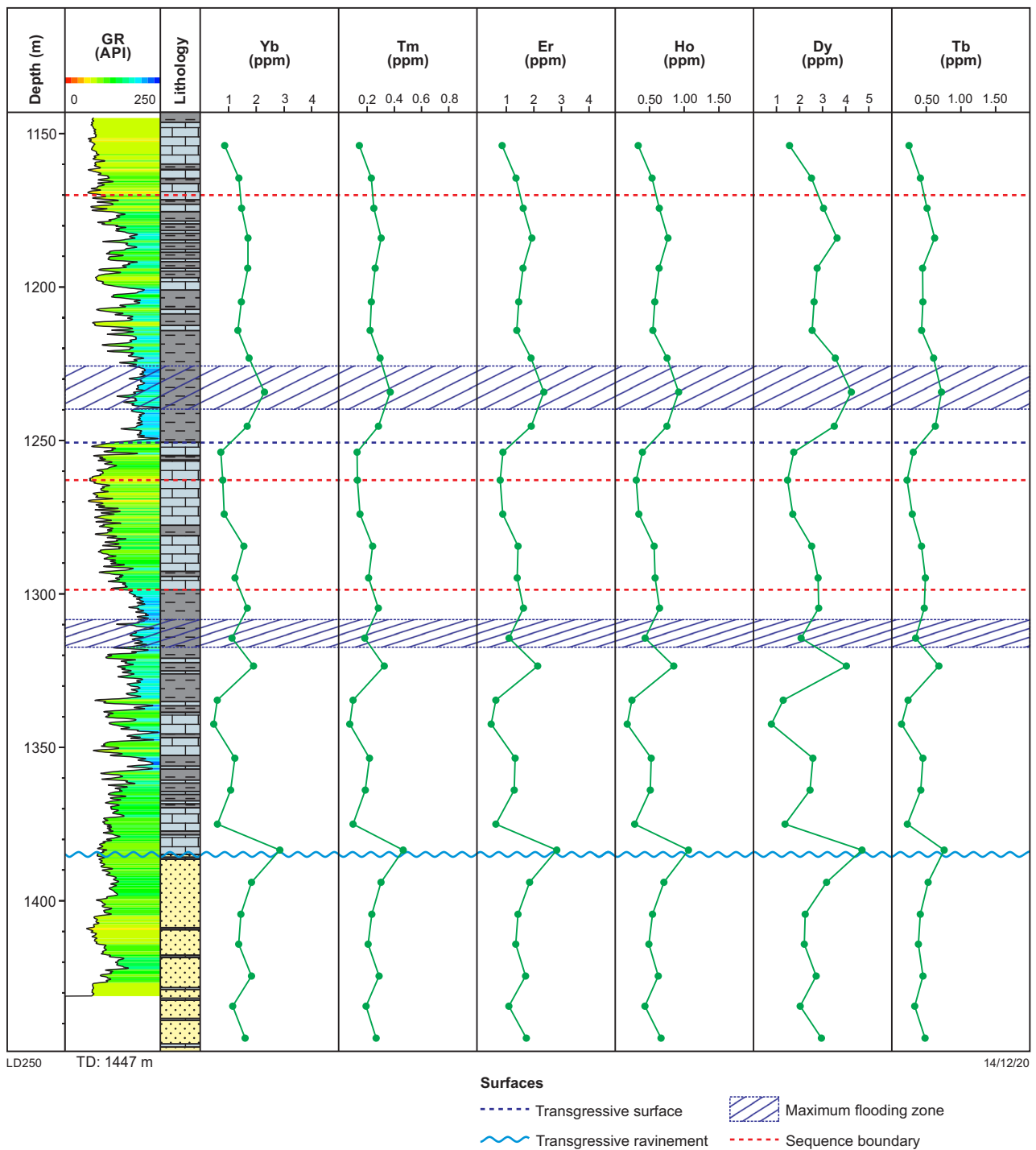


Figure 23. Concentration of heavy rare earth elements through the Nambéet Formation recorded by ICP-MS analysis

supported by the ?fluvial–?marginal marine interpretation of the Fly Flat Member equivalent in Dodonea 1 on the Barbwire Terrace (Hough and Weeden, 1986) and in Percival 1 (France, 1986) over 200 km to the southeast on the Barbwire Terrace (Fig. 1).

The sharp change from clastic-dominated deposits of the Fly Flat Member to the initially carbonate-dominated lithology of the overlying Samphire Marsh Member observed in Olympic 1 is interpreted to be the product of a second-order transgressive event resulting in widespread flooding and significant back-stepping of the paleoshoreline. Above and below the transgressive surface are shallow-water deposits,

and the main effect of the transgression was an abrupt cut-off of siliciclastic supply. The result was inundation of the Broom Platform to form a large shallow sea with a structure comparable to an epeiric platform or low-angle epeiric ramp.

An epeiric platform – epeiric ramp model is suggested based on two key characteristics of the sequence. First, the dominance of low-energy deposition in both proximal and distal settings. Inner-ramp areas in open oceans are generally characterized by high-energy deposition (Flügel, 2004); however, in epeiric seas both inner and outer areas are characterized by low-energy deposition (Irwin, 1965). This effect is observed in the shallow-water deposits

of CFA1 at the base of the Samphire Marsh Member, which are overlain by a series of carbonate-dominated lithologies from deeper low-energy environments CFA3, CFA4 and CFA6. Low-energy calcareous rhythmites are a common deposit in epeiric seas and on epeiric ramps (Westphal and Munnecke, 2003; Westphal et al., 2008) due to low sedimentation rate, shallow wave base and low relief. These processes favour fine-grained sedimentation and development of early diagenetic carbonate features such as the abundant carbonate nodules recorded from Olympic 1 (Wright and Burchette 1998; Westphal et al., 2008).

The second major indicator of epeiric settings is the presence of anoxic to euxinic conditions in shallow carbonate-producing environments. The vast expanses of shallow water in epeiric seas are thought to prevent or limit tide-processes causing development of large proximal areas with poor circulation (Flügel, 2004); in the classic epeiric sea model by Irwin (1965) these are defined as zone Z (Fig. 11). Anoxic to euxinic conditions are interpreted in the basal, shallow-marine sections of the Samphire Marsh Member (CFA1 and CFA2) in Olympic 1 and can likely be attributed to this effect.

The Samphire Marsh Member shows similar well log (gamma) signatures in wells proximal to Olympic 1, including Thangoo 2, Twin Buttes 1, Aquila 1 and Hedonia 1, consistent with transitional settings on a shallow inclined ramp. Thinner intervals of the Samphire Marsh Member are interpreted from wireline logs in wells drilled further to the south and east such as Pictor 1, Looma 1, Missing 1 and Edgar Range 1 (Appendix 1). This is consistent with gradual restriction of the marine system in more proximal settings and the resulting reduction in accommodation space within this ramp-style environment.

Moving east of Olympic 1 the lower Samphire Marsh Member preserves increasingly siliciclastic lithologies with common sandstone, sandy limestone and siltstone. (e.g. Setaria 1, Acacia 2, Dodonea 1, Mirbelia 2; Appendix 1). In these wells the transition to carbonate–mudstone-dominated lithofacies occurs only in upper parts of the member. D-INPEFA signatures indicate that carbonate–mudstone lithologies become dominant where the second major transgressive surface, at the base of CFA6, is encountered in Olympic 1. In these wells it is likely that the carbonate–mudstone package represents only the A1 transgressive–regressive cycle.

## Correlation

### Interformation correlation

#### Wilson Cliffs Sandstone

The Wilson Cliffs Sandstone is equivalent to the Fly Flat Member and possibly includes proximal equivalents to the lower sections of the Samphire Marsh Member of the Nambett Formation (Fig. 3). Conodont biozones have been determined from two of the four wells that contain the Wilson Cliffs Sandstone: Wilson Cliffs 1, Kidson 1, Patience 2

and Contention Heights 1. The *P. elegans* – *Berg. extensus* biozone is recorded through a significant depth interval (~375 m), and almost to the top of the formation in the type section at Wilson Cliffs 1 (Nicoll, 1993; Appendix 1). In this well a distinct change in lithofacies from sandstone and sandy limestone to mudstone is identified at the top of the Wilson Cliffs Sandstone. This lithological boundary is seen in all four wells where the formation is interpreted to be present (Appendix 1).

Previous interpretations (Haines, 2011) suggest that, in these four wells, the Wilson Cliffs Sandstone is unconformably overlain by the Goldwyer Formation. The *Phragmodus*–*Plectodina* and *Histodella holodenata* biozones are recorded in the mudstone–siltstone sequence overlying the Wilson Cliffs Sandstone in both Wilson Cliffs 1 and Contention Heights 1 wells. The *H. holodenata* biozone is recorded in the Goldwyer Formation and is well accepted to indicate the middle Darriwilian (Zhen et al., 2020). The Goldwyer Formation records a major transgressive event in the Canning Basin (Kennard et al., 1994), and interpretation of the formation overlying the Wilson Cliffs Sandstone is supported by the D-INPEFA correlation which consistently show transgressive trends over these mudstone–siltstone sequences.

Conversely, conodont biostratigraphy from Contention Heights 1 indicates that the interval directly above the Wilson Cliffs Sandstone contains faunas probably indicative of the *J. gananda* biozone (Nicoll, 1993). This biozone is now affiliated with the Willara Formation (Zhen et al., 2017). Samples with the potential *J. gananda* identification were taken from ditch cuttings, and we suggest that the material from Contention Heights 1 may need to be revised. The more confident identification of the *Phragmodus*–*Plectodina* and *H. holodenata* biozones in Wilson Cliffs 1 and Contention Heights 1, lithological changes, and D-INPEFA trends support interpretation of the Goldwyer Formation overlying the Wilson Cliffs Sandstone in this area of the basin. Further, the Willara Formation was deposited during a major regression. It seems unlikely that sediments deposited during a major regression would be represented by finer-grained marine deposits than that of the preceding transgressive phase.

One issue that remains unresolved is the two-part division of the Wilson Cliffs Sandstone at its type section. The upper portion is defined as a white, very fine- to fine-grained sandstone. The lower portion is red-brown and ferruginous with common medium to coarse grains. Both sections are tight and highly silicified with common quartz overgrowths (Creevey, 1969).

An unnamed sandstone package is also intersected in Patience 2 below the described Wilson Cliffs Sandstone. Haines (2011) suggests that this potentially correlates to some or all of the sandstone in Wilson Cliffs 1 or, represents a previously unreported older unit. It may also be possible that the lower sandstone package in Wilson Cliffs 1 and the unnamed sandstone package in Patience 1 are correlatives of the Fly Flat Member in Olympic 1. Considering the transition in lithology at the base of the Samphire Marsh Member between Olympic 1 and eastern wells, for example Setaria 1, Acacia 2, Dodonea 1 and Mirbelia 2, the upper sandstone in Wilson Cliffs 1 may represent a localized section of the most proximal Samphire Marsh Member deposits.

## Prices Creek Group

The Kunian Sandstone, the lowest formation in the Prices Creek Group, is described by Nicoll et al. (1993) as a 'quartz-lithic arenite with occasional glauconite-rich units throughout'. Nicoll et al (1993) interpreted the Kunian Sandstone as the basal transgressive unit of the basin based on the regional tectonic framework and lithology and consider it equivalent to what McTavish and Legg (1976) describe as the basal transgressive sands of the Nambeet Formation. The sandstone does not contain any fossil material (Zhen and Nicoll, 2009) but biostratigraphic control from the overlying Kudata Dolomite support this interpretation. As such it is considered to be equivalent to the lower Fly Flat Member.

The Kudata Dolomite does not contain datable macrofossils, but conodont species recovered suggest a Tremadocian age (Nicoll et al., 1993). Conodonts recovered from the Kudata Dolomite in BHP PCD 158 and the lowest datable Nambeet Formation conodont samples in Samphire Marsh 1 are assigned to the same biozone, *Drepanastodus-Paltodus* (Nicoll et al., 1993). Nicoll (1993) also tentatively identifies the *P. elegans* – *B. extensus* biozone in the Kudata Dolomite in the Grevillea 1 petroleum exploration well on the Lennard Shelf (Fig. 1). This suggests equivalence to either the Fly Flat Member or the lower part of the Samphire Marsh Member.

The Emanuel Formation is designated an age range from the Tremadocian to the Floian (Zhen and Nicoll, 2009; Zhen et al., 2017). The *Prioniodus adami* – *S. bilobatus* biozone is identified in the middle and upper Emanuel Formation (Zhen and Nicoll, 2009). The contact with the overlying Gap Creek Formation is interpreted at the first appearance of *O. communis* and the coinciding eponymous biozone (Nicoll and Ethington, 2004; Zhen and Nicoll, 2009). This indicates that the Emanuel Formation is equivalent to the lower part of the Samphire Marsh Member and possibly the upper part of the Fly Flat Member.

The *J. gananda* biozone has been identified in the Gap Creek Formation at the top of the Prices Creep Group from the Grevillea 1 well (Nicoll, 1993). This suggests that the Gap Creek Formation may be an equivalent to the upper part of the Samphire Marsh Member and lower Willara Formation (Fig. 3).

## Intraformation member correlation

### Chemostratigraphy

The new Fly Flat and Samphire Marsh Members can be correlated between wells using chemostratigraphic techniques where data exists. ICP-MS analysis was conducted on samples collected at approximately 10 m intervals across the cored section and at 20 m intervals within cuttings in the Olympic 1 well. Analytical methods are detailed in Chemostrat Australia (2016).

Chemostratigraphy characterizes and categorizes sediments based on their inorganic geochemical composition. Defining geochemical signatures or 'fingerprints' for packages of rock facilitate the correlation of like signatures between wells. More detail on the

process of defining geochemical signatures can be found in Chemostrat Australia (2016). Four geochemically distinct packages were identified in Olympic 1 (Fig. 24), S1-P2 to S1-P5. Distinction of these packages was based largely on variations in K/Rb, Ti/Zr and Th/U values, and levels of Cu and enrichment factor of molybdenum (EFMo) identified in Chemostrat Australia (2016) and summarized in Table 9.

The four packages identified in Olympic 1 were correlated to Canning Basin wells Nicolay 1 and Sally May 2, which also cored sections through the Willara and Nambeet Formations (Fig. 24). Based on the correlation to Sally May 2 and Nicolay 1, S1-P2 – S1-P4 identified divisions within the Nambeet Formation and S1-P5 occurred in the upper Nambeet Formation and lower Willara Formation. S1-P2 defines the Fly Flat Member while the S1-P3 – S1-P4 boundary is placed just below ~1270 m and divides the Samphire Marsh Member into two mudstone-carbonate progressions in the Olympic 1 well. The S1-P3 – S1-P4 boundary in Olympic 1 coincides with a third-order sequence boundary representing a point of maximum regression and separating two second-order cycles, A0 and A1, within the Samphire Marsh Member (Fig. 19).

## Economic geology

### Reservoir potential

#### Fly Flat Member

The Fly Flat Member generally has low measured core porosity and permeability in Olympic 1 (Fig. 25). Grain size is consistent throughout the member (very fine sand size), and the lower porosity values are attributed to the abundance of diagenetic quartz and carbonate cements. Scanning electron microscope analysis reveals some microporosity between clay flakes. Despite promising porosity of over 10% at the top of the Fly Flat Member in Olympic 1, elsewhere the basin porosity is poor to very poor, and well-cemented sandstone with both silica and carbonate cement frequently described. Based on XRD measurements, the poor permeability in Olympic 1 is not directly related to the clay content; illite/smectite, illite/mica and chlorite. The low permeability may be attributed to siltstone volume and, more likely, to the heterogeneity produced by bioturbation.

Porosity and permeability are highest in SFA3, middle to upper shoreface facies. This facies association has the lowest levels of siltstone and bioturbation recorded. SFA3 also has the highest levels of K-feldspar, which are commonly dissolved to form secondary porosity, and shows extensive dissolution of carbonate allochems not observed in SFA1 and SFA2. Increased porosity and permeability in upper shoreface environments are consistent with the general model of reservoir quality increasing up-section along a shoreface profile (Howell et al., 2008). This being the case, the best reservoir quality may be expected in wells east of Olympic 1 where more proximal upper shoreface and possibly foreshore sandstone would be deposited. Overall, the Fly Flat Member in Olympic 1 is a poor reservoir for oil but may be fair to good for gas.



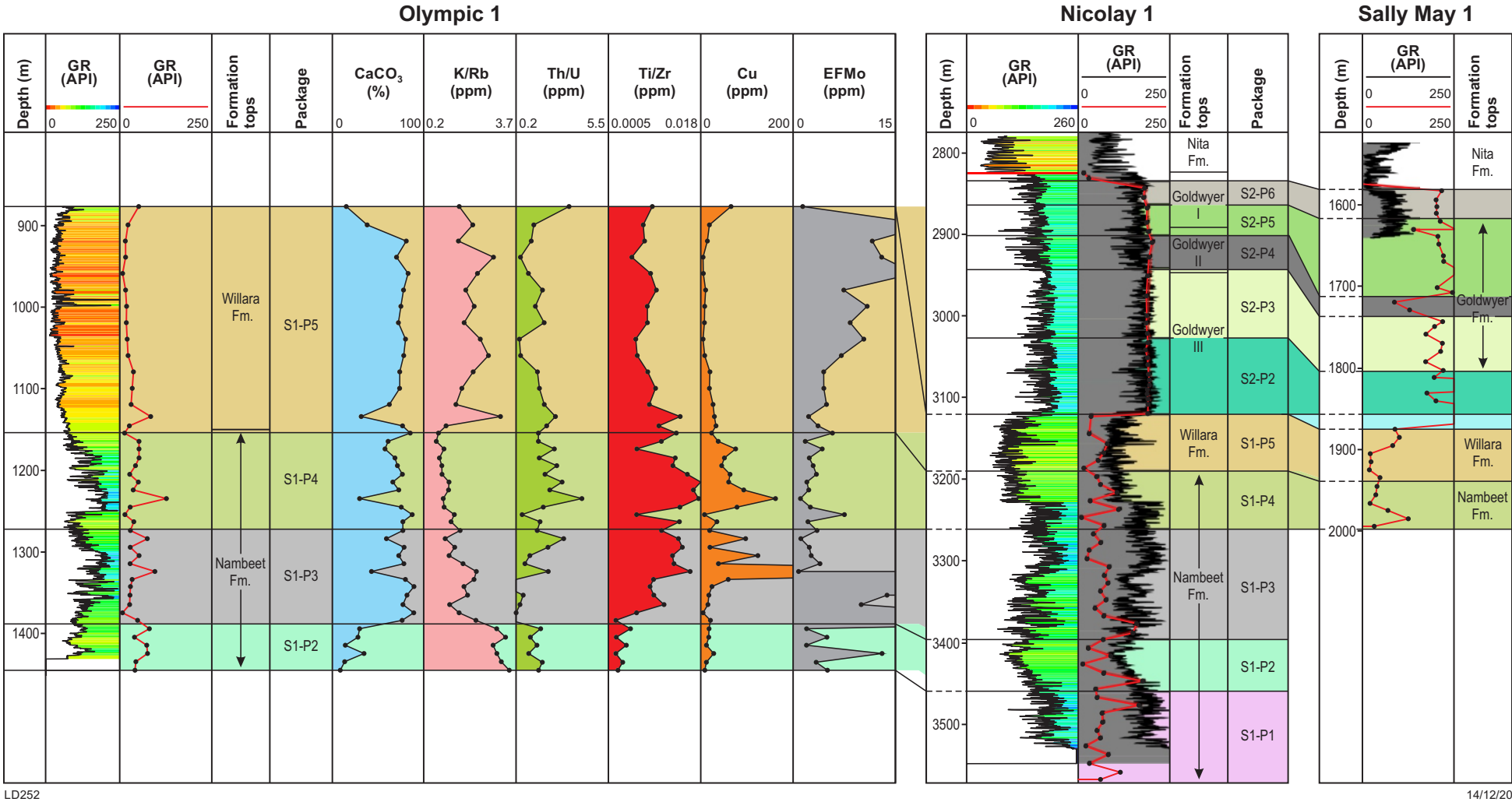


Figure 24. Chemostratigraphic packages of Olympic 1 correlated to Nicolay 1 and Sally May 2 (Chemostrat Australia, 2016). The red GR trace represents a chemical or calculated gamma value, see Chemostrat Australia (2016) for details

**Table 9. Distinguishing geochemical characteristics of the chemostratigraphic packages identified in Olympic 1, information summarized from Chemostrat Australia (2016)**

Depth (m)	GSWA sample number	Calculated age (Ma)	Mean square weighted deviation
1165.44	221598	470.18 ± 0.13	1.9
1239.27	221599	471.32 ± 0.11	1.0
1249.31	221600	471.78 ± 0.13	1.7
1264.61	221474	472.82 ± 0.13	0.6
1279.96	221475	Unproductive sample (non-uniform zircons)	-
1317.05	221476	Unproductive sample (non-uniform zircons)	-
1335.03	221477	477.07 ± 0.21	3.8
1339.56	221478	477.03 ± 0.16	1.4
1369.38	221479	Unproductive sample (non-uniform zircons)	-
1376.44	221496	Unproductive sample (no zircons)	-
1383.27	221480	479.37 ± 0.16	0.6

## Samphire Marsh Member

Porosity and permeability in the Samphire Marsh Member in Olympic 1 are low. The majority of carbonates are wackestone to grainstone. The principal pore types in both claystone, mudstone and carbonate lithologies are micropores, occurring between detrital clay flakes and micritic crystals. In mudstone lithologies, there is a weak correlation between increased clay content and decreased porosity. Minor secondary porosity is generated in carbonates by dissolution of bioclasts to form vugs (Fig. 18b). The diagenetic sequence in Olympic 1 shows that this secondary vug formation is the main porosity-enhancing event and occurs early. Later vugs are influenced by porosity-reducing events, including calcite and dolomite cementation. In general, the Samphire Marsh Member does not present good potential reservoir due to low measured core porosity and permeability (all under 1 mD) in both mudstones and carbonates (Fig. 25).

## Source and hydrocarbon potential

### Fly Flat Member

Olympic 1 has the most promising residual oil show in the formation, about 30 cm thick, in the upper section of the Fly Flat Member (Fig. 26). This show occurs at the boundary between SFA2 and SFA3 in thinly interbedded sandstone facies (*Hb*, *Sp* and *Sx*). The residual hydrocarbons are strongly facies controlled and their presence is related to lower levels of cementation (Fig. 26). The confinement of hydrocarbons to this thinly interbedded transition zone may reflect a local stratigraphic trapping mechanism between the lower permeability highly bioturbated silty sandstone beds (*Hb*) and more favourable planar-laminated (*Sp*) and cross-laminated sandstone (*Sx*) facies.

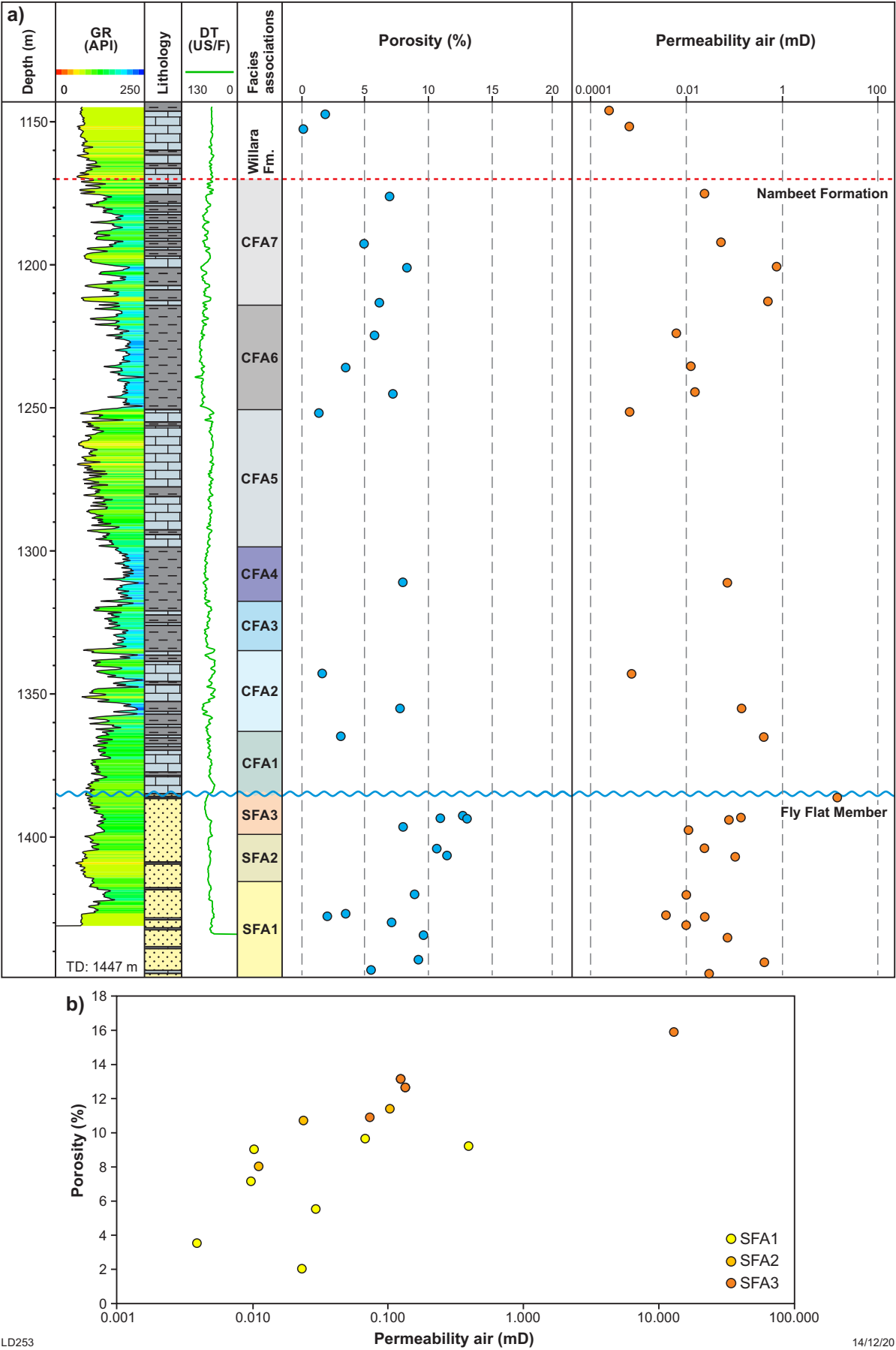
Minor gas peaks, predominantly C1, were recorded in a few wells and trace bitumen is documented in Olympic 1 and Hilltop 1 (Appendix 5). Fluorescence and minor shows are recorded in Olympic 1, Acacia 1, Sally May 2 and Setaria 1 (Appendix 5).

## Samphire Marsh Member

Traditionally the Nambeet Formation has been identified as a potential source rock in the Canning Basin but most data indicate low potential at best (Normore and Dent, 2017b; Fig. 27). An extensive set of TOC – Rock-Eval analyses across the Samphire Marsh Member in the Olympic 1 well shows two organic-rich zones (Fig. 5). These two zones correspond to the two mudstone-dominated intervals in the member.

The stratigraphically lower mudstone interval is more prospective for TOC, with fair to very good source potential and a maximum TOC value recorded at 3.28% (Fig. 25), while the upper mudstone interval is interpreted to have fair to good source potential (Fig. 27; Normore and Dent, 2017b). When evaluated from  $S_2$  values the source potential is fair in both intervals (Fig. 27). Rock-Eval analysis suggests Type II/III marine kerogens and a gas-prone source (Normore and Dent, 2017b). Strictly, a Type III source is impossible due to the absence of land plants at this time, further discussion on this can be found in Normore and Dent (2017b).

Minor quantities of gas have been recorded from the Samphire Marsh Member with the most notable being gas that flowed in Dodonea 1 at a rate of 85 m³/day from a drill stem test (Appendix 4). Rare residual hydrocarbons are observed in some wells and bitumen is associated with fractures in mineral hole PCD-158 (Appendix 4). Minor fluorescence and oil bleeds were observed in the Olympic 1 well associated with vugs in the otherwise tight carbonate facies.





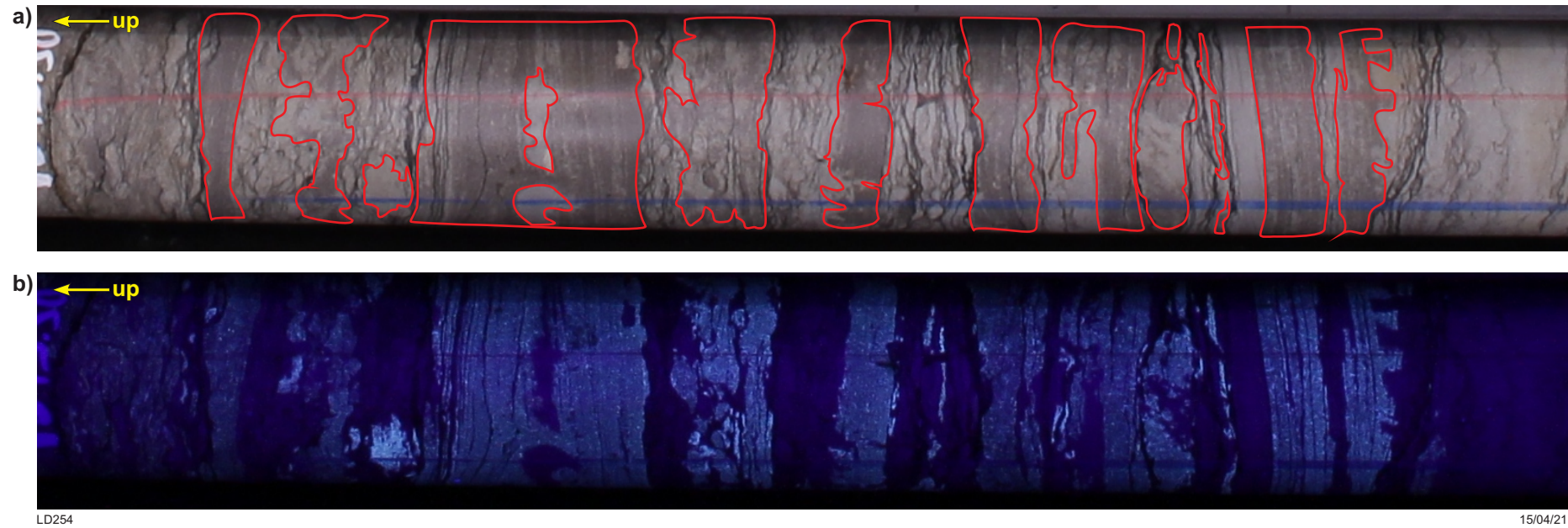
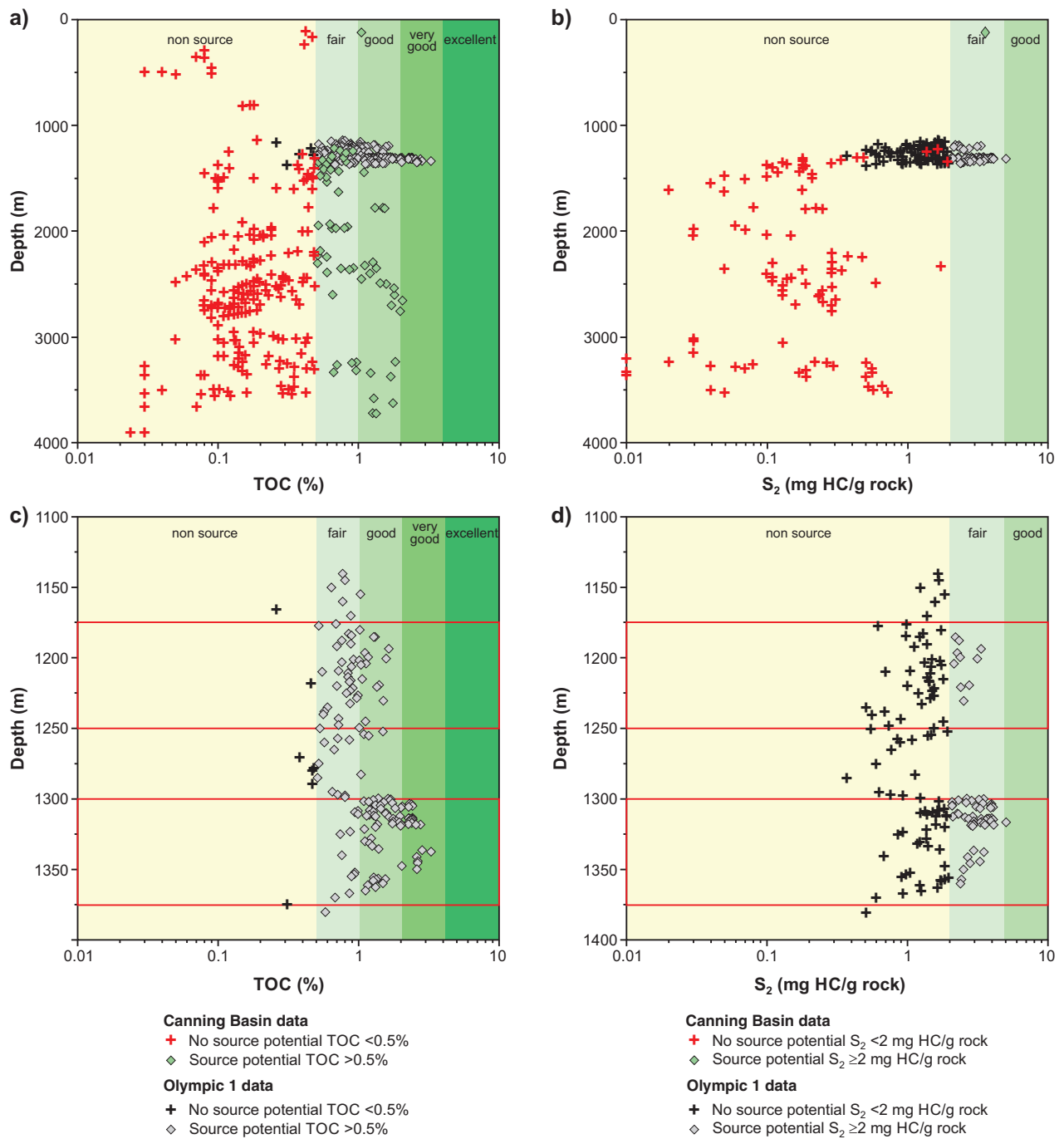


Figure 26. Core photos showing a 30 cm-long residual hydrocarbon show in Olympic 1: a) under white light; b) under ultraviolet light. Fluorescence, indicating the presence of hydrocarbons, is mainly associated with planar-laminated facies outlined in red, while interbedded, bioturbated sandstone lacks fluorescence



LD264

14/12/20

Figure 27. Source potential of the Nambeet Formation, historical data compared to new data from Olympic 1 (Normore and Dent, 2017b): a) TOC data from the Nambeet Formation, Canning Basin; b)  $S_2$  data from the Nambeet Formation, Canning Basin; c) TOC data from the Nambeet Formation in Olympic 1; d)  $S_2$  data from the Nambeet Formation in Olympic 1

## Conclusions

The 277.53 m of continuous core through the Nambett Formation in Olympic 1 well provides an excellent reference section for the formation.

The section can be divided into two members. The lower of these, the Fly Flat Member, is a subarkose siliciclastic sequence that overlies basement in Olympic 1. The member is divided into three facies associations SFA1–3 that record deposition in shallow-marine shoreface environments. Based on the presence of the *P. proteus* conodont biozone in the upper part of the Fly Flat Member in Olympic 1, deposition is estimated to have begun and ended in the Tremadocian. The member is interpreted as the earliest transgressive phase in the basin and marks the beginning of the A0 supersequence.

The overlying Samphire Marsh Member, a mixed carbonate–mudstone unit in Olympic 1, is comprised of seven facies associations CFA1–7 that record deposition in an epeiric sea along a low-angle ramp or platform type system. More proximal deposits of the member to the east of Olympic 1 contain variable amounts of sandstone and siltstone. Based on CA-IDTIMS zircon dates, ranging from  $479.37 \pm 0.18$  Ma at the base of the member to  $470.18 \pm 0.13$  Ma in the lowest part of the overlying Willara Formation, deposition of the Samphire Marsh Member is interpreted to have started in the Tremadocian and continued until the latest Floian. This age range is supported by the presence of conodont biozones *P. proteus* to *J. gananda*. The Samphire Marsh Member records the upper transgressive and regressive phase of supersequence A0 and the transgressive phase of the succeeding A1 supersequence.

Reservoir potential of both members in Olympic 1 is poor with sandstones of the Fly Flat Member having low porosity and permeability due to the occlusion of intergranular space by quartz overgrowths and calcite cements. The Samphire Marsh Member shows some potential as a source interval, particularly in the lower part of the stratigraphic section where TOC reaches a maximum of 3.28%.

## References

- Amberg, CEA, Collart, C, Salenbien, W, Eggern, LM, Munnecke, A, Nielsen, AT, Monnet, C, Hammer, O and Vandenbroucke, TRA 2016, The nature of Ordovician limestone-marl alternations in the Oslo-Asker District (Norway): witnesses of primary glacio-eustasy or diagenetic rhythms? *Scientific reports*, p. 1–13.
- Baliński, A and Sun, Y 2013, Preservation of soft tissues in an Ordovician linguloid brachiopod from China: *Acta Palaeontologica Polonica*, v. 58, p. 115–120.
- Buatois, LA, Mangano, GM and Carr, TR 1999, Sedimentology and ichnology of Paleozoic estuarine and shoreface reservoirs, Morrow Sandstone, Lower Pennsylvanian of southwest Kansas, USA: *Midcontinent Geoscience*, p. 1–35.
- Buatois, LA, Mángano, MG, Alissa, A and Carr, TR 2002, Sequence stratigraphic and sedimentologic significance of biogenic structures from a late Paleozoic marginal- to open-marine reservoir, Morrow Sandstone, subsurface of southwest Kansas, USA: *Sedimentary Geology*, v. 152, p. 99–132.
- Catuneanu, O, Abreu, V, Bhattacharya, JP, Blum, MD, Dalrymple, RW, Eriksson, PG, Fielding, CR, Fisher, WL, Galloway, WE, Gibling, MR, Giles, KA, Holbrook, JM, Jordan, R, St. Kendall, CGC, Macurda, B, Martinsen, OJ, Miall, AD, Neal, JE, Nummedal, D, Pomar, L, Posamentier, HW, Pratt, BR, Sarg, JF, Shanley, KW, Steel, RJ, Strasser, A, Tucker, ME and Winker, C 2009, Towards the standardization of sequence stratigraphy: *Earth Science Reviews*, v. 92, p. 1–33.
- Chemostat Australia 2016, Chemostratigraphic analysis of the Ordovician in the Canning Basin, Western Australia: Geological Survey of Western Australia, W21660 A3, 41p.
- Choi, YS and Simo, JA 1998, Ramp facies and sequence stratigraphic models in an epeiric sea: the Upper Ordovician mixed carbonate-siliciclastic Greenwood and Platteville Formations, Wisconsin, USA, in *Carbonate Ramps edited by* VP Wright and TP Burchette: Geological Society, London, Special Publications 149, p. 437–456.
- Christ, N, Immenhauser, A, Wood, RA, Darwich, K and Niedermayr, A 2015, Petrography and environmental controls on the formation of Phanerozoic marine carbonate hardgrounds: *Earth Science Reviews*, v. 151, p. 176–226.
- Clifton, HE 2006, A re-examination of facies models for clastic shorelines, in *Facies Models Revisited edited by* HW Posamentier and RG Walker: SEPM Society for Sedimentary Geology, v. 84, p. 293–338.
- Cohen, KM, Finney, SC, Gibbard, PL and Fan, J-X 2020, The ICS International Chronostratigraphic Chart (v 2020/03 update): *Episodes*, v. 36, p. 199–204.
- Combaz, A and Peniguel, G 1972, Etude palyno-stratigraphique se l'Ordovicien dans quelques sondages du Bassin de Canning (Australie Occidentale): *Bulletin du Centre de Recherches Pau-SNPA*, v. 6, p. 121–167.
- Cooper, RA 1998, Towards a general model for the depth ecology of graptolites, in *Proceedings of the sixth International Graptolite Conference and 1998 Field meeting IUGS Subcommission on Silurian Stratigraphy edited by* JC Gutiérrez-Marco and I Rábano, Madrid, Tamas Geológico-Mineros ITGE 23, p. 161–163.
- Cooper, RA 1999, Ecostratigraphy, zonation and global correlation of earliest Ordovician planktic graptolites: *Lethaia*, v. 32, p. 1–16.
- Cooper, RA, Fortey, RA and Lindholm, K 1991, Latitudinal and depth zonation of early Ordovician graptolites: *Lethaia*, v. 24, p. 199–218.
- Creevey, KJ 1969, Wilson Cliffs No. 1, PE 152, Western Australia, well completion report: Australian Aquitaine Petroleum Pty Ltd: Geological Survey of Western Australia, Statutory petroleum exploration report S419 A1, 40p.
- Dent, LM and Normore, LS 2017, Assessment of thermal maturity using bitumen, graptolite, and bioclast reflectance: Ordovician Nambett Formation, Canning Basin: Geological Survey of Western Australia, Report 170, 1111p.
- Donovan, JK 1992, Depositional environments and paleoecology of the Lower Ordovician Pogonip Group, Opd Unit, Arrow Canyon Ridge, Clark County, Nevada: UNLV Theses, Dissertations, Professional Papers, and Capstones, no. 1116.
- Drummond, BJ, Sexton, MJ, Barton, TJ and Shaw, RD 1991, The nature of faulting along the margins of the Fitzroy Trough, Canning Basin, and implications for the tectonic development of the trough: *Exploration Geophysics*, v. 22, p. 111–116.
- Dunham, RJ 1962, Classification of carbonate rocks according to depositional texture, in *Classification of carbonate rocks edited by* WE Hamm: American Association of Petroleum Geologists, Tulsa, Oklahoma, US, p. 108–121.
- Egenhoff, S and Maletz, J 2007, Graptolites as indicators of maximum flooding surfaces in monotonous deep-water shelf successions: *Palaiois*, v. 22, p. 373–383.
- Erick, M and Hinnov, LA 2007, Millennial-scale paleoclimate cycles recorded in widespread Palaeozoic deeper water rhythmites of North America: *Palaeogeography, Palaeoclimatology, Palaeoecology*, v. 243, p. 348–372.
- Flügel, E 2004, Microfacies of carbonate rocks: Analysis, interpretation and application: Springer-Verlag, New York, US, 984p.
- Flügel, E 2010, Microfacies of Carbonate Rocks: Analysis, Interpretation and Application (2nd edition): Springer-Verlag, Berlin, Heidelberg, Germany.



- Forman, DJ and Wales, DW 1981, Geological evolution of the Canning Basin, Western Australia: Bureau of Mineral Resources, Geology and Geophysics, Bulletin 210, 91p.
- France, RE 1986, Percival no. 1 well completion report: Volume 1 of 3; Western Mining Corporation Limited.: Geological Survey of Western Australia, Statutory petroleum exploration report W2819 A2 V1.
- Frogtech Geoscience 2017, 2017 Canning Basin SEEBASE study and GIS data package: Geological Survey of Western Australia, Report 182, 297p.
- Gowland, S 1996, Facies characteristics and depositional models of highly bioturbated shallow marine siliciclastic strata: an example from the Fulmar Formation (Late Jurassic), UK Central Graben: Geological Society London, Special Publications 114, no. 1, p. 185–214.
- Guppy, DJ and Opik, AA 1950, Discovery of Ordovician rocks, Kimberley Division: Australian Journal of Science, v. 12, p. 205–206.
- Guppy, DJ, Lindner, AW, Rattigan, JH and Casey, JN 1958, The geology of the Fitzroy Basin, Western Australia: Bureau of Mineral Resources, Geology and Geophysics, Bulletin 36, 136p.
- Haines, PW 2004, Depositional facies and regional correlations of the Ordovician Goldwyer and Nita Formations, Canning Basin, Western Australia, with implications for petroleum exploration: Geological Survey of Western Australia, Record 2004/7, 45p.
- Haines, PW 2011, Geological appraisal of petroleum exploration well Patience 2, Canning Basin, Western Australia: Geological Survey of Western Australia, Record 2011/11, 17p.
- Haines, PW and Wingate, MTD 2007, Fingerprinting reservoir sandstone provenance in the Canning Basin using detrital zircons, in Geological Survey of Western Australia Annual Review 2005–06: Geological Survey of Western Australia, p. 59–63.
- Haines, PW, Wingate, MTD, Zhan, Y and Maidment, DW 2018, Looking beneath the Canning Basin: new insights from geochronology, seismic and potential-field data, in GSWA 2018 extended abstracts: promoting the prospectivity of Western Australia: Geological Survey of Western Australia, Record 2018/2, p. 30–33.
- Hannaford C 2016, A palynological analysis of Olympic 1, Canning Basin, Western Australia: MGPALAE0, 8p.
- Hocking, RM, Mory, AJ and Williams, IR 1994, An atlas of Neoproterozoic and Phanerozoic basins of Western Australia, in The sedimentary basins of Western Australia edited by PG Purcell and RR Purcell: Petroleum Exploration Society of Australia, Western Australian Branch, Perth, Western Australia, p. 21–43.
- Hough, JK and Weeden, RJ 1986, Dodonea No. 1. Well Completion Report; Western Mining Corporation Ltd: Geological Survey of Western Australia, Statutory petroleum exploration report W2864A2.
- Howell, JA, Shorstad, A, MacDonald, A, Fordham, A, Flint, S, Fjellvoll, B and Manzocchi, T 2008, Sedimentological parameterization of shallow-marine reservoirs: Petroleum Geoscience, v. 14, p. 17–34.
- Hunt, D and Tucker, ME 1995, Stranded parasequences and the forced regressive wedge systems tract: deposition during base-level fall-reply: Sedimentary Geology, v. 95, no. 1–2, p. 147–160.
- Irwin, ML 1965, General theory of epeiric clear water sedimentation: American Association of Petroleum Geologists Bulletin, v. 49, p. 445–459.
- Jacque, M, Leslie, W and Tricot, P 1968a, Well completion report Edgar Range No. 1; Total Exploration Australia Pty. Ltd.: Geological Survey of Western Australia, Statutory petroleum exploration report W435 A1, 107p.
- Jacque, M, Sweeney, P and Tricot, P 1968b, Well completion report McLarty No. 1; Total Exploration Australia Pty. Ltd.: Geological Survey of Western Australia, Statutory petroleum exploration report W415 A1, 115p.
- Johnstone, MH (compiler) 1961, Samphire Marsh No. 1 Well, Western Australia: Bureau of Mineral Resources, Geology and Geophysics, Canberra, Petroleum Search Subsidy Acts.
- Kennard, JM, Jackson, MJ, Romine, KK, Shaw, RD and Southgate, PN 1994, Depositional sequences and associated petroleum systems of the Canning Basin, WA, in The sedimentary basins of Western Australia edited by PG Purcell and RR Purcell: Petroleum Exploration Society of Australia, Western Australian Branch, Perth, Western Australia, p. 657–676.
- Laurie, JR and Shergold, JH 1996a, Early Ordovician trilobite taxonomy and biostratigraphy of the Emanuel Formation, Canning Basin, Western Australia, Part 1: Palaeontographica Beiträge Zur Naturgeschichte der Vorzeit Abteilung A: Paläozoologie–Stratigraphie, v. 240, p. 65–103.
- Laurie, JR and Shergold, JH 1996b, Early Ordovician trilobite taxonomy and biostratigraphy of the Emanuel Formation, Canning Basin, Western Australia, Part 2: Palaeontographica Beiträge Zur Naturgeschichte der Vorzeit Abteilung A: Paläozoologie–Stratigraphie, v. 240, p. 105–144.
- Legg, DP 1976, Ordovician trilobites and graptolites from the Canning Basin, Western Australia: Geologica et Palaeontologica, v. 10, p. 1–58.
- McTavish, RA and Legg, DP 1976, The Ordovician of the Canning Basin, Western Australia, in Proceedings edited by MG Bassett, Palaeontological Association symposium, Birmingham, UK, 1974/09: University of Wales Press and National Museum of Wales, The Ordovician System, p. 447–478.
- Munnecke, A and Samtleben, C 1996, The formation of micritic limestones and the development of limestone-marl alternation in the Silurian of Gotland, Sweden: Facies, v. 34, p. 159–176.
- Munnecke, A and Westphal, H 2005, Variations in primary aragonite, calcite, and clay in fine-grained calcareous rhythmites of Cambrian to Jurassic age – an environmental archive? Facies, v. 51, p. 592–607.
- Nicoll, RS 1993, Ordovician conodont distribution in selected petroleum exploration wells, Canning Basin, Western Australia: Australian Geological Survey Organisation, Record 1993/17, 136p.
- Nicoll, RS and Ethington, RL 2004, *Lissoepikodus nudus* gen. et sp. nov. and *Oepikodus cleftus* sp. nov., new septimembrate conodont taxa from the Early Ordovician of Australia and Nevada: Courier Forschungsinstitut Senckenberg, v. 245, p. 427–461.
- Nicoll, RS, Laurie, JR and Roche, MT 1993, Revised stratigraphy of the Ordovician (late Tremadoc–Arenig) Prices Creek Group and Devonian Poulton Formation, Lennard Shelf, Canning Basin, Western Australia: Journal of Australian Geology and Geophysics, v. 14, p. 65–76.
- Nio, SD, Böhm, AR, Brouwer, JH, de Jong, MGG and Smith, DG 2006, Climate stratigraphy, principals and applications in subsurface correlation: European Association of Geoscientists and Engineers, Short Course Series 1, 130p.
- Nio, SD, Brouwer, J, Smith, D, de Jong, M and Böhm, A 2005, Spectral trend attribute analysis: Applications in the stratigraphic analysis of wireline logs: First Break, v. 23, p. 71–75.
- Normore, LS 2017, Provenance, depositional setting and regional correlations of the Ordovician Carranya Formation, Canning Basin: Geological Survey of Western Australia, Record 2017/3, 22p.
- Normore, LS and Dent, LM 2017a, Olympic 1, Canning Basin: Geological Survey of Western Australia, Digital Core Atlas Series, 212p., <www.dmr.wa.gov.au/wapims>.
- Normore, LS and Dent, LM 2017b, Petroleum source potential of the Ordovician Nambeet Formation, Canning Basin: Evidence from petroleum well Olympic 1: Geological Survey of Western Australia, Report 169, 20p.
- Normore, LS, Zhen, YY, Dent, LM, Crowley, JL, Percival, IG and Wingate, MTD 2018, Early Ordovician CA-IDTIMS U–Pb zircon dating and conodont biostratigraphy, Canning Basin, Western Australia: Australian Journal of Earth Sciences, v. 65, p. 61–73.
- Nummendal, D, Pilkey, OH and Howard, JD 1987, Transgressive stratigraphy at sequence-bounding unconformities: some principles derived from Holocene and Cretaceous examples: Sea-level fluctuation and coastal evolution: Society of Economic Paleontologists and Mineralogists (SEPM), Special Publication 41.
- Olsen, H, Briedis, NA and Renshaw, D 2017, Sedimentological analysis and reservoir characterisation of a multi-darcy, billion barrel oil field – The upper Jurassic shallow marine sandstones of the Johan Sverdrup field, North Sea, Norway: Marine and Petroleum Geology, v. 84, p. 102–134.
- Parra-Garcia, M, Sanchez, G, Dentith, MC and George, AD 2014, Regional structural and stratigraphic study of the Canning Basin, Western Australia: Geological Survey of Western Australia, Report 140, 215p.
- Partridge, AP 2006, Jurassic – Early Cretaceous spore–pollen and dinocyst zonations for Australia, in Australian Mesozoic and Cenozoic palynology – updated to the 2004 geological time scale edited by E Monteil: Geoscience Australia, Record 2006/23.

- Pearson, DL 1984, Pollen/spore colour "standard" version #2: Phillips Petroleum Company, Exploration Projects Section (unpublished).
- Phipps, J, Trupp, M and Nosiara, M 1998, Well Completion Report Interpretation Volume Looma-1 EP 353; Shell Development (Australia) Pty Ltd: Geological Survey of Western Australia, Statutory petroleum exploration report W20358 A2.
- Playford, G and Wicander, R 2016, Palynological report on samples from Buru Energy Olympic 1 Wells, Canning Basin, Western Australia: Geological Survey of Western Australia, Statutory petroleum exploration report W21660 A3.
- Playford, PE, Cope, RN, Cockbain, AE, Low, GH and Lowry, DC 1975, Canning Basin, in *The Geology of Western Australia: Geological Survey of Western Australia, Memoir 2*, p. 319–368.
- Rickards, B and Chapman, A 1991, Bendigonian graptolites (Hemichordata) of Victoria: *Memoirs of the Museum of Victoria*, v. 52, p. 1–135.
- Roberts, JJ and Boyd, R 2011, Late Quaternary core stratigraphy of the northern New South Wales continental shelf: *Australian Journal of Earth Sciences*, v. 51, p. 141–156.
- Romine, KK, Southgate, PN, Kennard, JM and Jackson, MJ 1994, The Ordovician to Silurian phase of the Canning Basin WA *edited by* PG Purcell and RR Purcell, West Australian Basins Symposium, Perth, Western Australia, 1994: Petroleum Exploration Society of Australia, Western Australian Branch, The Sedimentary Basins of Western Australia, p. 677–696.
- Schlaich, M and Aigner, T 2017, Facies and integrated sequence stratigraphy of an Epeiric Carbonate Ramp Succession: Dhurma Formation, Sultanate of Oman: The depositional record: *The Journal of the International Association of Sedimentologists*, v. 3, no. 1, p. 92–132.
- Shaw, RD, Sexton, M and Zeilinger, I 1994, The tectonic framework of the Canning Basin, WA, including 1:2 million structural elements map of the Canning Basin: Australian Geological Survey Organisation, Record 1994/48, 89p.
- Tada, R and Siever, R 1989, Pressure solution during diagenesis: *Annual Review of Earth and Planetary Sciences*, v. 17, p. 89–118, doi:10.1146/annurev.ea.17.050189.000513.
- Taylor, AM and Goldring, R 1993, Description and analysis of bioturbation and ichnofabric: *Journal of the Geological Society*, v. 150, no. 1, p. 141–148.
- Vachard, D, Clausen, S, Palafox, JJ, Buitrón, BE, Devaere, L, Hayart, V and Régnier, S 2017, Lower Ordovician microfacies and microfossils from Cerro San Pedro (San Pedro de la Cueva, Sonora, Mexico), as a westernmost outcrop of the newly defined Nuia Province: *Facies*, v. 63, p. 1–37.
- Vachard, D and Téllez-Grión, C 1986, El alga Nuia en el Ordovícico de México; hipótesis diversas: *Revista Instituto Mexicano Petroleo*, v. 18, no. 2, p. 12–25.
- Vandenberg, AHM and Cooper, RA 1992, The Ordovician graptolite sequence of Australasia: *Alcheringa: An Australasian Journal of Palaeontology*, v. 16, p. 33–85.
- van Wagoner, JC, Mitchum, RM, Campion, KM and Rahmanian, VD 1990, Siliciclastic sequence stratigraphy in well logs, cores, and outcrops: concepts for high-resolution correlation of time and facies: *American Association of Petroleum Geologists Methods in Exploration Series*, v. 7, p. 55.
- Westphal, H and Munnecke, A 2003, Limestone-marl alternations: A warm-water phenomenon? *Geology*, v. 31, no. 3, p. 263–266.
- Westphal, H, Munnecke, A, Böhm, F and Bornholdt, S 2008, Limestone-marl alternations in epeiric sea settings – witnesses of environmental changes or diagenesis? *Special Paper 48: Dynamics of Epeiric Seas*, p. 389–406.
- Wingate, MTD, Lu, Y and Haines, PW 2018, 199446: monzogranite, Samphire Marsh 1; *Geochronology Record 1525: Geological Survey of Western Australia*, 5p.
- Wright, VP, Burchette, T 1998, Carbonate ramps: an introduction in *Carbonate Ramps edited by* VP Wright and TP Burchette: Geological Society, London, Special Publications 149, p. 1–5.
- Zhen, Y, Percival, IG, Normore, LS and Dent, LM 2017, Floian (Early Ordovician) Conodonts of the Canning Basin, Western Australia – Biostratigraphy and Palaeobiogeographic Affinities with Chinese Faunas, in *Proceedings of the International Geoscience Programme (IGCP) Project 653 Annual Meeting*, p. 235–241.
- Zhen, YY and Nicoll, RS 2009, Biogeographic and biostratigraphic implications of the *Serratognathus bilobatus* fauna (Conodonta) from the Emanuel Formation (Early Ordovician) of the Canning Basin, Western Australia: *The Australian Museum, Sydney, NSW, Records of the Australian Museum* 61, 30p.
- Zhen, YY, Normore, LS, Dent, LM and Percival, IG 2020, Middle Ordovician (Darriwilian) conodonts from the Goldwyer Formation of the Canning Basin, Western Australia. *Alcheringa: An Australasian Journal of Palaeontology*, v. 44, no. 1, p. 25–55.

## Appendices

### Appendix 1. Revised stratigraphic picks for the top of the Nambeet Formation and equivalent formations, including the top Wilson Cliffs Sandstone and Prices Creek Group

**Table A1.1. Revised stratigraphic picks for the top Nambeet Formation and top Fly Flat Member based on petroleum and mineral exploration and stratigraphic wells**

Well or drillhole name	Total depth (m)	Nambeet top (m)	Nambeet base (m)	Nambeet interval (m)	Fly Flat Member top (m)	Sits on basement
Acacia 2	1573.00	1277.00	1502.50	225.50	1370.00	Yes
Aquila 1	1735.00	1364.00	1735.00	371.00	1554.00	Unknown
Calamia 1	1697.30	1337.00	1671.00	334.00	1541.40	Yes
Crystal Creek 1	2504.00	2403.00	2504.00	101.00	? (unclear)	Unknown
Dodonea 1	2215.00	1910.00	2185.00	275.00	2108.00	Yes
Edgar Range 1	1968.10	1754 (?) maybe 1648	1968.10	214.10	N/A (absent)	Unknown
Frankenstein 1	2803.00	2560.00	2666.00	106.00	2660?	Yes
Goldwyer 1	1439.00	1260.00	1420.40	160.40	1387.80	Yes
Hedonia 1	1543.00	1290.00	1501.00	211.00	1501.00	Yes
Hilltop 1	1770.00	1418.00	1736.00	318.00	1565.00	Yes
Leo 1	2411.00	2253 maybe 2060?	2319.50	66.50	2276.00	Yes
Looma 1	2535.00	2311.00	2494.00	183.00	?2360.00	Yes
McLarty 1	2591.00	2341.00	2590.80	249.80	2341.00	Unknown
Mirbelia 2	2818.00	2674.50	-		?2751.43	Unknown
Missing 1	1810.00	1680.00	1810.00	130.00	1746.00	Unknown
Munro 1	2116.00	1890.00	2105.90	215.90	2063?	Yes
Nicolay 1	3564.70	3228.00	3564.70	336.70	N/A (absent)	Unknown
Olympic 1	1447.53	1170.00	-		1383.57	Unknown
Pegasus 1	2995.00	2900.00	2995.00	79.00	2925.00	Unknown
Percival 1	2448.00	2229.00	2447.60	218.60	2300.00	Unknown
Pictor 1	2146.00	1932.00	2121.00	189.00	2028.20	Yes
Sally May 2	1994.10	1933.00	1994.10	61.10	1933.00	Unknown
Samphire Marsh 1	2031.20	1240.00	2015.00	775.00	?1878.20	Yes
Setaria 1	956.00	627.00	955.00	328.00	897.00	Unknown
Sharon Ann 1	1830.00	1501.70	1830.00	328.30	1779.00	Unknown
Solanum 1	834.00	805.90	834.00	28.10	815.00	Unknown
Tappers Inlet 1	2856.28	2202.50	2834.60	632.10	?2712.70	Yes
Thangoo 1A	1654.76	1278.46	1554.50	276.04	1499.60	Yes
Thangoo 2	1472.00	1149.00	1438.00	289.00	1366.40	Yes
Twin Buttes 1	1600.30	1358.00	1600.30	242.30	N/A (not deep enough)	Unknown
Willara 1	3903.00	3142.00	3656.00	514.00	3410.70	Unknown



**Table A1.2. Proposed equivalent stratigraphic picks for the top Nambeet Formation and top Fly Flat Member based on well and drillhole data**

Well or drillhole name	Total depth (m)	Nambeet top (m)	Nambeet base (m)	Nambeet interval (m)	Fly Flat Member top (m)	Sits on basement
Gap Creek 1	1541.20	1047.50	1527.80	480.30	1431.84	Yes
Grevillea No. 1	2586.00	2122.50	2556.50	434.00	2466.00	Yes
Justago 1	3150.00	2241.84	3150.00	908.16	?3016.52	Yes

**Table A1.3. Revised stratigraphic picks for the top Wilson Cliffs Sandstone based on petroleum and mineral exploration and stratigraphic wells**

Well or drillhole name	Total depth (m)	Wilson Cliffs Sandstone top (m)	Wilson Cliffs Sandstone base (m)	Wilson Cliffs Sandstone interval (m)	Sits on basement
Contention Heights 1	1790.70	1580.39	1790.70	210.31	Unknown
Kidson 1	4431.49	4412.50	4431.49	19.50	Unknown
Patience 2	4184.00	3163.50	4184.00	762.00	Unknown
Wilson Cliffs 1	3722.22	2848.43	3503.00	654.57	Yes

**Table A1.4. Stratigraphic picks for the Prices Creek Group based on well completion reports from petroleum and mineral exploration and stratigraphic wells**

Well or drillhole name	Total depth (m)	Prices Creek Group top (m)	Prices Creek Group base (m)	Gap Creek Formation top (m)	Emanuel Formation top (m)	Kudata Dolomite top (m)	Kunian Sandstone top (m)	Sits on basement
BMR 03 Noonkanbah	247.00	10.70	180.70	-	-	10.70	99.10	Unknown
BHP PCD158	213.80	113.10	205.80	111.60	115.00	145.00	173.50	Unknown
BHP PHD 001	668.10	70.90	643.60	-	70.90	465.00	550.00	Unknown
BHP PHD 002	119.20	93.00	119.20	-	93.00	?	?	Unknown
Gap Creek 1	1541.20	1047.50	1527.80	1047.50	1162.00	?1366.00	1450.00	Yes
Grevillea No. 1	2586.00	1953.00	2556.50	1953.00	2165.00	2399.00	2466.00	Yes
Justago 1	3150.00	2240.50	3150.00	2240.50	2575.00	2890.00	3050.50	Yes
Prices Creek 1	307.00	0.00	307.00	-	0.00	?	?	Unknown
Prices Creek 2	104.00	25.00	104.00	-	25.00	?	?	Unknown
Prices Creek 3	247.00	4.00	247.00	-	4.00	?	?	Unknown

## Appendix 2. Formation definition card — Fly Flat Member

DEFINITION CARD	
<b>NAME OF UNIT</b> ¹ : Fly Flat Member	<b>STATE(S)</b> ¹ : WA
<b>STATUS OF UNIT</b> : New Name	<b>RANK</b> : Member
<b>PROPOSER</b> : L Dent and L Normore	<b>DATE</b> : 18.01.2021
<b>RESERVED IN STRATIGRAPHIC UNITS DATABASE</b> : YES	
<b>PROPOSED PUBLICATION</b> : Dent, LM, Normore, LS and Martin, SK 2021, Reference section, revised stratigraphy and facies analysis of the Ordovician Nambeet Formation, Canning Basin, Western Australia, Geological Survey of Western Australia, Report in press.	
<b>DERIVATION OF NAME</b> ¹ : Fly Flat Bore ~21.3 km north-northwest of the Olympic 1 well. Approximate coordinates: Lat: 18.12768°S Lon: 122.55072°E	
<b>SYNONYMY, UNIT NAME HISTORY</b> (if any) ¹ : This unit has previously been informally referred to as the 'lower sandstone unit' of the Nambeet Formation including 'basal transgressive deposits' referred to by Kennard et al. (1994).	
<b>CONSTITUENT UNITS</b> ³ : N/A	
<b>PARENT UNIT</b> : Nambeet Formation	
<b>TYPE LOCALITY</b> (including Lat. & Long.) ² : Olympic 1 well (–18°17'57.60"S, 122°38'23.40"E) between 1383.57 – 1447.53 m depth (63.96 m continuous drillcore). Drillcore archived in Geological Survey of Western Australia Perth Core Library.	
<b>CONFIDENTIAL TYPE LOCALITY?</b> : No	
<b>DESCRIPTION AT TYPE LOCALITY</b> ² :	
<b>LITHOLOGY</b> ² : The Fly Flat Member is composed of well-sorted, very fine-grained subarkose sandstone and minor siltstone. Sandstone composition is dominated by quartz and feldspar, with calcareous allochems comprising between 5–50% of grains. Calcareous allochems are predominantly fossil fragments and the incertae sedis cyanobacteria, <i>Nuia</i> . Minor to common detrital clay matrix is observed and may be locally enriched in organic material. Glauconite is present in trace amounts. Bioturbation is common ranging from minor to locally extensive, and bored hardgrounds with glauconite veneers are observed in the lower parts of the member. In other parts of the basin the Fly Flat Member contains a basal conglomerate or medium- to coarse-grained poorly consolidated sandstone and granitic 'basement wash'. This conglomeratic unit is not always present. X-ray diffraction indicates a quartz content of 50.9 – 79.9%, a K-feldspar content between 6.4 and 23.8% and a carbonate content of between 10.2 and 31.4% for the Fly Flat Member at the type section.	
<b>THICKNESS</b> ² : 63.53 m was cored at the type locality; however, this is a minimum thickness as the base of the section was not recovered.	
<b>FOSSILS</b> : Conodonts, echinoderms, possible brachiopods, possible bivalves and the incertae sedis cyanobacteria, <i>Nuia</i> .	
<b>DIASTEMS OR HIATUSES</b> (if relevant): Sharp planar or bored hardground surfaces are found between 1417.0 – 1447.8 m at the type locality. The upper contact of the member with the overlying Samphire Marsh Member is represented by an abrupt sequence boundary.	
<b>RELATIONSHIPS &amp; BOUNDARY CRITERIA</b> ² : At the type section the Fly Flat Member lies stratigraphically between the Samphire Marsh Member (above) and basement (below). Although the depositional sequence from Fly Flat to Samphire Marsh Member is regionally continuous, the contact at the type section is likely a disconformity. The lower basement contact is interpreted from seismic data at the type locality and correlations to wells Hedonia 1, Hilltop 1, Goldwyer 1, Leo 1, Calamia 1, Samphire Marsh 1, Thangoo 1A, Thangoo 2 and Pictor 1 where drilling has shown it to overlie basement.	

<b>DISTINGUISHING OR IDENTIFYING FEATURES</b> ¹ : Distinguished from the overlying Samphire Marsh Member by the abrupt change from dominantly sandy siliciclastic to carbonate–mudstone lithologies.
<b>AGE &amp; EVIDENCE</b> ² : At the type section, the Fly Flat Member is assigned a Lower Ordovician, Tremadocian age based on the presence of the <i>Paroistodus proteus</i> conodont biozone recorded in the top ~60 m of the member and into the overlying Samphire Marsh Member (Zhen et al., 2017). A U–Pb radiometric date of 479.37 ± 0.16 Ma is recorded from a bentonite bed at 1383.27 m, 30 cm above the top of the member in the Samphire Marsh Member (Normore et al., 2017).
<b>CORRELATION WITH OTHER UNITS</b> ² : The Fly Flat Member is laterally equivalent to the lower Wilson Cliffs Sandstone, which is recorded in the south eastern sections of the Canning Basin (wells Contention Heights 1, Kidson 1, Patience 2 and Wilson Cliffs 1 [type section]). As deposition is continuous from the Fly Flat Member into the Samphire Marsh Member at most localities, it is likely that the very top of the Wilson Cliffs Sandstone is equivalent to the base of the Samphire Marsh Member. The lower portions of the Fly Flat Member are also considered equivalent to the Kunian Sandstone (Prices Creek Group) described by Nicoll et al. (1993) in far northern parts of the Canning Basin. It is also possibly equivalent to the overlying Kudata Dolomite of the same group also described by Nicoll et al. (1993).
<b>REGIONAL ASPECTS/GENERAL GEOLOGICAL DESCRIPTION</b> : The Fly Flat Member is identified as a sandstone package below a thick carbonate–mudstone sequence, most commonly overlying basement. A basal conglomerate or medium- to coarse-grained poorly consolidated sandstone and granitic ‘basement wash’ is present in some parts of the basin, particularly the northwest (e.g. wells Hedonia 1, Goldwyer 1 and Leo 1).
<b>EXTENT</b> : The Fly Flat Member is recorded across the central–western parts of the Canning Basin, although confident identification is restricted to locations where the Nambeet Formation has been intersected by drilling. It has been drilled on the following tectonic subdivisions: Broome Platform, Willara Sub-basin, Barbwire Terrace, Munro Arch and Kidson Sub-basin and recently identified in the Barnicarndy Graben. It is probable that the member is present in the Samphire Graben, and extends further south into the Kidson Sub-basin than indicated by current records. The Nambeet Formation, and thus the Fly Flat Member, is interpreted to be absent on the southwestern edge of the Broome Platform based on seismic (Zhan, 2019).
<b>GEOMORPHIC EXPRESSION</b> : The Fly Flat Member has been recorded only in the subsurface.
<b>THICKNESS VARIATIONS</b> : Thickness of the Fly Flat Member varies from as thin as ~42 m to just over ~200 m, interpreted at Hilltop 1.
<b>STRUCTURE AND METAMORPHISM</b> : Flat-lying to gently dipping depending on structural position. Locally affected by faulting (Zhan, 2019). No metamorphism.
<b>ALTERATION AND MINERALISATION</b> : None observed.
<b>GEOPHYSICAL EXPRESSION</b> : This member is not differentiated from the Samphire Marsh Member on seismic work completed to date.
<b>GEOCHEMISTRY</b> : No data.
<b>GENESIS/DEPOSITIONAL ENVIRONMENT</b> : At the type section the Fly Flat Member was deposited in shallow-marine, shoreface settings (ranging upper to lower). Deposition occurred as part of early marine transgression into the Canning Basin.
<b>COMMENTS</b> :
<b>REFERENCES</b> ¹ :  Kennard, JM, Jackson, MJ, Romine, KK, Shaw, RD and Southgate, PN 1994, Depositional sequences and associated petroleum systems of the Canning Basin, WA, in The sedimentary basins of Western Australia edited by PG Purcell and RR Purcell: Petroleum Exploration Society of Australia, Western Australian Branch, Perth, Western Australia, p. 657–676.  Nicoll, RS, Laurie, JR and Roche, MT 1993, Revised stratigraphy of the Ordovician (late Tremadoc–Arenig) Prices Creek Group and Devonian Poulton Formation, Lennard Shelf, Canning Basin, Western Australia: Journal of Australian Geology and Geophysics, v. 14, p. 65–76.



Normore, LS, Zhen, YY, Dent, LM, Crowley, JL, Percival, IG and Wingate, MTD 2018, Early Ordovician CA-IDTIMS U-Pb zircon dating and conodont biostratigraphy, Canning Basin, Western Australia: Australian Journal of Earth Sciences, v. 65, p. 61–73.

Zhan, Y 2019, A seismic interpretation of the Broome Platform, Willara Sub-basin and Munro Arch of the Canning Basin, Western Australia: Geological Survey of Western Australia, Report 193, 43p.

Zhen, Y, Percival, IG, Normore, LS and Dent, LM 2017, Floian (Early Ordovician) Conodonts of the Canning Basin, Western Australia — Biostratigraphy and Palaeobiogeographic Affinities with Chinese Faunas, in Proceedings of the International Geoscience Programme (IGCP) Project 653 Annual Meeting, p. 235–241.

### Appendix 3. Formation definition card — Samphire Marsh Member

DEFINITION CARD	
<b>NAME OF UNIT</b> ¹ : Samphire Marsh Member	<b>STATE(S)</b> ¹ : WA
<b>STATUS OF UNIT</b> : New Name	<b>RANK</b> : Member
<b>PROPOSER</b> : L Dent and L Normore	<b>DATE</b> : 18.01.2021
<b>RESERVED IN STRATIGRAPHIC UNITS DATABASE</b> : YES	
<b>PROPOSED PUBLICATION</b> : Dent, LM, Normore, LS and Martin, SK 2021, Reference section, revised stratigraphy and facies analysis of the Ordovician Nambeet Formation, Canning Basin, Western Australia, Geological Survey of Western Australia, Report in press.	
<b>DERIVATION OF NAME</b> ¹ : Samphire Marsh 1, petroleum exploration well where the original Nambeet Formation type section is designated. Location: Lat: -19.520°S, Long: 121.183°E.	
<b>SYNONYMY, UNIT NAME HISTORY</b> (if any) ¹ : This member has previously just been included in the overall definition of the Nambeet Formation.	
<b>CONSTITUENT UNITS</b> ³ : N/A	
<b>PARENT UNIT</b> : Nambeet Formation	
<b>TYPE LOCALITY</b> (including Lat. & Long.) ² : Olympic 1 well (-18°17'57.60"S, 122°38'23.40"E) between 1170.00 and 1383.57 m depth (213.57 m thick; continuous drillcore). Drillcore archived in Geological Survey of Western Australia Perth Core Library.	
<b>CONFIDENTIAL TYPE LOCALITY?</b> : No	
<b>DESCRIPTION AT TYPE LOCALITY</b> ² :	
<b>LITHOLOGY</b> ² : Samphire Marsh Member consists of interbedded and nodular carbonate–mudstone sequences. Limestone bed textures range from grainstone to lime mudstone and nodule textures vary from wackestone to lime mudstone. Transitions between interbedded and nodular sections and coarser to finer carbonate fabrics are gradational throughout the sequence. Mudstones in both interbedded and nodular sections are calcareous. X-ray diffraction indicates a quartz content of 4.1 – 29.8%, a total clay content between 3.8 and 43.8%, a calcite content of between 9.9 and 85.9%, and a dolomite content between 0 and 12.2% across the Samphire Marsh Member at the type section.	
<b>THICKNESS</b> ² : ~213.57 m thick at the type locality, with a transitional upper contact. Whole section recovered.	
<b>FOSSILS</b> : Conodonts, trilobites, graptolites, brachiopods, bivalves, nautiloids sensu lato, echinoderms. Minor taxa include gastropods, macheridians, bryozoans, scolecodonts and the incertae sedis cyanobacteria, <i>Nuia</i> .	
<b>DIASTEMS OR HIATUSES</b> (if relevant): Bored hardgrounds are observed in the lower–middle parts of the member at the type locality. The lower contact of the member with the underlying Fly Flat Member is represented by an abrupt sequence boundary which may represent a disconformity at this locality.	
<b>RELATIONSHIPS &amp; BOUNDARY CRITERIA</b> ² : At the type section the Samphire Marsh Member lies stratigraphically between the Fly Flat Member (below) and the Willara Formation (above). Although the depositional sequence from Fly Flat to Samphire Marsh Member is continuous elsewhere, the contact at the type section is likely a disconformity. In the Samphire Marsh 1 well, the Samphire Marsh Member is atypically and unconformably overlain by the Permo-carboniferous Grant Group.	
<b>DISTINGUISHING OR IDENTIFYING FEATURES</b> ¹ : Distinguished from the underlying Fly Flat Member by the abrupt change from dominantly sandy siliciclastic to carbonate–mudstone lithologies.	

<p><b>AGE &amp; EVIDENCE</b> ²: At the type section, the Samphire Marsh Member is assigned a Lower–Middle Ordovician, Tremadocian to possible earliest Dapingian age. This is based on the presence of the <i>Jumodontus gananda</i>, <i>Oepikodus communis</i>, <i>Prioniodus oepiki</i> – <i>Serratognathus bilobatus</i> and <i>Paroistodus proteus</i> conodont biozones (Zhen et al. 2017). Six U–Pb radiometric dates are recorded from bentonite beds. Derived ages range from $479.37 \pm 0.16$ Ma at 1383.27 m (30 cm above the base of the member) to $470.18 \pm 0.13$ Ma at 1165.44 m (just above the interpreted Samphire Marsh Member – Willara Formation contact) (Normore et al., 2017).</p>
<p><b>CORRELATION WITH OTHER UNITS</b> ²: The basal section of the Samphire Marsh Member may be equivalent to the uppermost deposits of the Wilson Cliffs Sandstone which is recorded in the south eastern sections of the Canning Basin (wells Contention Heights 1, Kidson 1, Patience 2 and Wilson Cliffs 1 [type section]). Based on conodont biostratigraphy, the lower parts of the Samphire Marsh Member are considered equivalent to the Kudata Dolomite as described by Nicoll et al. (1993), and the Emanuel Formation, while the upper parts of the member may be equivalent to the lower parts of the Gap Creek Formation (all Prices Creek Group) as described by Nicoll and Ethington (2004) and Zhen and Nicoll (2009).</p>
<p><b>REGIONAL ASPECTS/GENERAL GEOLOGICAL DESCRIPTION</b>: The Samphire Marsh Member is identified as a thick carbonate–mudstone sequence, overlying a siliciclastic package and transitioning into carbonate-dominated sediments of the overlying Willara Formation.</p>
<p><b>EXTENT</b>: The Samphire Marsh Member is recorded across the central–western parts of the Canning Basin, although confident identification is restricted to locations where the Nambeet Formation has been intersected by drilling. It has been drilled on the following tectonic sub-divisions: Broome Platform, Willara Sub-basin, Barbwire Terrace, Munro Arch and Kidson Sub-basin and recently identified in the Barnicarndy Graben.</p>
<p><b>GEOMORPHIC EXPRESSION</b>: The Samphire Marsh Member has been recorded only in the subsurface.</p>
<p><b>THICKNESS VARIATIONS</b>: Thickness of the Samphire Marsh Member varies from as thin as an estimated ~50 m to almost 640 m in Samphire Marsh 1.</p>
<p><b>STRUCTURE AND METAMORPHISM</b>: Flat-lying to gently dipping depending on structural position. Locally affected by faulting (Zhan 2019). No metamorphism.</p>
<p><b>ALTERATION AND MINERALISATION</b>: None observed.</p>
<p><b>GEOPHYSICAL EXPRESSION</b>: This member is not differentiated from the Fly Flat Member on seismic work completed to date.</p>
<p><b>GEOCHEMISTRY</b>: No data.</p>
<p><b>GENESIS/DEPOSITIONAL ENVIRONMENT</b>: At the type section, the Samphire Marsh Member was deposited on an epeiric platform or very low-angle epeiric ramp environment (restricted inner-ramp to outer-ramp settings).</p>
<p><b>COMMENTS</b>:</p>
<p><b>REFERENCES</b> ¹:</p> <p>Nicoll, RS, Laurie, JR and Roche, MT 1993, Revised stratigraphy of the Ordovician (late Tremadoc-Arenig) Prices Creek Group and Devonian Poulton Formation, Lennard Shelf, Canning Basin, Western Australia: <i>Journal of Australian Geology and Geophysics</i>, v. 14, p. 65–76.</p> <p>Nicoll, RS and Ethington, RL 2004, <i>Lissoepikodus nudus</i> gen. et sp. nov. and <i>Oepikodus cleftus</i> sp. nov., new septimembrate conodont taxa from the Early Ordovician of Australia and Nevada: <i>Courier Forschungsinstitut Senckenberg</i>, v. 245, p. 427–461.</p> <p>Normore, LS, Zhen, YY, Dent, LM, Crowley, JL, Percival, IG and Wingate, MTD 2018, Early Ordovician CA-IDTIMS U–Pb zircon dating and conodont biostratigraphy, Canning Basin, Western Australia: <i>Australian Journal of Earth Sciences</i>, v. 65, p. 61–73.</p> <p>Zhan, Y 2019, A seismic interpretation of the Broome Platform, Willara Sub-basin and Munro Arch of the Canning Basin, Western Australia: <i>Geological Survey of Western Australia, Report 193</i>, 43p.</p>



Zhen, Y, Percival, IG, Normore, LS and Dent, LM 2017, Floian (Early Ordovician) Conodonts of the Canning Basin, Western Australia — Biostratigraphy and Palaeobiogeographic Affinities with Chinese Faunas, *in* Proceedings of the International Geoscience Programme (IGCP) Project 653 Annual Meeting, p. 235–241.

Zhen, YY and Nicoll, RS 2009, Biogeographic and biostratigraphic implications of the *Serratognathus bilobatus* fauna (Conodonta) from the Emanuel Formation (Early Ordovician) of the Canning Basin, Western Australia: The Australian Museum, Sydney, NSW, Records of the Australian Museum 61, 30p.

## Appendix 4. Micro-brachiopod report by I Percival

Appendix plates 1–4 available with the PDF of this Report as an accompanying digital resource

Micro-brachiopod analysis of samples from Olympic 1, Canning Basin,  
Western Australia

By  
*Ian Percival*  
Geological Survey of New South Wales

Prepared for: Geological Survey of Western Australia  
December 2016

*Scale bars on all images are 200 microns except where otherwise noted.

<i>Depth (m)</i>	<i>GSWA sample</i>	<i>Image code</i>	<i>Formation</i>	<i>Member</i>
1128.98	221578	IAN-A_0001	lower Willara Fm.	-

- One specimen only of very highly conical acrotretide ventral valve with apical foramen:

cf. *Semitreta* aff. *S. magna* (Gorjansky 1969) of Popov & Holmer (1994) – Plate 1a.

<i>Depth (m)</i>	<i>GSWA sample</i>	<i>Image code</i>	<i>Formation</i>	<i>Member</i>
1158.93	221580	IAN-A_0001–0010	lower Willara Fm.	-

- Very highly conical acrotretide ventral valve with apical foramen (0002), with probable associated dorsal valve (0003): cf. *Semitreta* aff. *S. magna* (Gorjansky 1969) of Popov & Holmer (1994) - Plate 1b.

- Ventral & dorsal valves (0004–0010): cf. *Wahwahlingula? emanuelensis* Brock & Holmer (2004) - Plate 1 c and d.

<i>Depth (m)</i>	<i>GSWA sample</i>	<i>Image code</i>	<i>Formation</i>	<i>Member</i>
1173.96	221581	IAN-A_0011–0036	Basal Willara Fm.	-

- Fragment of indeterminate large lingulide with strong ridges crossing pitted proparea (0011–0012). ventral & dorsal valves (0013?, 0014–0017) of ?*Libecoviella divaricata* Brock & Holmer 2004 - Plate 1e.

- Acrotretide dorsal valve with single or double spines at anterior termination of median septum (0018–0023, 0031?, 0032); ventral valve with convex pseudointerarea (0024–0030) lacking interr ridge: *Conotreta* sp. nov. - Plate 1 f and g.

<i>Depth (m)</i>	<i>GSWA sample</i>	<i>Image code</i>	<i>Formation</i>	<i>Member</i>
1188.00	221582	IAN-B_0002–0006	Nambett Formation	Samphire Marsh Mbr

- Fragment of indeterminate large lingulide with strong ridges crossing pitted proparea (0003–0004). ?*Eopaterula* sp. - Plate 1h.

- Indeterminate Acrotretide dorsal valve devoid of median septum (0006), identical with IAN-A_0031

<i>Depth (m)</i>	<i>GSWA sample</i>	<i>Image code</i>	<i>Formation</i>	<i>Member</i>
1249.72	221584	IAN-B_0007–0032; IAN-C_0001–0023	Nambett Formation.	Samphire Marsh Mbr.

- Ventral valve fragment (0026, 0027) of *Schizotreta* sp. - Plate 1i.



- Acrotretide with transverse outline, dorsal valve characterised internally by median septum bearing spine halfway along its length, and very short but wide pseudointerarea (IAN-B_0011-0015, IANC_0001-0008), ventral valve with wide planar pseudointerarea (IAN-B_0010, 0028, 0030-0031); *Torynelasma* sp. nov. - Plate 1 j and k.
- Acrotretide with transversely ovoid to subcircular outline, dorsal valve with prominent concave shelflike plate, stout median buttress and simple low rounded median septum (IAN-B_0016-0021), associated with ventral valve with relatively large foramen confined to larval shell, procline convex pseudointerarea with a low interr ridge in some specimens to match rounded protruding dorsal valve beak (IAN-B_0007-0009, 0022-0025, 0029, 0032): acrotretid gen. nov. - Plate 1 l and m.
- Dorsal valves (IAN-C_0010-0018) of *Wahwahlingula? emanuelensis* Brock & Holmer (2004) - Plate 2 a and b
- Fragment of dorsal valve exterior (IAN-C_0019-0020) of *Libecoviella? sp.* [scale bar 500 microns] Plate 2c.
- Exterior fragments with distinctive ornament of short, sharp, prone spines (IAN-C_0021-0023): *?Spinilingula* sp. - Plate 2d.

Depth (m)	GSWA sample	Image code	Formation	Member
1263.95	221585	IAN-C_0024-0029	Nambeet Formation.	Samphire Marsh Mbr.

- Ventral valve (0024-0026) possibly attributable to *Torynelasma* sp. nov. - Plate 2e.
- Dorsal (and ventral) valves (0027-0029) of acrotretid gen. nov. - Plate 2f.

Depth (m)	GSWA sample	Image code	Formation	Member
1338.94	221590	IAN-D_0001-0005	Nambeet Formation.	Samphire Marsh Mbr.

- Fragmentary ventral valves (exterior & interior) of indeterminate paterinide - Plate 2g.

Depth (m)	GSWA sample	Image code	Formation	Member
1351.44	221591	IAN-D_0006-0021; IAN-E_0001-0016	Nambeet Formation.	Samphire Marsh Mbr.

- *Libecoviella?* fragment (0006) dorsal & ventral valves (IAN-D_0007-0021): *Wahwahlingula? emanuelensis* Brock & Holmer (2004) [scale bar 500 microns] - Plate 2 h, i, and j.
- Dorsal valves (IAN-E_0001-0004, 0005?, 0007?, 0008?); corresponding ventral valves may include 0009-0016, one with prominent interr ridge (0014), of acrotretid gen. nov. - Plate 2 k and l.

<i>Depth (m)</i>	<i>GSWA sample</i>	<i>Image code</i>	<i>Formation</i>	<i>Member</i>
1368.84	221592	IAN-E_00017–0026; IAN-F_0001–0010	Nambeet Formation.	?Wilson Cliffs Mbr.

- Fragment with ornament (E 0017), & fragment of ventral valve internal (E 0018) of *Libecoviella?* sp. [scale bar 500 microns] - Plate 3a.
- Unidentified lingulid(?) ventral valves with pitted post-larval shell & pointed beak, faint radial ribbing (E 0019-0020, 0022?) dorsal valve (E 0021) & ventral valves (E 0024-0026) of acrotretid gen. nov. [scale bar 500 microns] - Plate 3 b and c.
- Dorsal & ventral valves (IAN-F_0001-0010) of *Wahwahlingula? emanuelensis* Brock & Holmer (2004) [scale bar 500 microns] - Plate d and e.

<i>Depth (m)</i>	<i>GSWA sample</i>	<i>Image code</i>	<i>Formation</i>	<i>Member</i>
1382.60	221593	IAN-F_0011–0016	Nambeet Formation.	?Wilson Cliffs Mbr.

- Exterior fragments (0011, 0012) cf. *zhanatellidae?* n. gen. A of Brock & Holmer 2004 - Plate 3f.
- Robust acrotretide dorsal valve (0015), and possibly the associated ventral valve (0016) with large apical process, cf. *Semitreta lauriei* Brock & Holmer (2004) [scale bar 500 microns] - Plate 3g.

## Appendix 5. Hydrocarbon shows recorded in the Nambeet Formation and laterally correlative units

**Table A5.1. Hydrocarbon shows in petroleum exploration, mineral exploration and stratigraphic wells intersecting the Nambeet Formation, Wilson Cliffs Sandstone and Prices Creek Group, recorded from well completion reports**

Well or drillhole name	Total depth (m)	Formation/member	Depth (m)	Gas	Oil	Description
Acacia 2	1573	Fly Flat Member	1468–1472	X	X	1% orange-yellow fluorescence with dull blue-white fluorescing cut and moderate blue-white fluorescing residue; associated with 3–6 units of gas
		Fly Flat Member	1484–1487	X	X	20–30% bright yellow to dull gold fluorescence with dull yellow fluorescing cut and thin residue; associated with 35 units gas
		Fly Flat Member	1487–1493	X	X	Trace to 5% fluorescence as above with 3–7 units of gas
Aquila 1	1735	No shows recorded				
BMR 03 Noonkanbah	247	No shows recorded				
BHP PCD158	213.8	Kudata Dolomite – Kunian Sandstone	145.6 – 183.0		X	Bitumen in fractures; slow flow of bitumen on initial exposure
BHP PHD 001	668.1			?		
BHP PHD 002	119.2			?		
Calamia 1	1697.3	Samphire Marsh Member	1461.4 – 1540.4	X		Trace of background gas with occasional peaks up to 1 unit, comprising 100% methane
		Fly Flat Member	1540.3 – 1671.4	X		Increased background gas 1–2 units with peaks up to 4 units
Contention Heights 1	1790.7	No shows recorded				
Crystal Creek 1	2504	Samphire Marsh Member	2410	X		Peak of 90 units total gas
		Samphire Marsh Member	2249.5 – 2504		X	Dead oil laminae/patches are present
Dodonea 1	2215	Samphire Marsh Member	1995–2000		X	Pale yellow to yellow-green fluorescence with moderate to fast yellow cut
		Samphire Marsh Member	2000–2005	X	X	10% pale, gold to yellow-white fluorescence with a slow pale yellow crush cut; associated with a gas level of 416/235/70/36/15 at 2004 m
		Samphire Marsh Member	2015–2020	X	X	40–95% dull yellow-green fluorescence with a yellow cut; associated with gas level of 1136/1089/153/44/8/trace at 2019 m
		Samphire Marsh Member	2024–2029	X	X	Traces of oil staining in sandstone cuttings and light-brown oil: flowed gas at a rate of 85 m3/day from the Nambeet Formation; drill stem test #2 (2114.03 – 2033.42 m)
		Samphire Marsh Member	2033.4 – 2042.3		X	Core No. 3, minor spotty oil with pale blue-yellow to white fluorescence bleeding from sandstone and siltstone lithologies
		Samphire Marsh Member	2082–2087	X		Gas peak of 160-192/111-124/22-26/11/trace
		Fly Flat Member	2109–2110	X		Gas peak of 120/101/8/trace
		Fly Flat Member	2141		X	Very weak to trace oil stains with no fluorescence and white-yellow cut recorded
		Fly Flat Member	2162–2176	X		Gas peak of 1683/1232/141/20

**Table A5.1. Hydrocarbon shows in petroleum exploration, mineral exploration and stratigraphic wells intersecting the Nambeet Formation, Wilson Cliffs Sandstone and Prices Creek Group, recorded from well completion reports**

Well or drillhole name	Total depth (m)	Formation/member	Depth (m)	Gas	Oil	Description
Edgar Range 1	1968.1	Samphire Marsh Member	1778.51 – 1785.52	X		Core No. 13, dark grey to black shale showed gas bubbles in some vertical fractures
Frankenstein 1	2803	No shows recorded				
Gap Creek 1	1541.2	Samphire Marsh Member (Emanuel Formation)	1395		X	Rare dull orange fluorescing bitumen
Goldwyer 1	1439	No shows recorded				
Grevillea No. 1	2586	Samphire Marsh Member (Kudata Dolomite)	2399–2465		X	Rare residual hydrocarbons, no fluorescence but occasional weal to moderate blue-white to white crush cut with a thin spotty white ring
Hedonia 1	1543	Samphire Marsh Member	1309–1310	X		450 units total gas; 30800/5160/5720/2400/800
		Samphire Marsh Member	1329–1330	X		500 units total gas; 30800/4680/6006/3228/2000
		Samphire Marsh Member	1486–1489	X		160 units total gas; 14168/3612/2860/8087/600
Hilltop 1	1770	Fly Flat Member	1640 – 1716.5		X	Occasional trace bitumen in sandstones but no shows
Justago 1	3150	No shows recorded				
Kidson 1	4431.49	No shows recorded				
Leo 1	2411	No shows recorded				
Looma 1	2535	Fly Flat Member	2362–2373	X		Presence of gas indicated by mud readings, C1 only.
		Fly Flat Member	2409–2440	X		Presence of gas indicated by mud readings, C1 only.
McLarty 1	2591	No shows recorded				
Mirbelia 2	2818	No shows recorded				
Missing 1	1810	No shows recorded				
Munro 1	2116	No shows recorded				
Nicolay 1	3564.7	Samphire Marsh Member	3357–3348		X	8 units total gas, mainly C1
		Samphire Marsh Member	3384		X	Trip gas 15 units, mainly C1
		Samphire Marsh Member	3451–3476		X	7 units total gas, mainly C1
		Samphire Marsh Member	3474		X	25 units total gas, mainly C1
		Samphire Marsh Member	3477		X	42 units total gas; 8244/63/5
		Samphire Marsh Member	3564		X	15 units total gas, mainly C1



**Table A5.1. Hydrocarbon shows in petroleum exploration, mineral exploration and stratigraphic wells intersecting the Nambet Formation, Wilson Cliffs Sandstone and Prices Creek Group, recorded from well completion reports**

Well or drillhole name	Total depth (m)	Formation/member	Depth (m)	Gas	Oil	Description
Patience 2	4184	Samphire Marsh Member	1362.1 – 1362.2		X	Moderate, whitish blue fluorescence in limestone. Weak, white streaming cut – weak white blooming crush. Weak, white, mottled residual film. Very poor
		Fly Flat Member	1393.5 – 1393.8		X	Moderate, whitish green fluorescence in sandstone, mottled white streaming cut grading to milky bloom. Weak yellow green residual ring. Weak white resin film. Poor
		Wilson Cliffs Sandstone	3177	X		Gas shows up to 13 units
		Wilson Cliffs Sandstone	3348–3879	X		Traces of C1–C4
		Wilson Cliffs Sandstone	3325–3429		X	Isolated weak oil shows
		Wilson Cliffs Sandstone	3395	X		Max gas trip
		Wilson Cliffs Sandstone	3405–3429		X	Fluorescence in sandstone cuttings, pale yellow, no instant cut, very slow crust cut and residual ring
		Wilson Cliffs Sandstone	3650–3780		X	Oil fluorescence in large sandstone cuttings
Pegasus 1	2995	Wilson Cliffs Sandstone	3861–3864		X	Isolated oil shows
		Wilson Cliffs Sandstone	4132–4170	X		Traces of C1–C4
Percival 1	2448	Fly Flat Member	2229 – 2447.6	X		Formation gas from 0.5 to 1 unit, background from contamination was 9–15 units.
Pictor 1	2146	Fly Flat Member	2090	X		Gas erratically declined from 100 ppm C1 and 90 ppm C2 at 2255 to a trace of C1 at total depth. No heavier gases or fluorescence were detected
Prices Creek 1	307	Emanuel Formation	42.6 – 76.8		X	25 units trip gas
Prices Creek 2	104	Emanuel Formation			X	Trace mineral oil from six samples
Prices Creek 3	247	Emanuel Formation			X	Trace mineral oil from surface to total depth
Sally May 2	1994.1	Fly Flat Member	1938.5 – 1942.95		X	Trace mineral oil from surface to total depth
		Fly Flat Member	1938.5 – 1942.95		X	Minor oil show, 0–5% of the rock present as patches and spots that are more obvious on the core surface after several hours
		Fly Flat Member	1941.3 – 1941.37		X	Fluorescence, bright white over 55% of the interval. One 1–2 cm continuous band
		Fly Flat Member	1941.76 – 1941.88		X	Fluorescence, bright white with instant bright white cut. Forms as patches over 20% of the show zone
		Fly Flat Member	1958.05 – 1958.25		X	Spotty fluorescence that becomes a semi-continuous blocky oil stain band after several hours
		Fly Flat Member	1962.2 – 1962.5		X	Patchy oil stain observed after several hours
		Fly Flat Member	1970.39 – 1970.47		X	Fluorescence, bright white over 70% of the interval, patchy and semi-continuous
		Fly Flat Member	1970.66 – 1970.8		X	Fluorescence, bright white in continuous band, fluorescence over 10% of the area, chip samples showed strong, slow streaming yellow-white cut
Sally May 2	1994.1	Fly Flat Member	1973.8 – 1973.9		X	Fluorescence, bright white, patchy and discontinuous
		Fly Flat Member	1975.4 – 1984.2		X	Fluorescence, rare isolated spots

**Table A5.1. Hydrocarbon shows in petroleum exploration, mineral exploration and stratigraphic wells intersecting the Nambeet Formation, Wilson Cliffs Sandstone and Prices Creek Group, recorded from well completion reports**

Well or drillhole name	Total depth (m)	Formation/member	Depth (m)	Gas	Oil	Description
Samphire Marsh 1	2031.2	Fly Flat Member	1988.1 – 1988.6		X	Fluorescence observed directly after recovery, dull to moderately bright white with patches of bright white
		Fly Flat Member	1988.6 – 1989		X	Faint patchy oil shows
Setaria 1	956	No shows recorded				
Setaria 1	956		633–658	X	X	Trace dull yellow fluorescence with no associated cut and low mudlog gas readings (800–2000 ppm C1)
			747–759		X	Trace oil stains, bright yellow fluorescence and cut observed in cuttings. Mudlog gas low (900–2000 ppm C1)
			843–883	X		Trace to 50 ppm C1–C4
			895–942	X	X	Fluorescence and oil stains in cuttings at 900 m. Mudlog gas consistently 2000 ppm C1, increasing to 6500 ppm C1 between 932–942 m
Sharon Ann 1	1830	No shows recorded				
Solanum 1	834	No shows recorded				
Tappers Inlet 1	2856.28		2064	X		Slight increase in mud gas below 2064 m possibly related to source material
Thangoo 1A	1654.76				X	Slight staining and fluorescence in some dolomite veins in the upper part of the tight basal sandstone
Thangoo 2	1472	No shows recorded				
Twin Buttes 1	1600.3	No shows recorded				
Willara 1	3903	No shows recorded				
Wilson Cliffs 1	3722.22	Wilson Cliffs Sandstone	3000 – 3003.8		X	Weak greenish yellow fluorescence detected on sandstone cuttings, possibly solid hydrocarbons

The Lower Ordovician Nambheet Formation represents some of the earliest deposits in the Canning Basin. The Olympic 1 petroleum exploration well recovered 319.53 m of continuous core that includes the conformable contact between the Nambheet Formation and overlying Willara Formation, and 277.53 m of the Nambheet Formation. The cored section from the Olympic 1 well is proposed as a reference section for the Nambheet Formation, Canning Basin. This Report details the range of analysis undertaken on the Nambheet Formation cored section in the Olympic 1 well including: conodont and palynological biostratigraphy, bentonite geochronology, organic geochemistry, HyLogger analysis, chemostratigraphy and facies analysis. Based on the results of this analysis, this Report proposes that the Nambheet Formation should be divided into two formal members: the upper Samphire Marsh Member and the underlying Fly Flat Member.



Further details of geoscience products are available from:

Information Centre  
Department of Mines, Industry Regulation and Safety  
100 Plain Street  
EAST PERTH WA 6004  
Phone: (08) 9222 3459 Email: [publications@dmirs.wa.gov.au](mailto:publications@dmirs.wa.gov.au)  
[www.dmirs.wa.gov.au/GSWApublications](http://www.dmirs.wa.gov.au/GSWApublications)

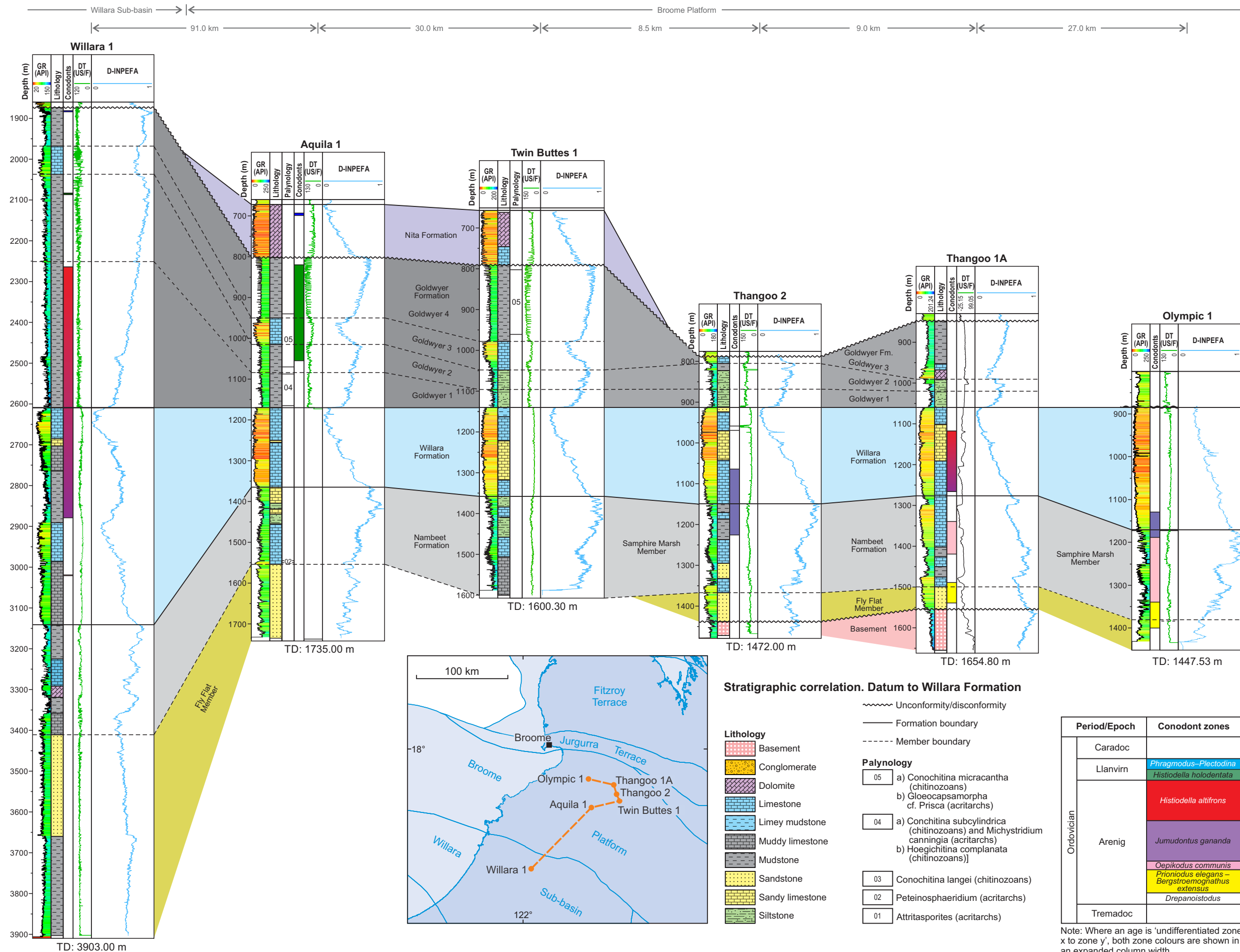


Plate 1. Correlation panel through wells on the Broome Platform and Willara Sub-basin



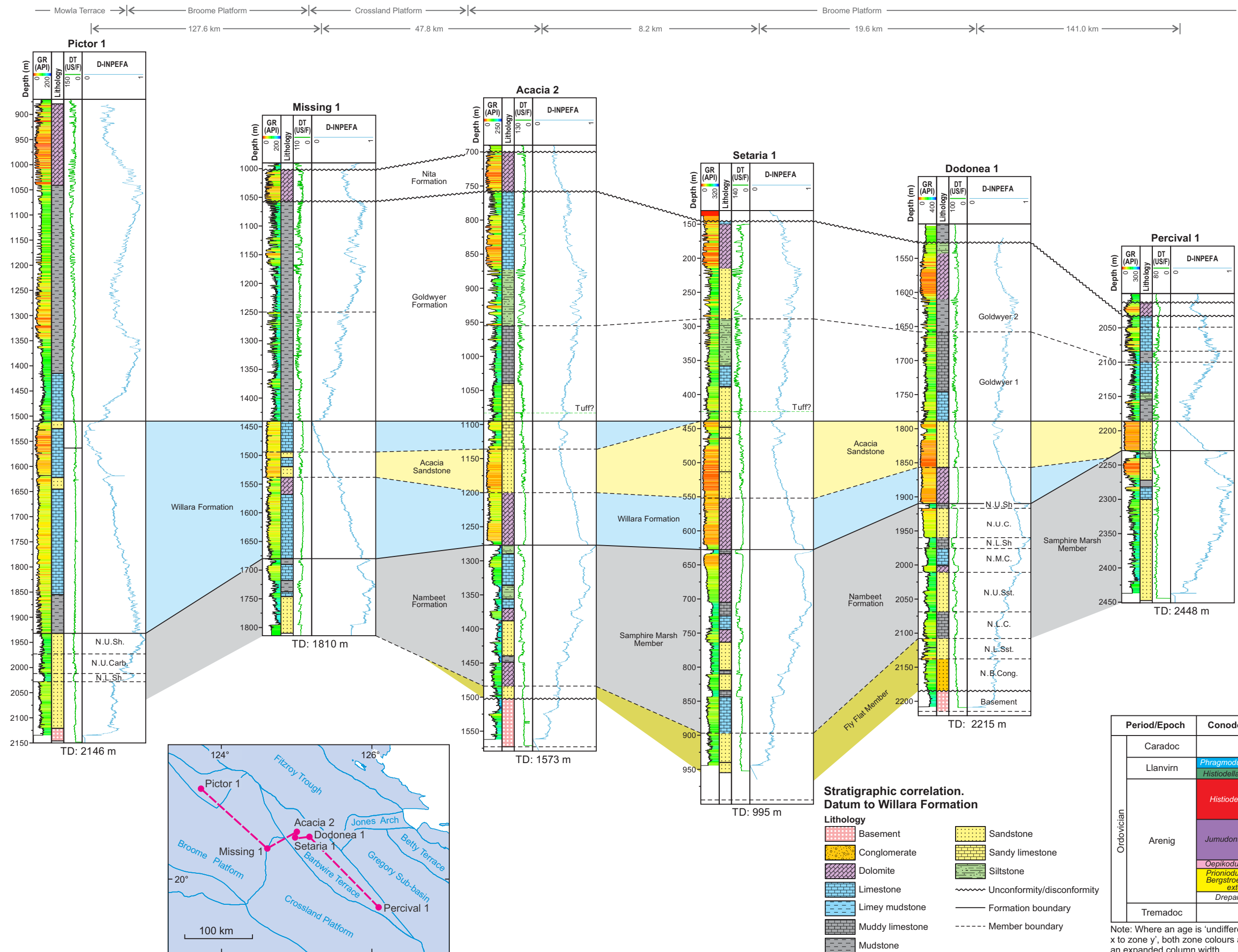


Plate 2. Correlation panel through wells on the Broome Platform, Mowla Terrace and Barbwire Terrace

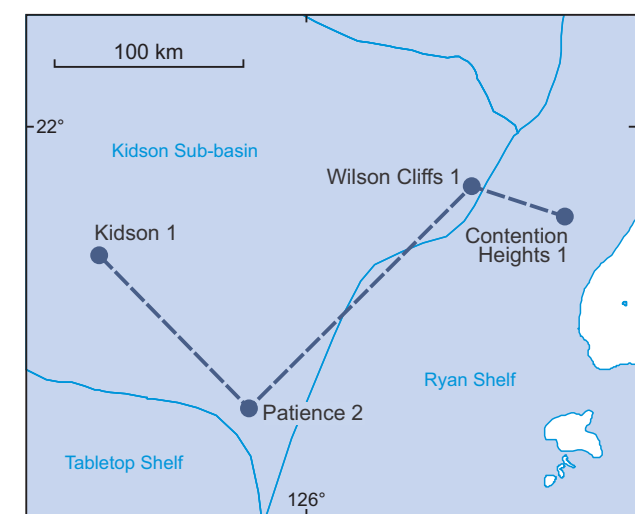
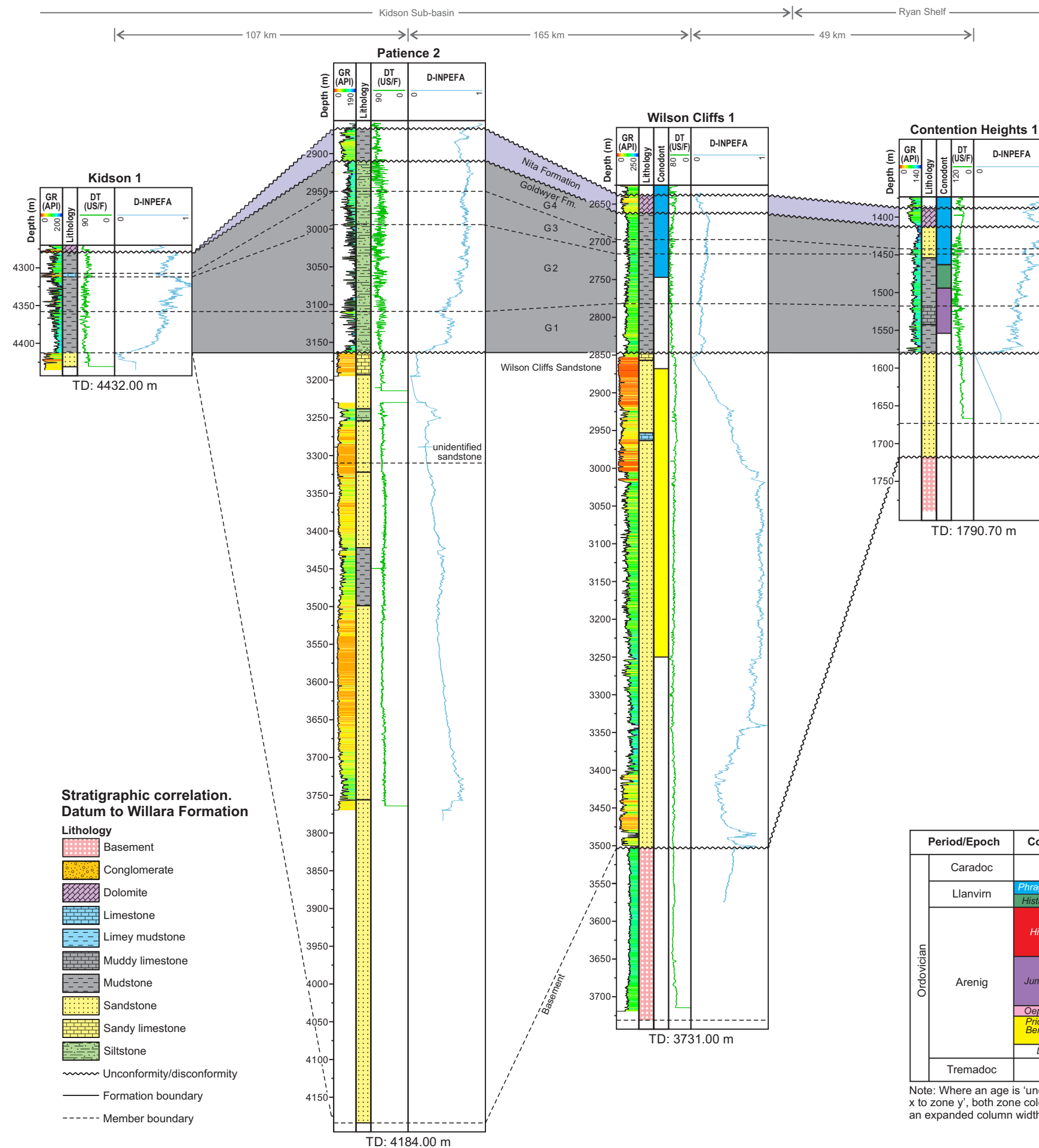
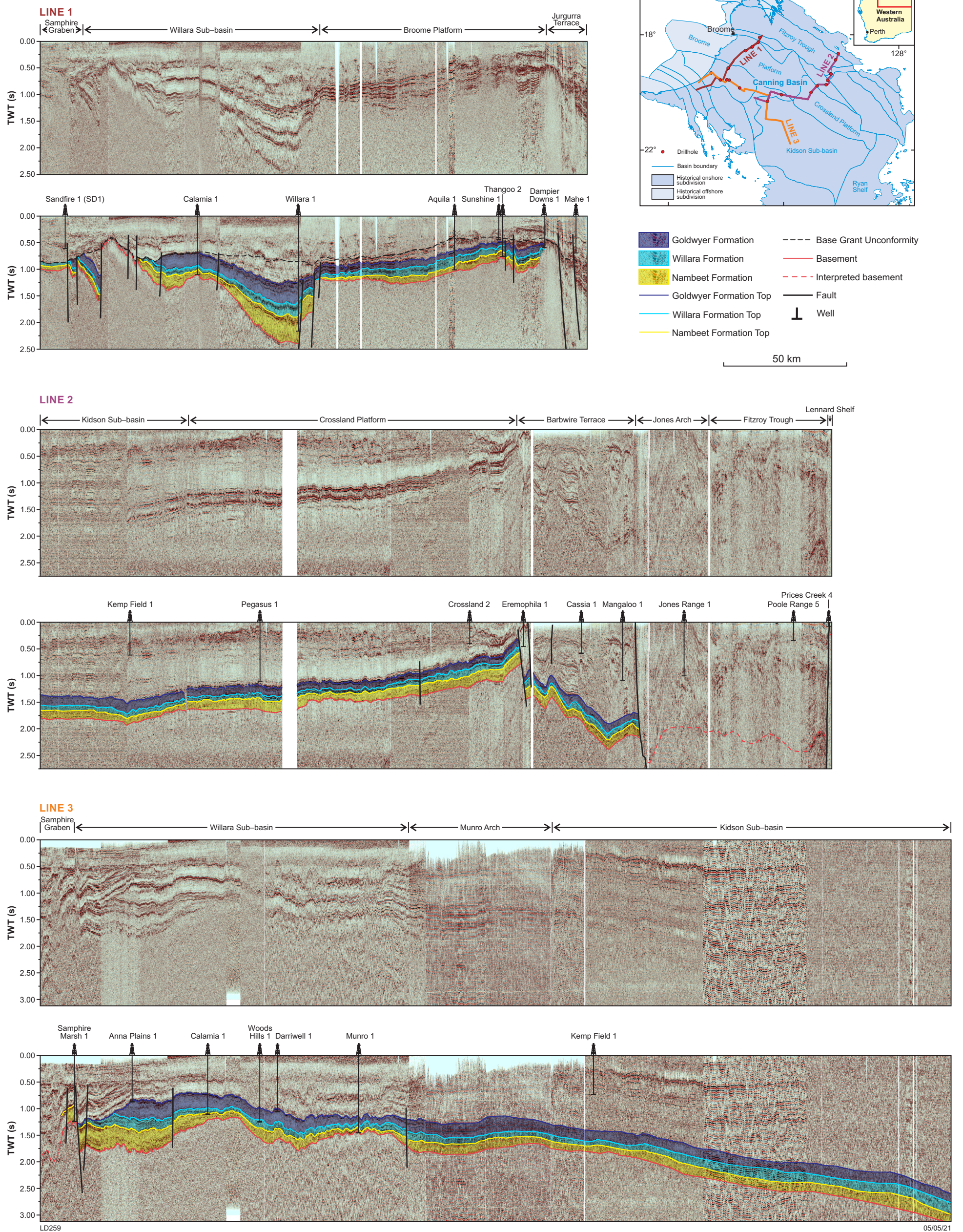


Plate 3. Correlation panel of wells where the Wilson Cliffs Sandstone has been identified



SW

NE



**Plate 4. Seismic lines showing interpreted Nambeet Formation, Willara Formation and Goldwyer Formation packages in three sections across the Canning Basin**